TTU-ES-70-3

STRESS WAVES IN SANDWICH PLATES

by

RAY KINSLOW

and

BRIAN DELANO

Prepared For

NATIONAL AERONAUTICS AND SPACE ADMINISTRATION

MANNED SPACECRAFT CENTER

HOUSTON, TEXAS

GRANT NUMBER NGR 43-003-007

AUGUST, 1970

TENNESSEE TECHNOLOGICAL UNIVERSITY

DEPARTMENT OF ENGINEERING SCIENCE

COOKEVILLE, TENNESSEE 38501

TTU-ES-70-3

STRESS WAVES IN SANDWICH PLATES

by

Ray Kinslow

and

Brian Delano

Prepared For

NATIONAL AERONAUTICS AND SPACE ADMINISTRATION

MANNED SPACECRAFT CENTER

HOUSTON, TEXAS

GRANT NUMBER NGR 43-003-007

August, 1970

TENNESSEE TECHNOLOGICAL UNIVERSITY

DEPARTMENT OF ENGINEERING SCIENCE

COOKEVILLE, TENNESSEE 38501

ABSTRACT

A mathematical stress wave model is formulated for use in predicting the effects of various material combinations and geometry in the design of sandwich plates that may be subjected to high velocity impact. In the experimental investigations the bounding layers were of a birefringent material and stresses were determined by means of a dynamic polariscope utilizing a high-speed framing camera. A comparison is made of the theoretical and experimental results.

CONTENTS

ILLUSTRATIONS

Figure

ILLUSTRATIONS, Continued

ILLUSTRATIONS, Continued

TABLES

NOMENCLATURE

a, b	leading and trailing edges of pressure pulse
a', b'	leading and trailing edges of reflected pressure pulse
c	wave velocity
A, AA, AAA B, BB, BBB C, CC, CCC	pulse amplitudes resulting from front surface reflections
E	Young's modulus
f	photoelastic constant
h	model thickness
k	constants
K	impedance mismatch
L	pulse or wave length
N	fringe order
O	point of impact
p_0	pressure at cavity surface
$\bar{p}_0$	non-dimensional unit of pressure
P	pulse amplitude
S	a point
r	radius vector
r_0	cavity radius
t	time
$\bar{t}$	non-dimensional unit of time
T	lamination thickness

NOMENCLATURE, Continued

u	particle displacement
v	particle velocity
y	distance from free surface of target
Y	target thickness
α	decay constant
ε_r	radial strain
ε_θ	tangential strain
λ, μ	Lamé constants
ν	Poisson's ratio
ϕ	scalar displacement potential
ρ	material density
σ_r	radial stress
σ_θ	tangential stress
$\bar{\sigma}$	non-dimensional unit of stress
τ	shear stress

SECTION I

INTRODUCTION

Meteoroids and other debris in outer space pose potential hazards to astronauts, spacecraft, and missiles. Although the impacted body may have sufficient strength and thickness to resist actual puncture, damage may be caused by strong shock waves resulting from the impact. When such a stress wave encounters a free surface, it is reflected, generally as a tensile wave. If the amplitude of this reflected wave is equal to or greater than the strength of the "target" material, fracture will occur. Such fractures may appear as cracks near the surface, weakening the structure; as rear surface bulges which could jam mechanisms or block flow in pipes; or as a complete detachment of target material, creating a shrapnel effect, endangering equipment or personnel.

It has been demonstrated that damage caused by stress waves produced by hypervelocity impact can, in many cases, be reduced by employing laminated targets (Reference 1). The results of such experiments have served to alert the design engineer to the possibility of reducing the probability of damage or of using a thinner or lighter material as the outer skin or hull of spacecraft. It is perhaps more important to realize that the use of laminates does not necessarily reduce the probability of damage, but may, in some cases, actually result in increased damage to the structure (Reference 2).

This study is an attempt to formulate a mathematical model that can be utilized to predict the action of laminates in affecting the stress waves induced by impact. Such a model should include all parameters that may affect the ability of structures to resist fracture caused by hypervelocity collisions before it can be used with confidence.

This study is limited to an investigation of elastic waves in sandwich plates or targets of only three layers, the two bounding layers being of one material and the center layer, or core, being of a different material. It deals only with stress amplitudes and not with material strengths and fracture criteria.

A brief theoretical analysis of the propagation and reflection of spherical waves in solid homogeneous targets is first made, followed by the study of waves in sandwich plates. This includes the effects of material properties (such as Poisson's ratio, density, modulus of elasticity), target geometry (target thickness, lamination thicknesses, core location), and the stress wave characteristics (amplitude, wave or pulse length, wave form, decay rate).

The next section describes the experimental investigation of the stresses developed in both homogeneous and laminated targets. The outer layers were transparent birefringent materials that could be studied by photoelastic methods. Stresses are determined only in the third layer of the target, this being the region of maximum tensile stress when waves are reflected from the free surface.

A theoretical model is next formulated that duplicates the experimentally determined stresses in a homogeneous target as closely as possible. This is called a "quasi-theoretical" method (Reference 3). By using this theoretical model, the effects of the core are calculated and compared with those determined experimentally.

SECTION II

THEORETICAL ANALYSIS

Spherical dilatational wave propagation in homogeneous, isotropic material can be specified by the equation

$$\frac{\partial^2 \phi}{\partial t^2} = c^2 \left(\frac{\partial^2 \phi}{\partial r^2} + \frac{2}{r} \frac{\partial \phi}{\partial r} \right)$$

where ϕ is a scalar displacement potential, c is the wave velocity, and t is time. Particle displacement (u) and velocity (v) are specified by the relations

$$u = \frac{\partial \phi}{\partial r} \qquad \text{and} \qquad v = \frac{\partial u}{\partial t}$$

where r denotes the radius vector from the point of projectile impact. The radial and tangential stresses are given by the relations

$$\sigma_r = (\lambda + 2\mu) \left(\frac{\partial u}{\partial r} \right) + 2\lambda \left(\frac{u}{r} \right)$$

and

$$\sigma_\theta = \lambda \left(\frac{\partial u}{\partial r} \right) + 2(\lambda + \mu) \left(\frac{u}{r} \right)$$

where λ and μ are the Lamé constants and are related to Young's modulus (E)

and Poisson's ratio (ν) as follows

$$\lambda = \frac{\nu E}{(1 + \nu)(1 - 2\nu)}$$

$$\mu = \frac{E}{2(1 + \nu)}$$

The mathematical model used in this investigation for generating spherical elastic waves is that described in References 4 and 5. It is assumed that there is a hollow hemispherical cavity in the target with its center at the point of impact and that a time-varying pressure or forcing function is applied to the cavity surface, generating stress waves in the target. The pressure (p_0) applied to the cavity surface is an impulse that may be described by the relation

$$P_0 = k_1 e^{-\alpha_1 t} + k_2 e^{-\alpha_2 t} + k_3 e^{-\alpha_3 t} + \ldots$$

where α_1, α_2, . . . are decay constants, t is elapsed time, and k_1, k_2, . . . are constants. By the proper choice of values of k and α, various wave forms can be generated.

The solution of the wave equation based upon Blake's work and described in Reference 5 is employed in this study.

Reflected stress waves are created in so-called "image cavities." The velocity of both the incident wave and the reflected spherical wave is given by the relation

$$c = \left[\frac{E(1 - \nu)}{\rho(1 + \nu)(1 - 2\nu)}\right]^{1/2}$$

Solid Homogeneous Targets

Figure 1 shows the target being considered. Its thickness is denoted by Y and the distance of a point (S) from the rear surface is given by y. Only stresses developed along the axis passing through point O and normal to the target's rear surface have been considered.

Nondimensional units of stress and time are used in this theoretical part of the study as follows:

$$\bar{\sigma} = \sigma/E \qquad \text{and} \qquad \bar{t} = tc/Y$$

Unless otherwise specified, the following values are also used:

$$r_0 = 0.2Y, \qquad \nu = 0.333, \qquad c = 1.000$$

The first case to be investigated is that of the application of a constant and continuous pressure to the cavity surface in a solid homogeneous target. The tangential stress ($\bar{\sigma}_\theta$) and radial stress ($\bar{\sigma}_r$) were computed at points 0.1Y, 0.2Y, 0.3Y, and 0.4Y distance from the free surface. Results are shown in Figure 2. The stress indicated by a-a is developed as the wave front reaches the point under consideration. As this wave is reflected from the free surface as a tensile wave, it produces a sudden change in stress denoted by a'-a'. The curves of radial stress at the four points are compared in Figure 3. It is seen that the maximum tensile stress resulting from this wave has a value of approximately 20 (actually 20E) at a point about 0.23Y distance from the free surface.

The effect of the wave or pulse length upon the developed stress was next investigated. Figure 4 shows the stress-time relation at the four points for a square wave input having a length of 0.75. In this case, there will not only be discontinuities caused by the passage and

reflection of the wave front, but also by the trailing edge of the pulse. Figures 5 and 6 show the resulting stress for pulse lengths of 0.50 and 0.25, respectively. It is obvious that not only the pulse amplitude, but also its length, contributes to the developed stress. These are summarized in Figure 7. The top curve shows the maximum compressive stress developed as the pulse moves toward the free surface. The second curve (indicated by $L = \infty$) shows the tensile stresses developed by the reflection of the wave generated by a constant and continuous forcing function. The various points show the maximum tensile stresses produced at the four points being considered by impulses of various lengths. It can be seen that in every case, the maximum tensile stress will occur when the reflected wave front coincides with the forward moving trailing edge. The lower curve is for these cases. It can be concluded that in any analysis of the developed stresses, the pulse length will be an important factor. For example, in the case of a very long pulse, the maximum tensile stress has been shown to have a value of about 20 at a distance of 0.23Y from the free surface, but a short pulse having a length of 0.25 will develop a tensile stress of about 35 at $y = 0.1Y$, and one having a length of 0.75 will produce a stress of approximately 50 about 0.35Y from the free surface.

Forcing functions more nearly simulating impact or explosives may be formulated. Figure 8 shows waves resulting from a function that closely represents an explosive input. The small sketch of the load-time curve approximates that of an electrical primer (Reference 6, page 347). Stress-time curves showing the effect of the decay constant, α, for decaying inputs are given in Figure 9. The results from an input that increases from zero and approaches a maximum value are shown in Figure 10. In these analyses, the cavity radius has arbitrarily been assumed to have a value of 0.20Y. The effect of using values of 0.10Y and 0.05Y is shown in Figure 11.

Laminated Targets

An abrupt change in the physical properties of a material will result in the modification of a pressure pulse as it encounters this change. In general, a portion of the pulse will be transmitted, and a portion will be reflected. The relations which describe the modification of a pulse are based upon the boundary conditions of continuity of pressure and continuity of particle velocity across the interface between two materials. These relations depend upon the value of ρc, called the "characteristic impedance," of the two materials. If $\rho_0 c_0$ is for the first, and $\rho_t c_t$ is for the second laminate, and P_0 is the pulse amplitude in the first, the amplitude of the transmitted component is

$$P_t = \left[\frac{2\rho_t c_t}{\rho_t c_t + \rho_0 c_0} \right] P_0$$

and the reflected component is

$$P_r = \left[\frac{\rho_t c_t - \rho_0 c_0}{\rho_t c_t + \rho_0 c_0} \right] P_0$$

These relations are somewhat simplified by letting

$$K = \frac{\rho_t c_t}{\rho_0 c_0}$$

giving

$$P_t = \left[\frac{2K}{K + 1} \right] P_0$$

and

$$P_r = \left[\frac{K - 1}{K + 1} \right] P_0$$

The sandwich structure under consideration is shown in Figure 12. Its total thickness is Y, the thicknesses of the first and last layers of material are T_0 and T_2, respectively. The characteristic impedance of

both is $\rho_0 c_0$. The middle lamination has a thickness of T_1 and a characteristic impedance of $\rho_1 c_1$. This figure shows the distance-time relation of the wave fronts. Starting at time zero at point r_0, the wave moves with a velocity of c_0 through the first layer. Upon reaching the first interface, the amplitude of the transmitted component is $\left[\frac{2K}{K+1}\right] P_0$ which moves through the core at a velocity of c_1. As this pulse reaches the second interface, a portion will again be transmitted, and a part will be reflected. However, the value of the impedance mismatch at this interface is not K, but has a value of 1/K. The amplitude of the pulse transmitted is, therefore,

$$\left[\frac{2K}{K+1}\right]\left[\frac{2/K}{(1/K)+1}\right] P_0 = \left[\frac{2K}{K+1}\right]\left[\frac{2}{K+1}\right] P_0 = \left[\frac{4K}{(K+1)^2}\right] P_0$$

and is denoted by $P_{1\text{-}0\text{-}0}$. As only the stress developed in the last layer of the target is under consideration, it can be assumed that the target is composed of this material only, and that the initial pulse has an amplitude of $\left[\frac{4K}{(K+1)^2}\right] P_0$ instead of P_0. The time required, however, for this pulse to reach any point is not the same as for a homogeneous target due to the change in velocity through the core. It must be adjusted by the amount

$$t_{1\text{-}0\text{-}0} = \left[\frac{c_0 - c_1}{c_0 c_1}\right] T_1$$

The component of the pulse reflected from the second interface is $\left[\frac{K-1}{K+1}\right] P_0$, which, upon again reaching the first interface, will be reflected with an amplitude of $\left[\frac{K-1}{K+1}\right]^2 P_0$. A portion will then be transmitted through the second interface, this being

$$P_{2\text{-}0\text{-}0} = \left[\frac{K-1}{K+1}\right]^2 \left[\frac{4K}{(K+1)^2}\right] P_0 = \left[\frac{4K\,(1-K)^2}{(1+K)^4}\right] P_0$$

If the transmitted pulse amplitudes in this layer are denoted by P_{A-B-C}, the other pulses P_{A-0-0} may be specified as

$$P_{A-0-0} = \frac{4K(1 - K)^{2(A - 1)}}{(1 + K)^{2A}}$$

These pulse amplitudes, P_{1-0-0}, P_{2-0-0}, P_{3-0-0} . . . form a rapidly converging series, the sum of which approaches the value of P_0. This is to be expected, because pulse attenuation and energy losses have been neglected up to this time. The time adjustments for these waves are given by the relation

$$t_{A-0-0} = \left[\frac{(2A - 1)c_0 - c_1}{c_0 c_1}\right] T_1$$

This series of transmitted waves, as well as others that will be discussed, can be seen more clearly on the second and third pages of Figure 12. Figure 13 gives the amplitudes of P_{A-0-0} as functions of the impedance mismatch, K.

Returning to the pulse P_{1-0-0}, it is seen that this will be totally reflected from the free surface as a tensile wave. When this reflected pulse reaches the second lamination, a portion will be transmitted into the core and a part will be reflected back into the third layer as P_{1-1-0}, which, in turn, will be reflected from the free surface as was P_{1-0-0}, resulting in P_{1-2-0}, and then in P_{1-3-0}, etc. Pulse P_{2-0-0}, P_{3-0-0}, . . . will likewise result in multiple reflections, the amplitudes of which are given by the relation

$$P_{A-B-0} = \frac{4K(1 - K)^{(2A + B - 2)}}{(1 + K)^{(2A + B)}}$$

The corresponding time delays are given by

$$t_{A-B-0} = t_{A-0-0} + \frac{2BT_2}{c_0}$$

These amplitudes are given on the first page of Figure 14 for various values of K. The values of P_{A-B-0} are given as percentages of P_0 in this figure. Consider the case of K having a value of 0.5.

$P_{1-0-0} = 0.889P_0$ $\quad P_{2-0-0} = 0.099P_0$ $\quad P_{3-0-0} = 0.011P_0$

$P_{1-1-0} = 0.296P_0$ $\quad P_{2-1-0} = 0.033P_0$

$P_{1-2-0} = 0.099P_0$ $\quad P_{2-2-0} = 0.011P_0$

$P_{1-3-0} = 0.033P_0$

$P_{1-4-0} = 0.011P_0$

Values of P less than $0.01P_0$ are not shown.

As previously stated, $P_{1-0-0} + P_{2-0-0} + P_{3-0-0} + \ldots = P_0$. This may be illustrated for this instance of K = 0.5,

$$0.889 + 0.099 + 0.011 = 0.999.$$

It can also be shown that the sum of all the transmitted pulse amplitudes,

$$\Sigma P_{A-B-0} = \frac{1 + K}{2K}$$

In this case of K = 0.5, the sum would be 1.5. The values given above have a total of 1.482. Where K has a small value, say 0.1, the sum of these pulse amplitudes is 5.5. This means that, although the magnitudes decrease very rapidly as they undergo multiple reflections, their sum may be several times that of the transmitted pulse in a homogeneous target. The conditions under which this may occur will be shown later.

Magnitudes of P_{A-B-0} given in Figure 14 for values of K ranging from 0.1 to 0.9, also apply for values of 1/K except that for odd values of B,

P_{A-B-0} will be negative. This explains why the sum of all the transmitted waves for K = 2.0, for example, is only 0.75. One should not come to the conclusion at this point in the study that the center core should always have a characteristic impedance greater than the boundary layers in order that the total stress developed in the last layer will be reduced. Under some conditions this would result in an increase in stress as the reflected tensile waves from P_{1-0-0}, P_{2-0-0}, etc. may meet the transmitted tensile waves, P_{1-1-0}, P_{2-1-0}, P_{1-3-0}, etc. and combine to increase the total tensile stress.

Referring again to Figure 12, it will be seen that there are additional transmitted waves not yet discussed. These are P_{1-0-1}, P_{1-0-2}, P_{1-1-1}, etc. These amplitudes are given by the relation

$$P_{A-B-C} = - \frac{16K^2 (1 - K)^{(2A + B + 2C - 3)}}{(1 + K)^{(2A + B + 2C + 1)}} \qquad (C \neq 0)$$

and the time differential by

$$t_{A-B-C} = t_{A-B-0} + \frac{2T_2}{c_0} + \frac{2CT_1}{c_1}$$

These waves may have significant magnitudes as shown on the second page of Figure 14; however, they usually occur at such a late time and have been attenuated by traveling through great distances by their successive reflections, that no instance has been found where they contribute significantly to the maximum tensile stress developed. Therefore, they have not been included in the examples given.

Wave reflections from the front surface of the target have not been considered in this analysis. If a crater is produced by the impact, the reflections would be from the expanding crater. If it is assumed, however,

that these reflections are from the original stress-free surface, they will have the amplitudes given in Figure 15. Each of these waves, A, B, C, AA, BB, CC, AAA, . . ., would produce another series of waves such as shown in Figure 12, having the amplitudes and times shown. In some instances their effects would be significant.

The thickness of the core (T_1) and its distance from the free surface (T_2) are significant factors in determining the resulting stress. From Figure 12 it can be seen that if the thickness T_1 is very small, the time between the wave fronts of P_{A-0-0} will also be small. The relation given for t_{A-0-0} also indicates that the time intervals are directly proportional to the thickness T_1. This may have little effect upon the total developed stress if the pulses are very short. If they are long, however, and T_1 is small, the transmitted components will overlap; and the total amplitude may be as great as if there were no lamination. The time intervals of the other pulses, P_{A-B-0}, depend upon the thickness T_2. These effects will be noted in the examples that follow. In Figures 16 through 24, the forcing function is a constant, that is, the waves should be relatively long. Figure 16 shows the effect of the core thickness upon the stress developed at a point 0.10Y distance from the free surface and an impedance mismatch value, K, of 0.25. It is seen that both the maximum compressive stress produced by the transmitted wave and the maximum tensile stress resulting from the reflected wave occurred at this point when T_1 was only 0.01Y. The superposition and overlapping of the wave fronts are clearly seen. This did not occur in the case of thicker cores, and the stress magnitude depended very little upon the core thickness in these cases. At other distances from the free surface, the maximum stress was also developed in the case of the thinner core, but it will also be noted that at y = 0.30Y the tensile stress resulting from

the core thickness of 0.20Y is greater than in the case of the intermediate thicknesses of 0.05Y and 0.10Y.

For K = 0.50 there was not as much dependence upon the core thickness. In this case, a smaller number of transmitted waves had significant values, and a still smaller number when K = 0.75.

The effect of the pulse length is shown in Figures 25 and 26. Comparing with Figures 20 through 23, it is seen that the tensile stress was more than twice as great in the case of a shorter pulse.

In these examples of the effects of laminations, the amplitudes of the transmitted waves were not as given in Figure 14, but were smaller because of attenuation due to distance. It has been assumed that the wave amplitude attenuates at a rate inversely proportional to the distance traveled.

The effect of lamination thickness upon stress in the case of a wave that more nearly represents the conditions of impact is shown in Figure 27.

SECTION III

EXPERIMENTAL INVESTIGATION

In the experimental investigation described in this report, a Beckman and Whitley Model 201 synchronous framing camera was used to record the dynamic fringe pattern generated in the model. The camera is a rotating mirror type, making twelve 0.7 X 0.9-inch photographs on a 4 X 5-inch film at speeds up to one million frames per second. Exposure time for each photograph at this speed is approximately 0.6 microsecond. Figure 28 is a diagram of the camera and related equipment.

The two pulse generators deliver 100 Joules each at 5 KV. One was used to provide energy for the light source. After much experimentation with exploding wires and other devices, it was found that a Buss type AGC-1 safety fuse was an ideal light source. This fuse, when exploded, provides an intense light with a sufficiently long duration for satisfactory exposure of all twelve frames.

The other pulse generator was used as the energy source for generating stress waves in the model as a simulation of hypervelocity impact. After experimenting with many kinds of model materials, PSM-1, a clear polyester sheet manufactured by Photolastic, Inc., was selected as the basic material to be used in this study. Its manufacturer claims that it has the highest photoelastic sensitivity of any model material available and has a wave velocity of about 60,000 inches per second, sufficiently low to be photographed without apparent wave movement during exposure. Another important

factor is that it is practically free of creep and edge effects. This plastic can be easily machined, polished, and cemented to other materials. The most consistent stress waves were generated by exploding a fine wire in contact with one edge of the model. The amplitudes of these waves, however, were not sufficiently great for accurate comparison of waves having only slight differences in amplitude. A stronger shock, giving a greater number of fringes, resulted when a small amount of explosive was added. Urea nitrate was the explosive used in this investigation.

Separation of the stresses is possible without additional experimental data since the waves in this case propagate without rotation. Stresses are developed both along and perpendicular to the direction of wave propagation. Displacement occurs, however, only in the direction of wave motion. The displacements are specified by:

$$u_r = f(r) \quad , \quad u_\theta = 0$$

and the strain-displacement relations by

$$\varepsilon_r = \frac{du_r}{dr} \quad , \quad \varepsilon_\theta = \frac{u_r}{r}$$

The stress-strain equations are

$$\sigma_r = \frac{E}{1 - \nu^2} \left[\varepsilon_r + \nu\varepsilon_\theta\right] \quad , \quad \sigma_\theta = \frac{E}{1 - \nu^2} \left[\varepsilon_\theta + \nu\varepsilon_r\right]$$

and the shear stress has the value

$$\tau = \pm \frac{\sigma_\theta - \sigma_r}{2}$$

where E is Young's modulus and ν is Poisson's ratio.

From these relations

$$2\tau = \sigma_\theta - \sigma_r = \frac{E}{1 + \nu} \left[\varepsilon_\theta - \varepsilon_r\right] = \frac{E}{1 + \nu} \left[\frac{u_r}{r} - \frac{du_r}{dr}\right]$$

but

$$\frac{d}{dr}\left(\frac{u_r}{r}\right) = \frac{1}{r}\left[\frac{du_r}{dr} - \frac{u_r}{r}\right]$$

So

$$\sigma_\theta - \sigma_r = -\frac{E}{(1+\nu)}\left[r\frac{d}{dr}\left(\frac{u_r}{r}\right)\right]$$

$$\frac{d}{dr}\left(\frac{u_r}{r}\right) = -\frac{(1+\nu)}{E}\left(\frac{\sigma_\theta - \sigma_r}{r}\right)$$

$$\frac{u_r}{r} = -\frac{(1+\nu)}{E}\int\frac{\sigma_\theta - \sigma_r}{r}\,dr$$

$$\varepsilon_\theta = \frac{u_r}{r} = -\frac{2(1+\nu)}{E}\int\frac{\tau}{r}\,dr$$

$$\varepsilon_r = \varepsilon_\theta - \frac{2(1+\nu)}{E}\tau = -\frac{2(1+\nu)}{E}\left[\tau + \int\frac{\tau}{r}\,dr\right]$$

The radial and tangential stresses are, therefore,

$$\sigma_r = -\left(\frac{2}{1-\nu}\right)\left[\tau + (1+\nu)\int\frac{\tau}{r}\,dr\right]$$

$$\sigma_\theta = -\left(\frac{2}{1-\nu}\right)\left[\nu\tau + (1+\nu)\int\frac{\tau}{r}\,dr\right]$$

This derivation is essentially the same as that described in Reference 7. The stress-optic relation is

$$\tau = \frac{Nf}{2h}$$

where N is the fringe order, f is the photoelastic constant of the material, and h is the model thickness.

These relations may be stated in terms of the model material properties and the fringe order

$$u_r = -\frac{(1+\nu)f}{Eh}\left[r\int\frac{N}{r}\,dr\right] = r\varepsilon_\theta$$

$$\varepsilon_r = -\frac{(1+\nu)f}{Eh}\left[N + \int\frac{N}{r}\,dr\right] = \frac{du_r}{dr}$$

$$\varepsilon_\theta = -\frac{(1+\nu)f}{Eh}\left[\int\frac{N}{r}\,dr\right]$$

$$\sigma_r = -\frac{f}{h(1-\nu)}\left[N + (1-\nu)\int\frac{N}{r}\,dr\right]$$

$$\sigma_\theta = -\frac{f}{h(1-\nu)}\left[\nu N + (1+\nu)\int\frac{N}{r}\,dr\right]$$

Values of displacement, strain, and stress may now be determined by numerical integration.

As the objective of the present research is to compare the stresses developed in a laminated target with those produced in a homogeneous target under the same dynamic impulse, the properties of the material, such as the dynamic modulus of elasticity and photoelastic constant, have not been determined. Resulting strains, displacements, and stresses are, therefore, relative values only and are designated by $k_1\varepsilon$, $k_1 u$, and $k_2\sigma$ where $k_1 = E/f$ and $k_2 = 1/f$. Values of other properties for the target material, PSM-1, are: Poisson's ratio (ν) = 0.38, density (ρ) = 20 grams per cubic inch, thickness (h) = 0.25 inch, and wave velocity (c) = 60,500 inches per second. The characteristic impedance values of this and some other materials are given in Table I.

It was found that a light field polariscope utilizing circular polaroids, and a dark red filter gave the most satisfactory photographs

of the stress pattern. Figure 29 is a typical photograph showing the fringe order values. Figure 30 was prepared from three sets of photographs, shots 175, 176, and 177, and show fringe locations for each frame. Frame 12 of shot 175 was identical with frame 1 of shot 176, but there was a slight gap between the last frame of shot 176 and the first frame of shot 177. In the last frame of 176 the wave front is approaching the rear edge of the model and in 177 the wave is being reflected. The zero fringe (wave front) cannot be seen in these photographs because of the light field being used, so this fringe was determined by extrapolation from the other fringes. The broken line shows the approximate location of the reflected wave front.

Displacements, strains, and stresses were computed from values of r and N read from this figure. Figure 31 shows the photographs and computed results. Shots 175 and 176 were considered continuous with the frame numbers indicated as being from 1 to 23. Shot 177 was not included in the computations as this report does not deal with the waves reflected from a free surface.

A plot of fringe order versus distance for various times is shown in Figure 32. Computed displacements are shown in Figure 33; strains in Figure 34; and stresses in Figure 35. The different scales for the radial and tangential strain and stress should be noted.

Two targets were next prepared having cores of aluminum cemented to the PSM-1 with Eastman 910 epoxy. Referring to Table II, which gives impedance mismatch values for various combinations of materials, it is seen that the impedance mismatch between PSM-1 and aluminum is about nine.

In the first target, the core thickness was only 1/8 inch. Figure 36 shows ten frames of this shot (No. 240). The second target had a core

thickness of 1.0 inch. Figure 37 shows photographs of this shot (No. 226). Plots of the fringe order at a time of 68 microseconds and the computed stresses are shown in Figure 38. Only fringes 0.5 and 1.5 were developed in the latter, and as fringe number 1.5 was barely distinguishable, it was the maximum point on this curve.

The time of 68 microseconds corresponded to Frame 14 of the homogeneous target. A comparison of the stress waves in the homogeneous target and the two sandwich plates is made in Figure 39. The distances traveled are, of course, not the same, as the wave velocity in the aluminum was about four times as great as in the plastic.

SECTION IV

A QUASI-THEORETICAL SOLUTION

It was shown in Section II of this report that forcing functions can be selected that will closely simulate explosive impulses or hypervelocity impact. Therefore, it was desired to formulate a function that would approximately duplicate the experimentally determined pressure waves. Without going into the details of the procedure, it was found that the function

$$p_0 = 9{,}161\, e^{-0.01\,t} - 52{,}194\, e^{-0.02\,t} + 116{,}950\, e^{-0.03\,t} - 129{,}079\, e^{-0.04\,t} + 70{,}283\, e^{-0.05\,t} - 15{,}121\, e^{-0.06\,t}$$

shown in Figure 40 will, when multiplied by the proper constant and applied to a 2-inch spherical cavity, create a wave at a time of 68 microseconds that approximates the experimental wave as shown in Figure 41. The time of the theoretical wave has been adjusted by 32.6 microseconds, the time required for the wave to travel two inches, the assumed cavity radius. By employing a greater number of terms in the equation representing the forcing function, the theoretical wave could have been made to coincide with the experimental wave as closely as desired. Values of radial and tangential stresses at other times were computed and are shown in Figure 42. By comparing Figures 35 and 42 it is seen that the waves have the same amplitudes at a time of 68 microseconds but that the stress amplitudes do not attenuate at the

same rate. This is to be expected. The theoretical solution is for spherical waves which decay at a rate proportional to r^{-1}, but the experimental ones would be expected to be cylindrical waves in a thin plate. Theoretically, cylindrical waves attenuate at a rate proportional to $r^{-0.5}$. The expected attenuation of both spherical and cylindrical waves are compared with the experimental results in Figure 43. This shows that in reality, the experimental results are in closer agreement with the spherical than with the cylindrical wave attenuation.

Distance-time plots of the waves in the targets having 1/8- and 1.0-inch aluminum cores are given in Figure 44. It is seen that because of the geometry of the targets, only the waves P_{A-0-0} contribute to the stress in the third layer at the time under consideration.

The same forcing function applied to the homogeneous target was also applied to the sandwich plates. The radial stress-distance relations at the time of 68 microseconds were computed. The results are shown in Figure 45. This figure also shows each of the transmitted components, P_{A-0-0}, as well as their resultants. A comparison of these theoretical stresses in homogeneous and laminated targets is given in Figure 46.

SECTION V

CONCLUSION

The experimental and theoretical results given in Figures 39 and 46 are shown in Figure 47 with values normalized for comparison of maximum stresses. These may be summarized as follows:

	Maximum Stress Compared With Homogeneous Target	
	1/8" Core	1.0" Core
Experimental	0.72	0.41
Theoretical	0.86	0.42

There is practically no difference between the experimental and theoretical results in the case of the target with the one-inch core. In fact, one would expect the experimental error to be greater than the small difference that can be detected.

In the case of the 1/8-inch core, however, the agreement between theory and experiment is not as good. The experimental study indicated that the amplitude of the stress wave after passing through the core would be 72 percent of its amplitude in a homogeneous material. The theoretical analysis gives an amplitude of 86 percent.

There are several possible explanations of discrepancies between theoretical and experimental values. Some of these will be discussed briefly

so that they may be taken into consideration in future studies and may lead to more accurate and dependable results.

1. The experimental waves were generated and analyzed in 0.25-inch sheets, but the theoretical results were computed for spherical waves in semi-infinite targets. Close agreement would not be expected. Three-dimensional experiments employing an imbedded polariscope are being planned.
2. Explosives that generated the stress waves probably varied somewhat from shot to shot. More consistent results were obtained when wires were exploded without the use of chemical explosives. A more powerful energy source is needed so that a wire alone can be used and a greater number of fringes will be generated. Reference to Figure 38 will show that more fringes are needed to accurately define the amplitude of the stress wave that had passed through the 1/8-inch core. Although only the 0.5 and 1.5 fringes were created in the target having the 1.0-inch core, the peak of the wave was more accurately determined because the 1.5 fringe was barely visible in that frame.
3. It has been assumed that the cemented joints have no effect upon the transmitted and reflected waves. Two sheets of PSM-1 were cemented together and a stress wave photographed as it passed through the joint. No attenuation of the wave could be detected. As long as the effect

of the joint is small it will not materially affect the results in the case of a relatively thick core. With a one-inch laminate only two transmitted waves contributed to the maximum stress (Figure 45). The situation is much different when the core is thin. In the instance of the 1/8-inch core the resultant stress was dependent upon at least nine transmitted components. In this case there were ten waves transmitted through and sixteen reflections from the cemented joints. It is apparent that although an attenuation of stress may not be detected at a single joint it can be quite significant when there is a large number of reflections and transmissions. As previously stated, Eastman 910 cement was used in the construction of the models used in this study. More attention should probably be given to selecting a cement having a characteristic impedance equal to that of the model material. Any voids in the cemented joint will, of course, have a large effect on the experimental results.

4. It has been assumed that the wave velocity remains constant in any given material. Only the first component ($P_{1\text{-}0\text{-}0}$) passes through undisturbed material. The reflected waves may traverse the core material many times. The material density and elastic constants will probably be changed slightly, perhaps due

to heating of the material. This will cause some change in the wave velocity and in the characteristic impedance (ρc) of the material. (It has been shown that the velocity of a reflected wave in Lucite is about 80 percent of that of the incident wave [Reference 2]).

5. Energy losses have been neglected. This is obviously not a valid assumption although these losses may be small.

As it is impossible to experimentally test even a small percentage of all possible material combinations of which sandwich plates may be constructed, a dependable theoretical method of analysis is needed. It is believed that the semi-empirical method developed in this study may be used to predict the effects of various material combinations and be of value in the design of sandwich plates that may be subjected to high velocity impact. It is shown that the multiple reflections within the structure must be taken into consideration.

REFERENCES

1. Kinslow, Ray, "Stress Waves in Composite Laminates," AEDC-TR-65-69, June, 1965.

2. Kinslow, Ray, "Observations of Hypervelocity Impact of Transparent Plastic Targets," AEDC-TDR-64-49 (AD438947), May, 1964.

3. Cosby, William A., and Lyle, Robert G., "The Meteoroid Environment and Its Effects on Materials and Equipment," NASA SP-78, 1965.

4. Kinslow, Ray, "Properties of Reflected Stress Waves," AEDC-TR-67-112 (AD818630), August, 1967.

5. Kinslow, Ray, "Properties of Spherical Stress Waves Produced by Hypervelocity Impact," AEDC-TDR-63-197 (AD421578), October, 1963.

6. Durelli, A. J., and Riley, W. F., Introduction to Photomechanics, Prentice-Hall, Inc., Englewood Cliffs, N. J., 1965.

7. Dally, J. W., and Riley, W. F., "Stress Wave Propagation in a Half-Plane Due to Transient Point Load," Developments in Theoretical and Applied Mechanics, ed. by W. A. Shaw, Vol. 3, Pergamon Press, London, 1967, pp. 357-377.

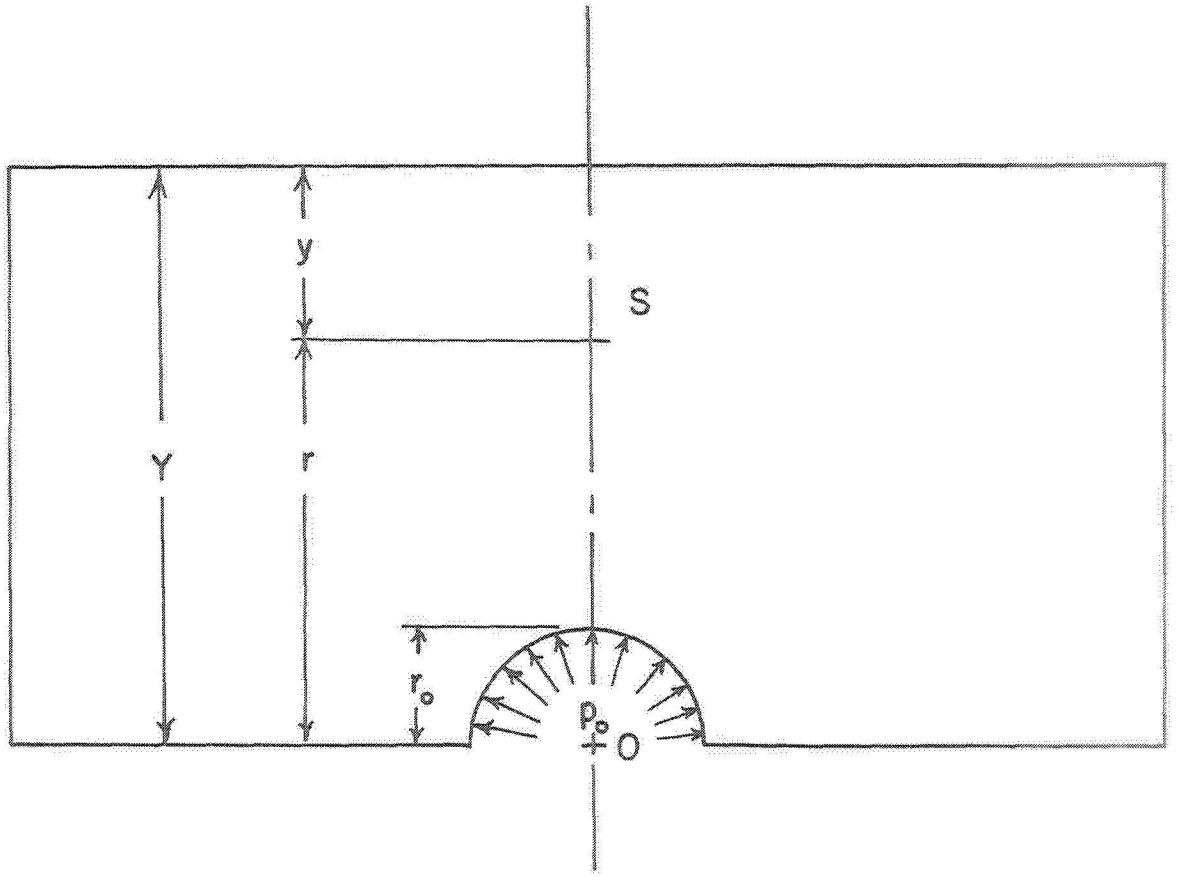

FIGURE 1

TARGET DIMENSIONS AND COORDINATES

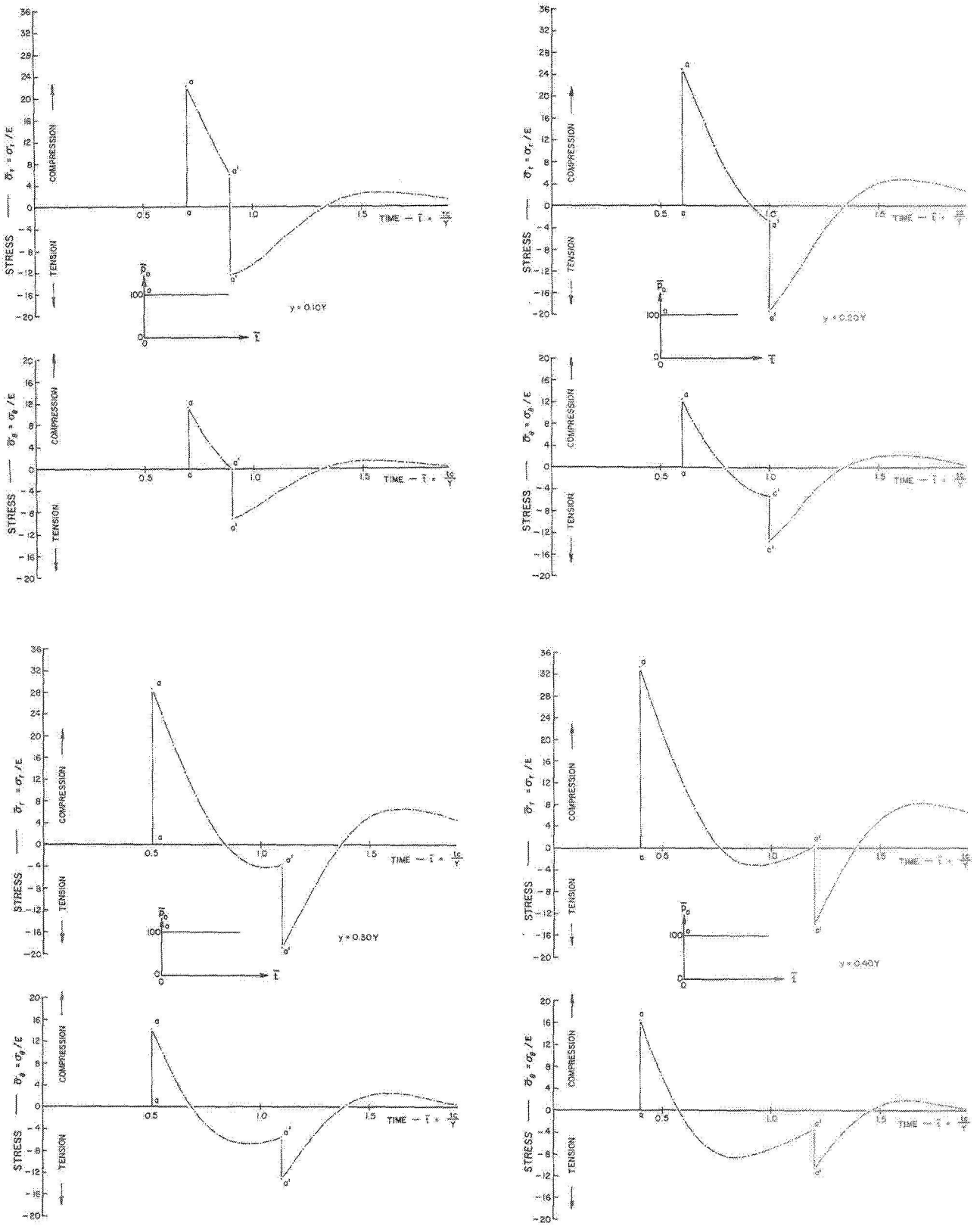

FIGURE 2

STRESS-TIME RELATIONS

($\bar{p}_o$ = CONSTANT)

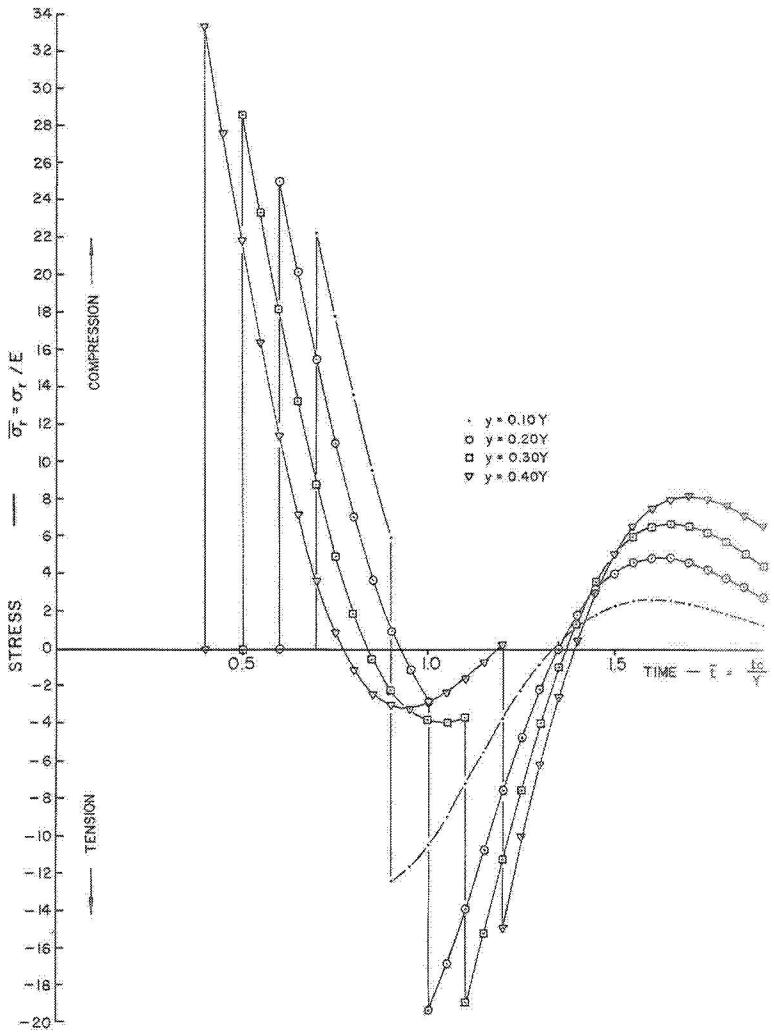

FIGURE 3

COMPARISON OF RADIAL STRESSES

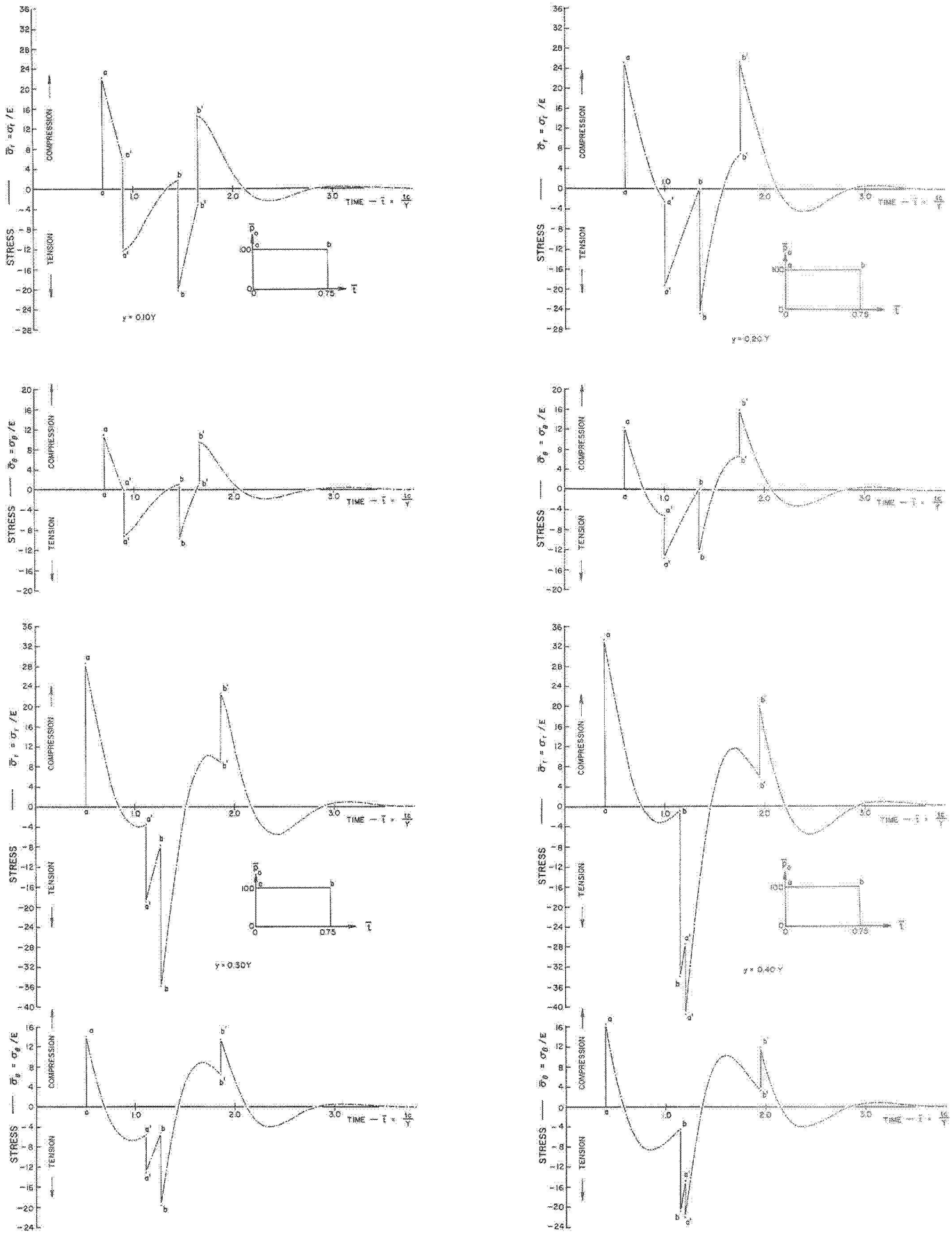

FIGURE 4

STRESS-TIME RELATIONS

($\bar{p}_o$ = IMPULSE, L = 0.75)

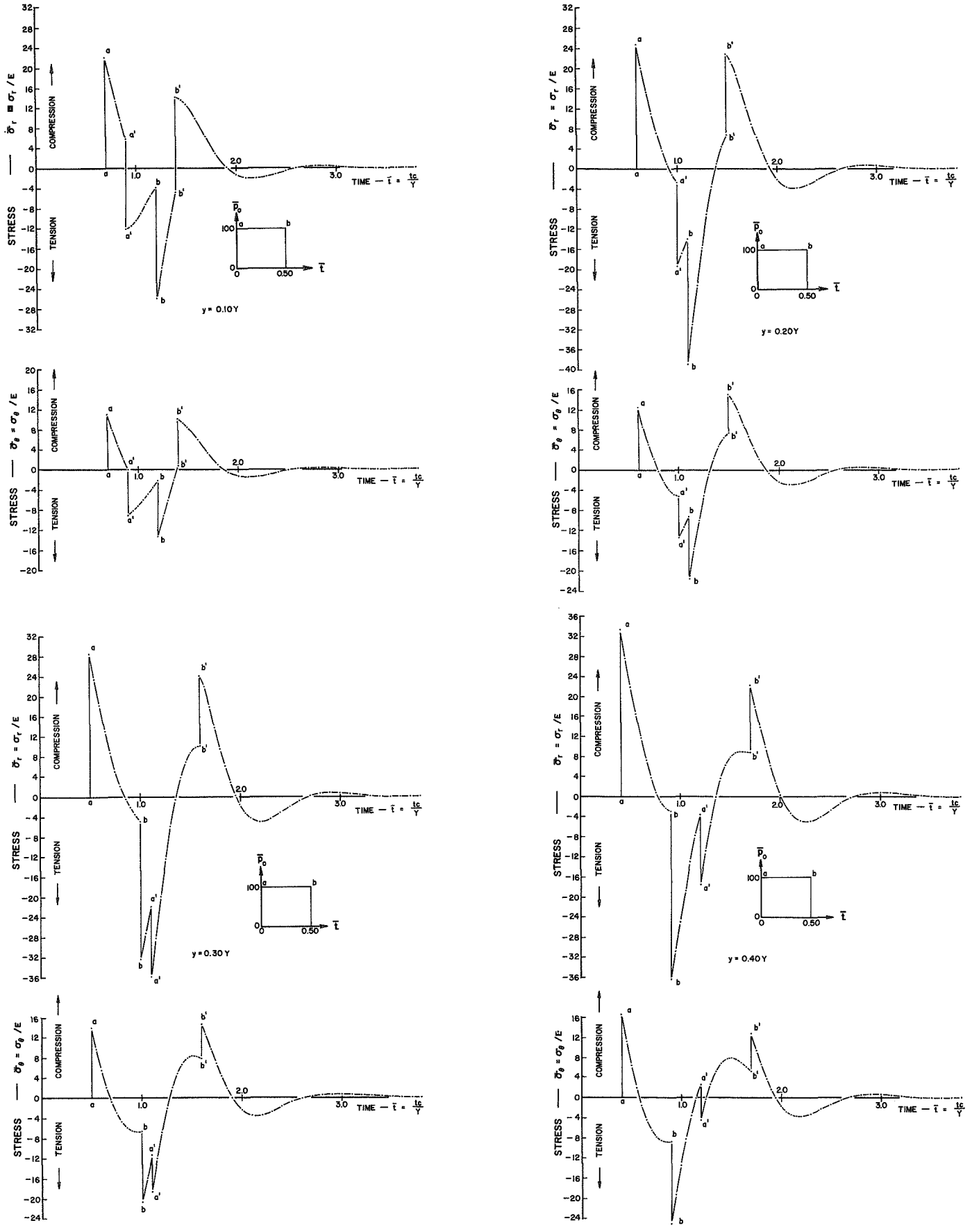

FIGURE 5

STRESS-TIME RELATIONS

($\bar{p}_o$ = IMPULSE, L = 0.50)

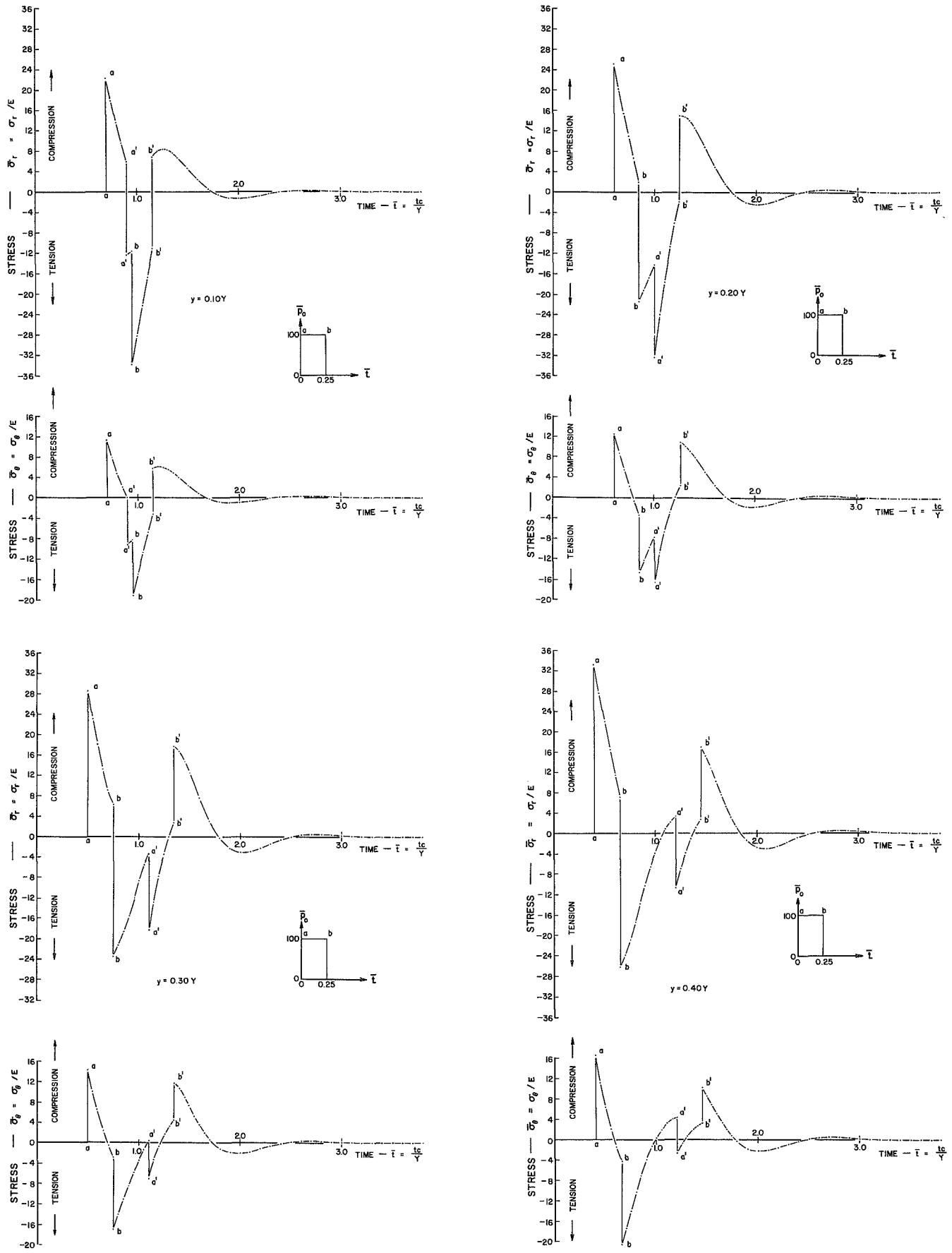

FIGURE 6

STRESS-TIME RELATIONS

($\bar{p}_o$ = IMPULSE, L = 0.25)

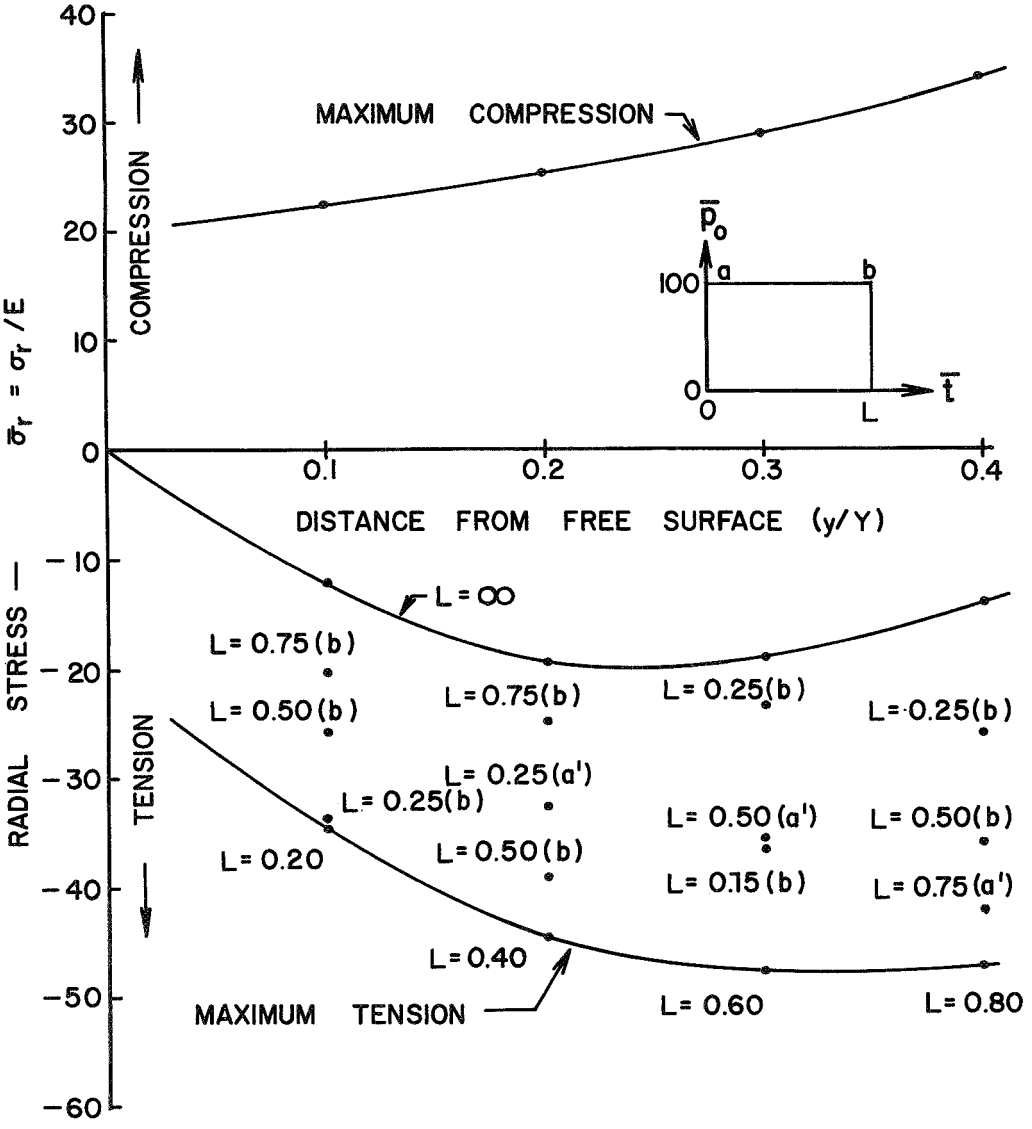

FIGURE 7

MAXIMUM STRESS NEAR FREE SURFACE

(STEP INPUTS)

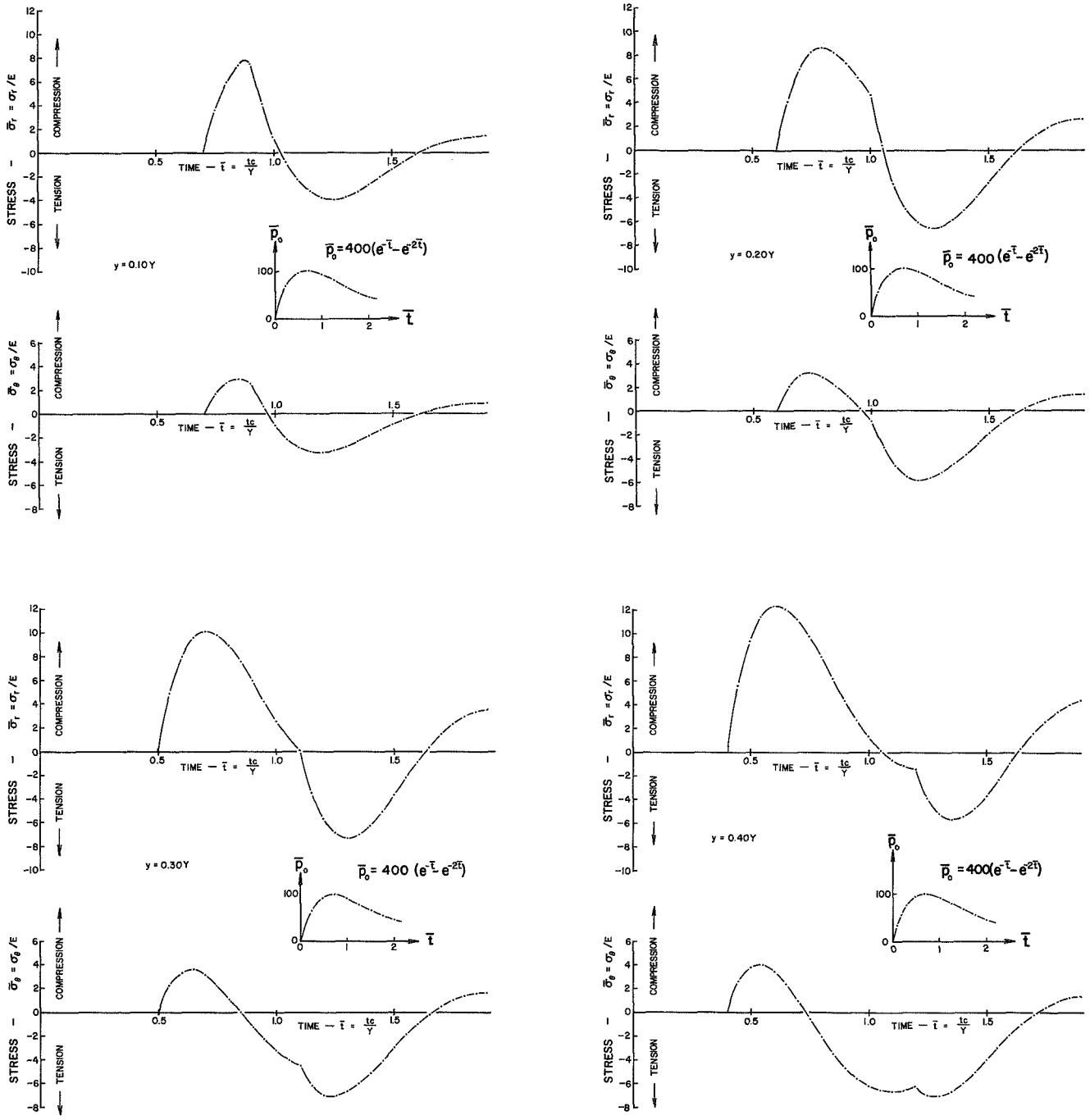

FIGURE 8

STRESS-TIME RELATIONS

$[\bar{p}_o = 400(e^{-\bar{t}} - e^{-2\bar{t}})]$

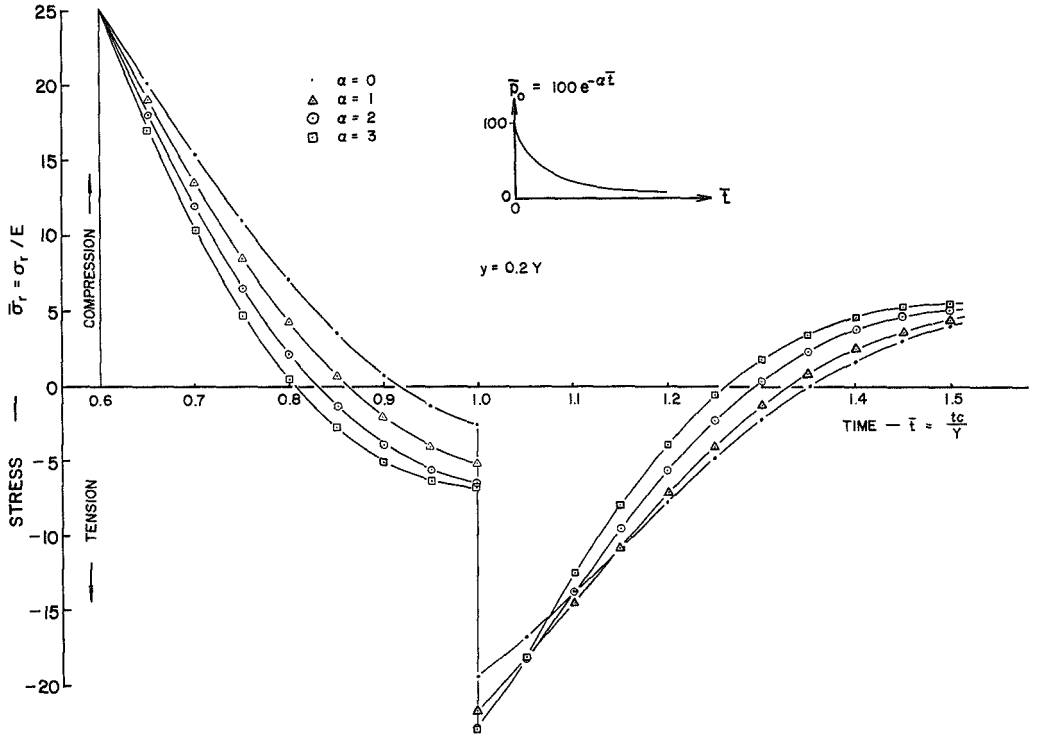

FIGURE 9

STRESS-TIME RELATIONS

(DECAYING INPUT)

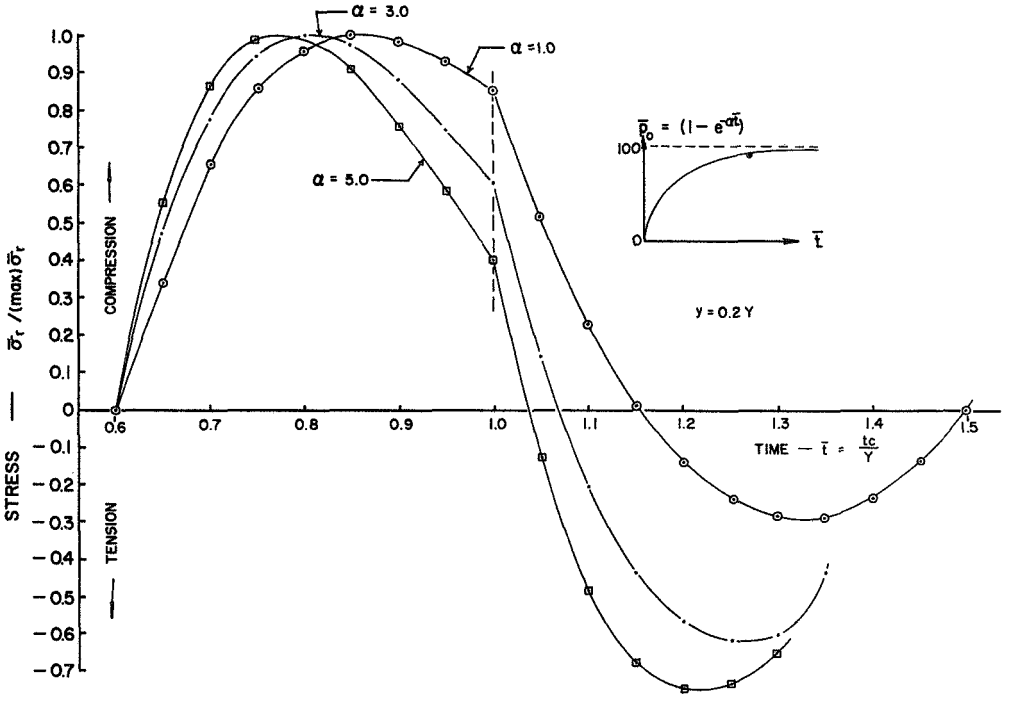

FIGURE 10

STRESS-TIME RELATIONS

$\bar{p}_o = (1 - e^{-\alpha \bar{t}})$

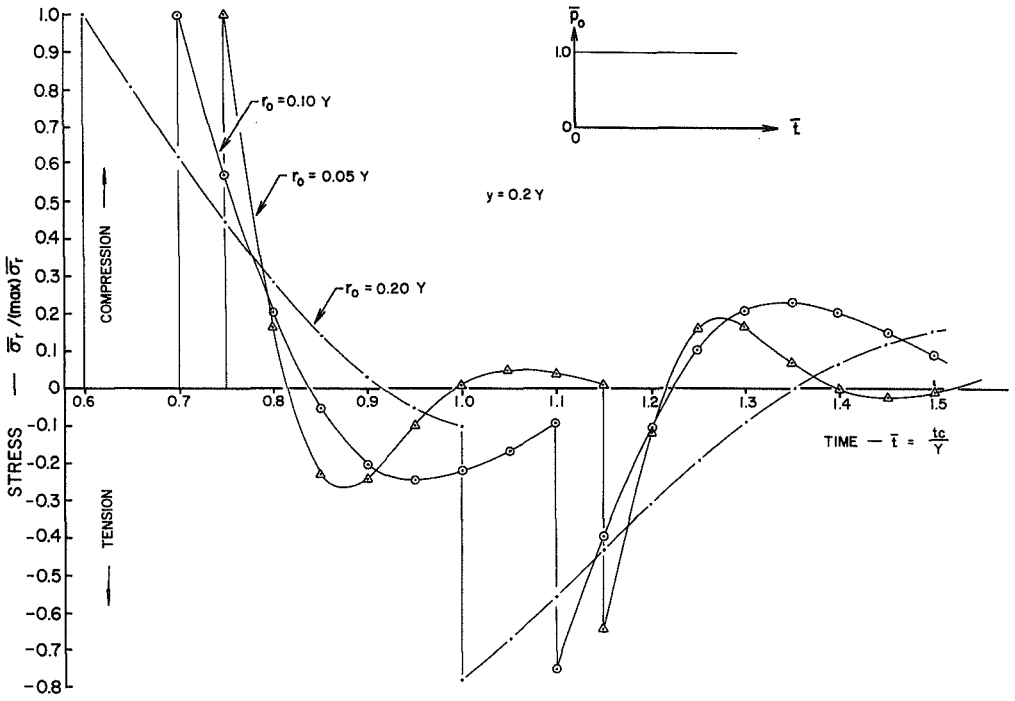

FIGURE II

EFFECT OF CAVITY RADIUS

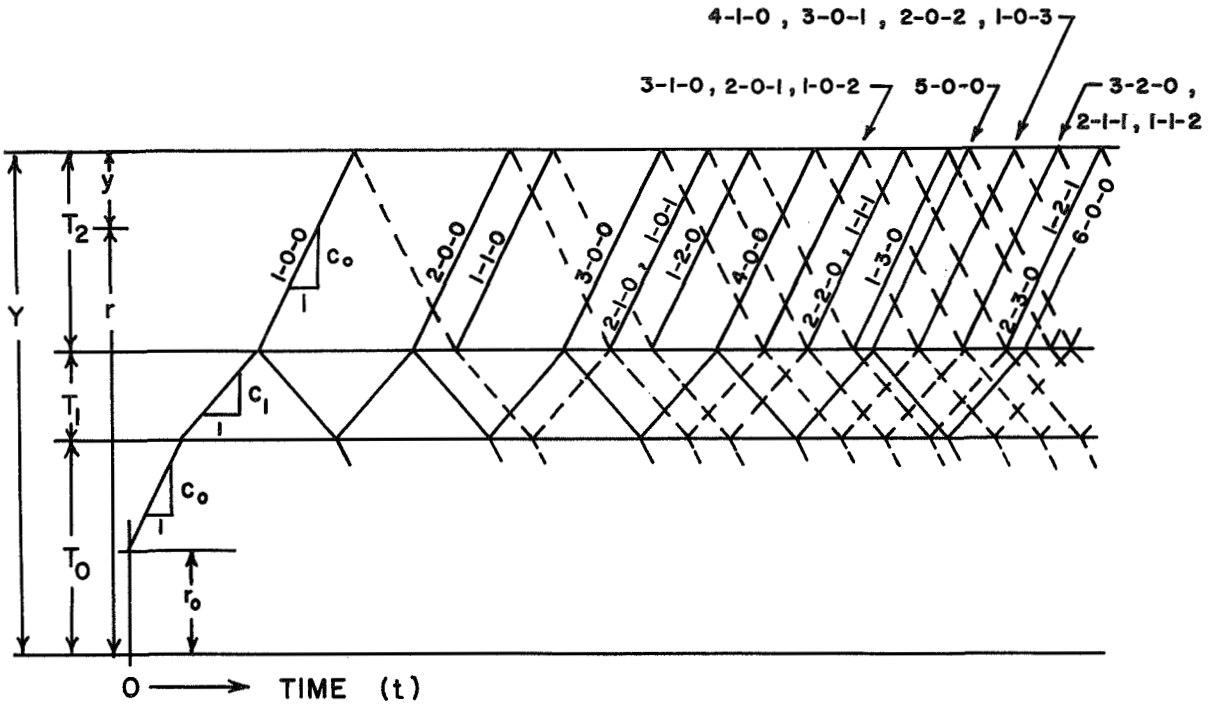

$$t_{A-0-0} = \left[\frac{(2A-1)C_0 - (C_1)}{C_0 C_1}\right] T_1$$

$$t_{A-B-0} = t_{A-0-0} + \frac{2BT_2}{C_0}$$

$$t_{A-B-C} = t_{A-B-0} + \frac{2T_2}{C_0} + \frac{2CT_1}{C_1}$$

FIGURE 12

REFLECTED AND TRANSMITTED STRESS WAVES IN LAMINATED TARGETS

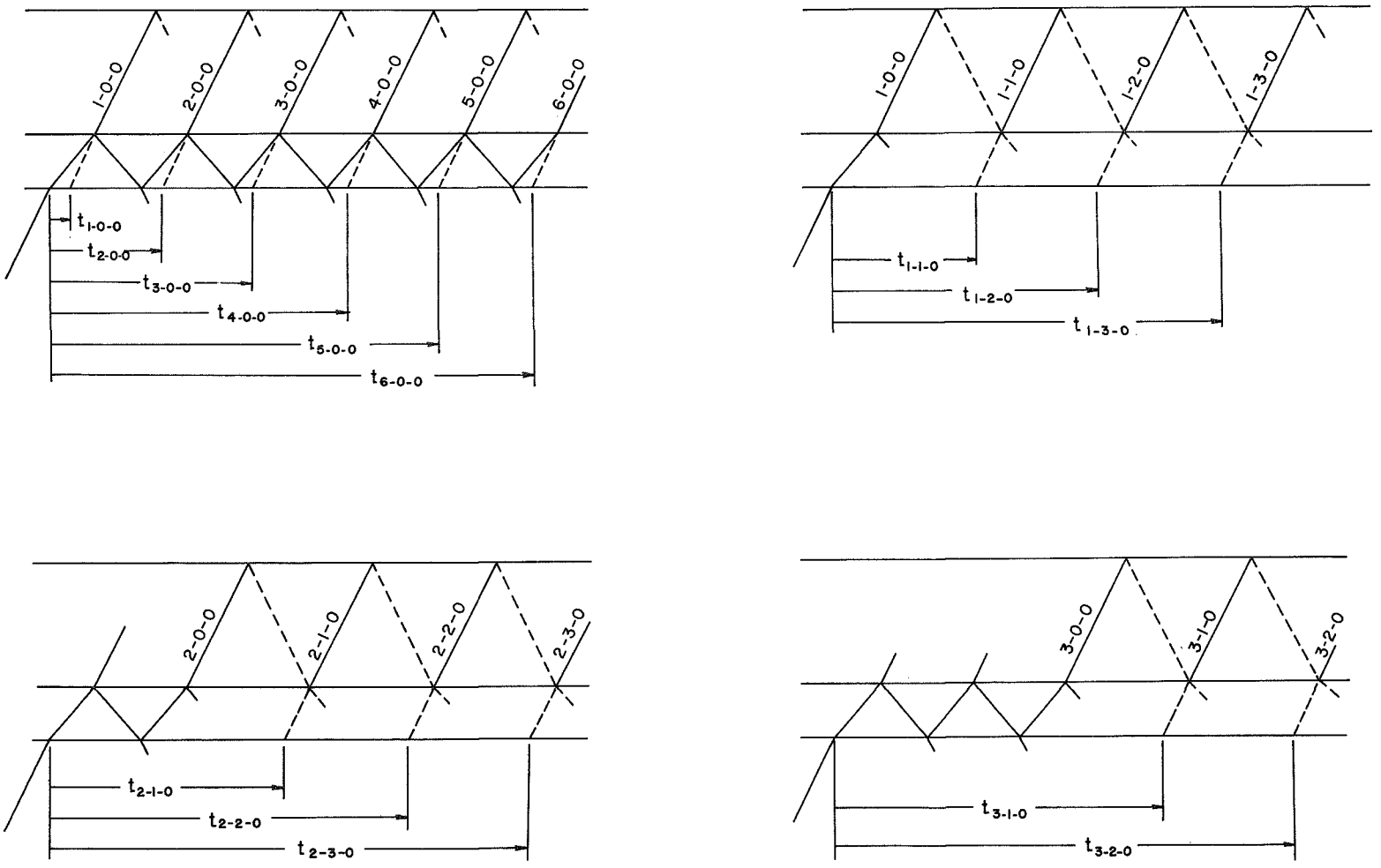

FIGURE 12 CONTINUED

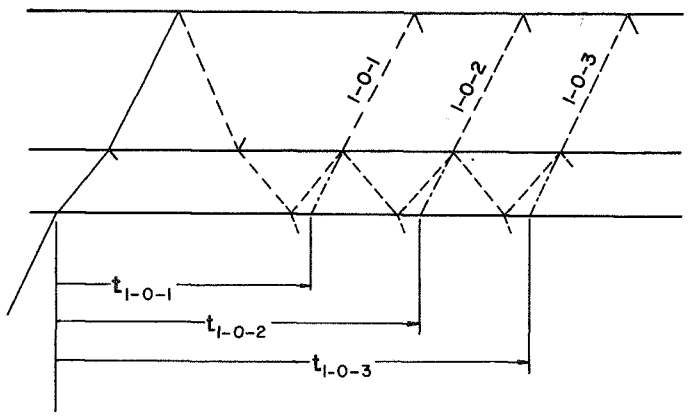

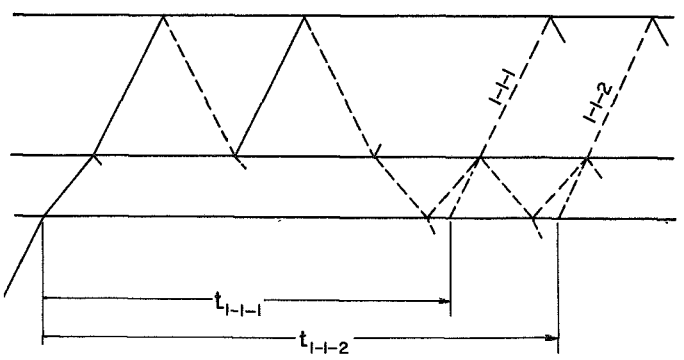

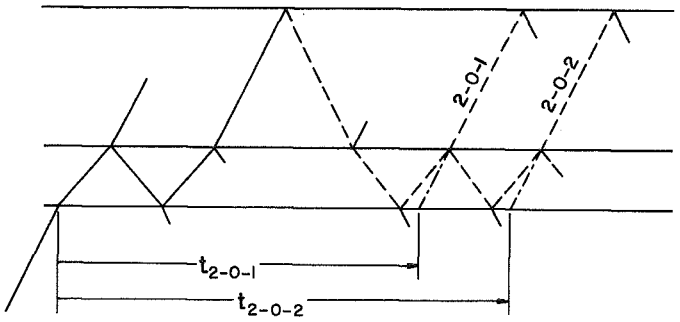

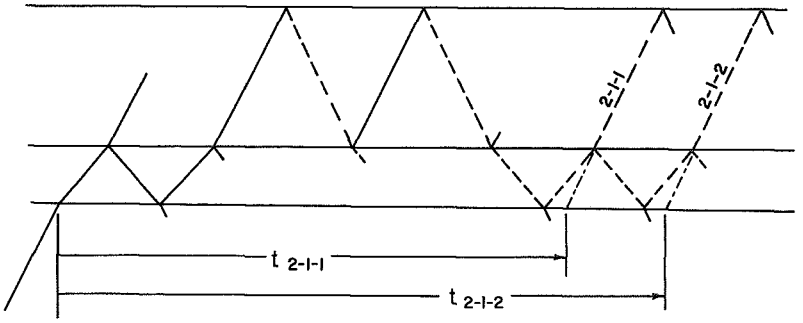

FIGURE 12 CONCLUDED

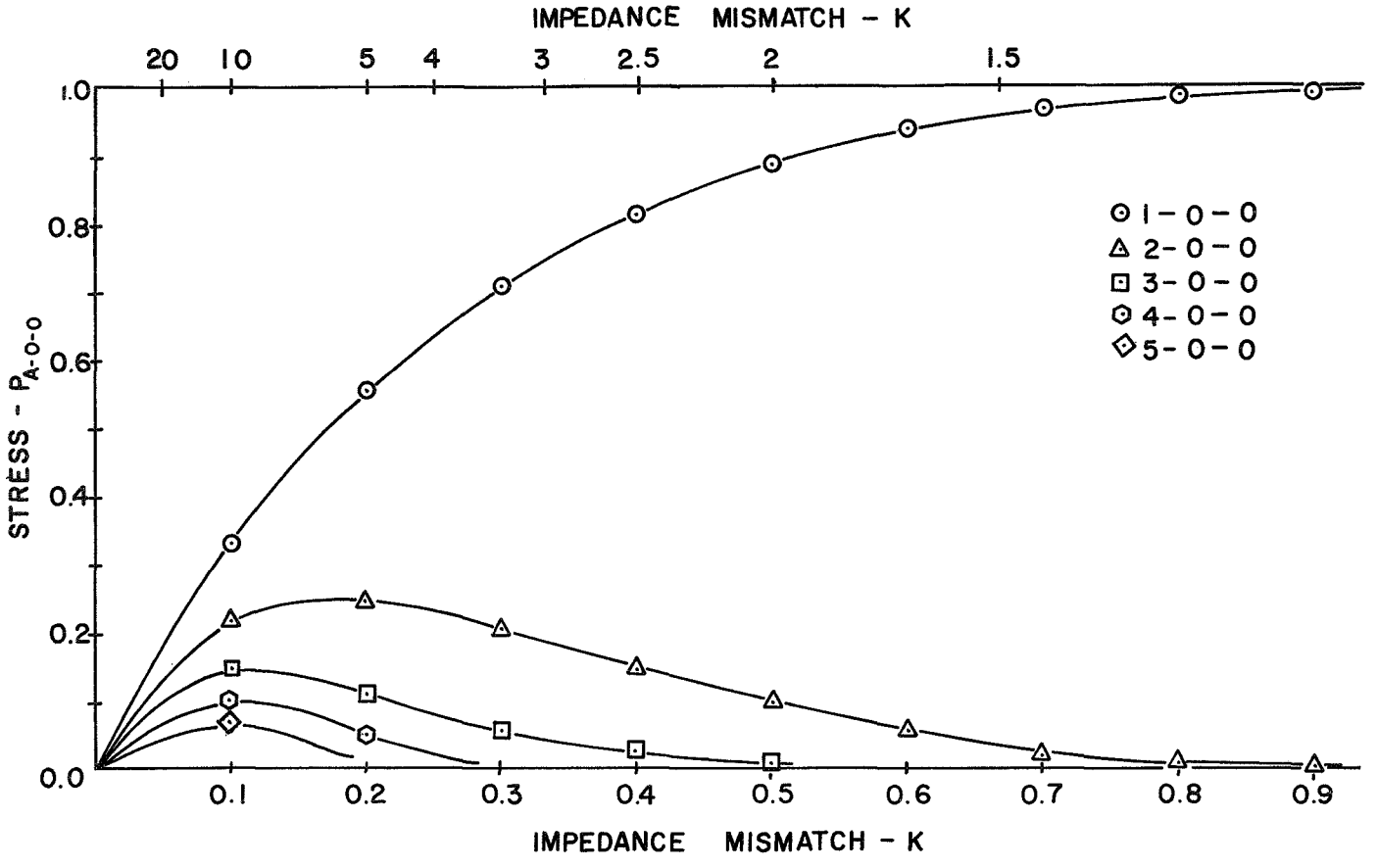

FIGURE 13

STRESS AMPLITUDE - IMPEDANCE MISMATCH RELATIONS

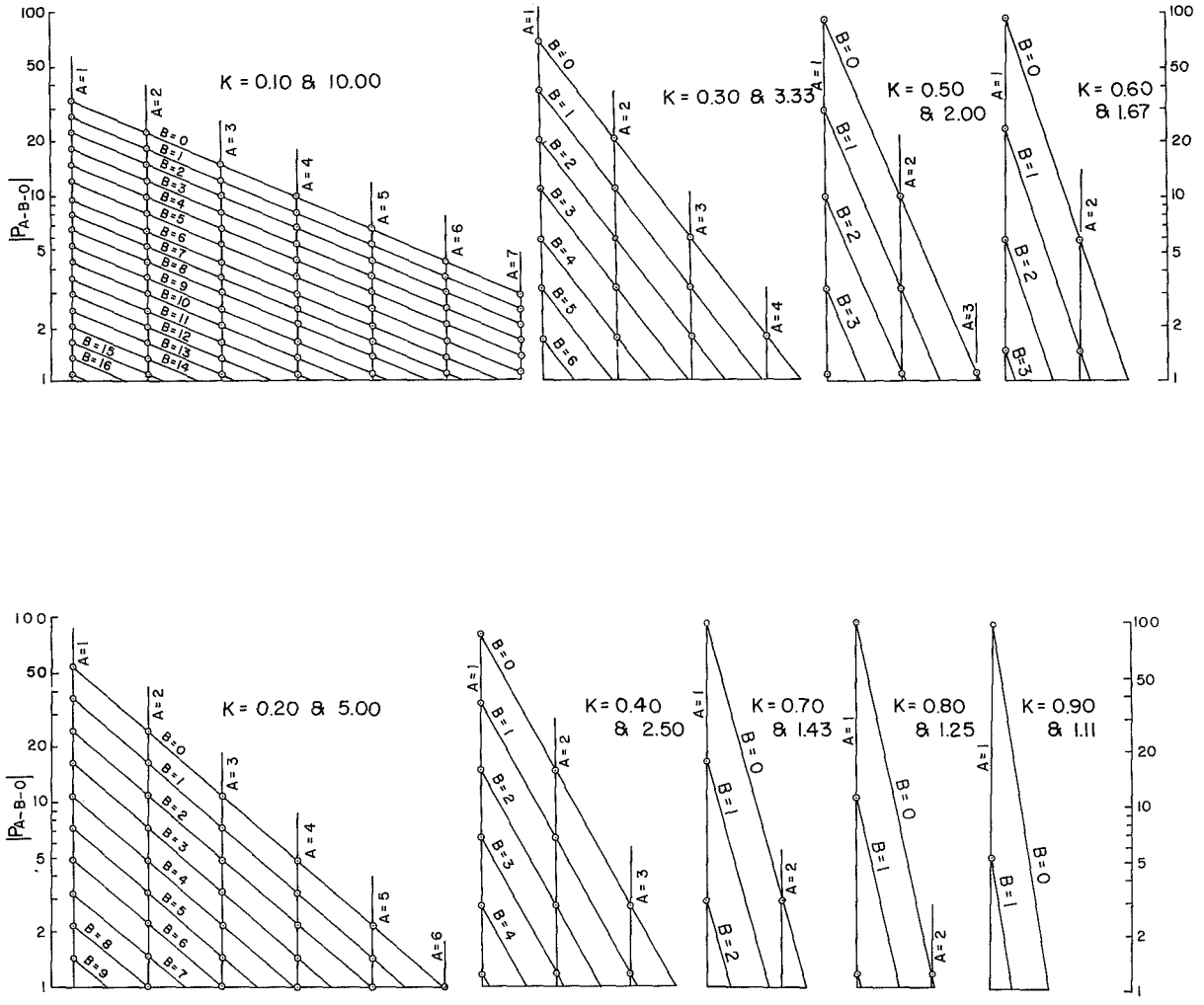

IF $K<1$, $P_{A-B-0} = +|P_{A-B-0}|$

IF $K>1$, { IF B IS EVEN, $P_{A-B-0} = +|P_{A-B-0}|$; IF B IS ODD, $P_{A-B-0} = -|P_{A-B-0}|$

FIGURE 14

AMPLITUDES OF VARIOUS TRANSMITTED WAVES

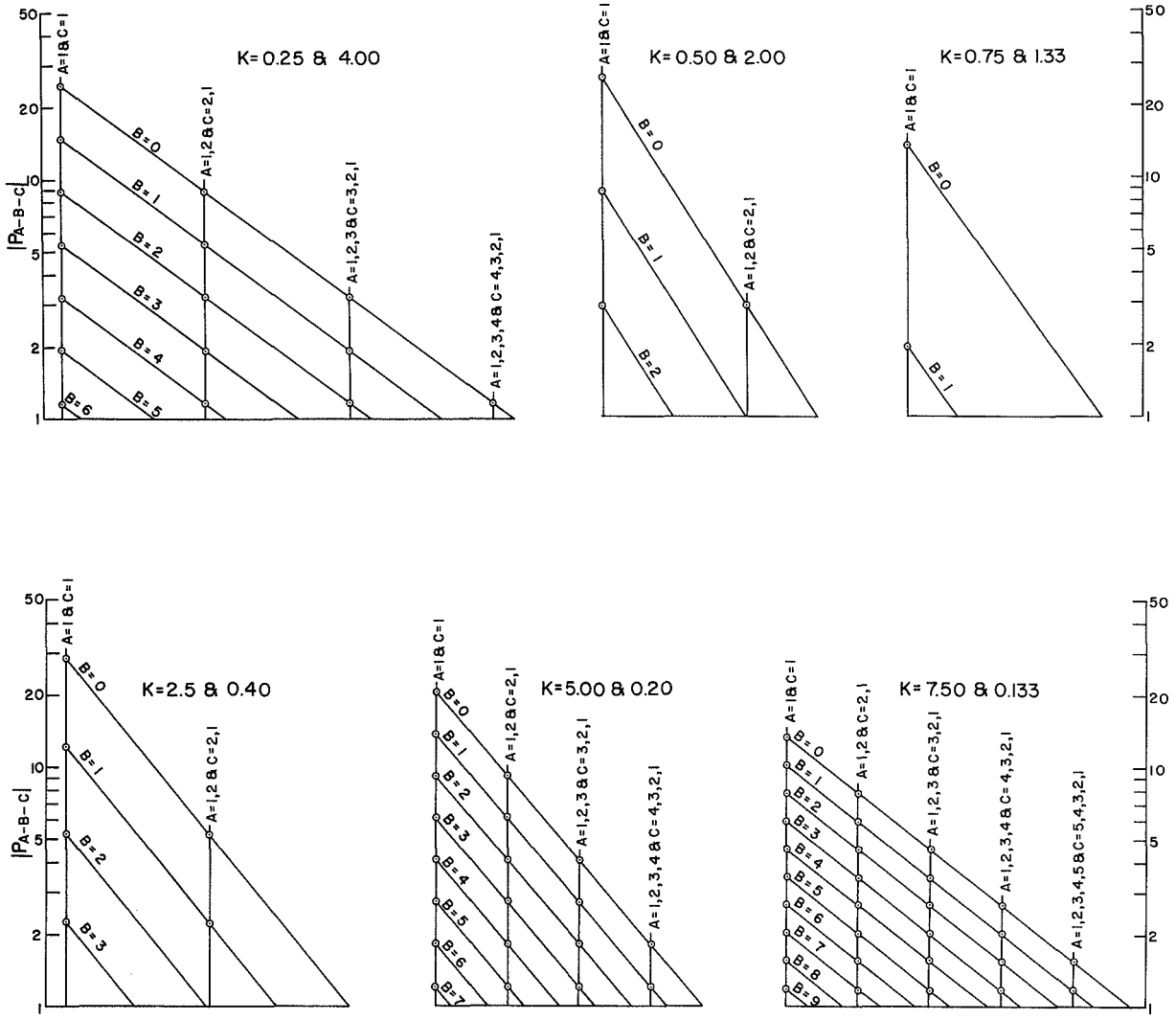

IF $K<1$, $P_{A-B-C} = -|P_{A-B-C}|$

IF $K>1$, { IF B IS EVEN, $P_{A-B-C} = +|P_{A-B-C}|$
IF B IS ODD, $P_{A-B-C} = -|P_{A-B-C}|$

FIGURE 14 CONCLUDED

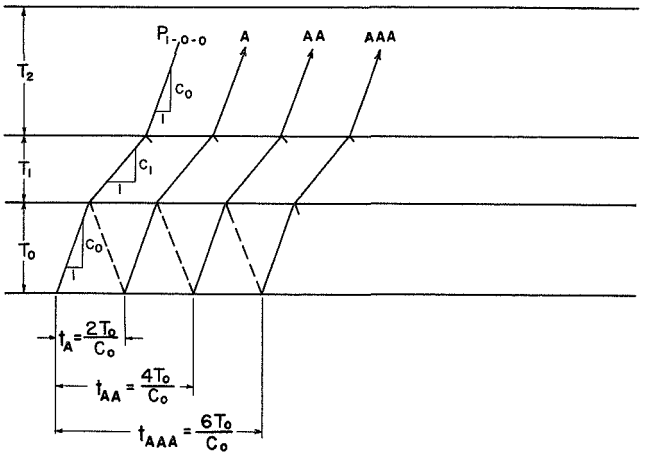

	AMPLITUDE AS FRACTION OF P_{1-0-0}				
		K=0.25	K=0.75	K=2.50	K=7.50
A	$\frac{1-K}{1+K}$	0.600	0.143	-0.429	-0.765
AA	$\left(\frac{1-K}{1+K}\right)^2$	0.360	0.020	0.184	0.585
AAA	$\left(\frac{1-K}{1+K}\right)^3$	0.216	0.003	-0.079	-0.448

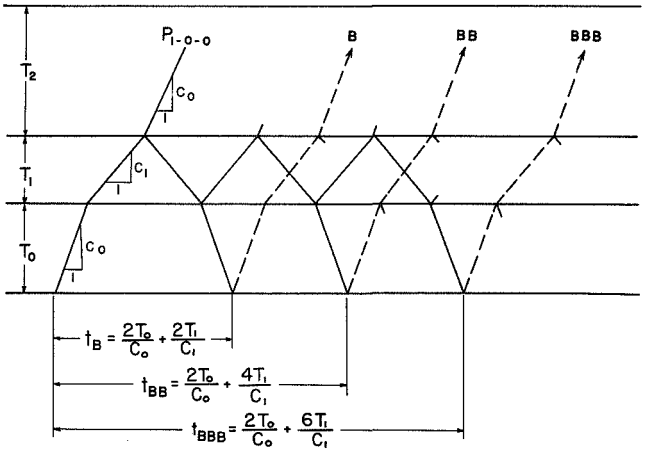

	AMPLITUDE AS FRACTION OF P_{1-0-0}				
		K=0.25	K=0.75	K=2.50	K=7.50
B	$\frac{-4K(1-K)}{(1+K)^3}$	-0.384	-0.140	0.350	0.318
BB	$\frac{-4K(1-K)^3}{(1+K)^5}$	-0.138	-0.003	0.064	0.186
BBB	$\frac{-4K(1-K)^5}{(1+K)^7}$	-0.050	-0.000	0.012	0.109

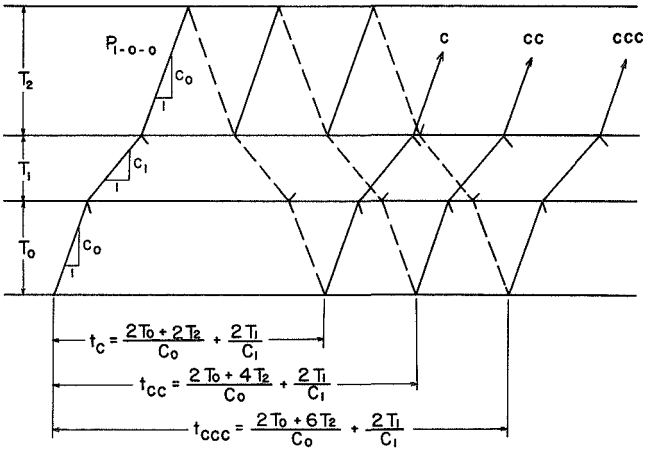

	AMPLITUDE AS FRACTION OF P_{1-0-0}				
		K=0.25	K=0.75	K=2.50	K=7.50
C	$\frac{16K^2}{(1+K)^4}$	0.410	0.960	0.666	0.172
CC	$\frac{16K^2(1-K)}{(1+K)^5}$	0.246	0.137	-0.286	-0.132
CCC	$\frac{16K^2(1-K)^2}{(1+K)^6}$	0.148	0.020	0.123	0.101

FIGURE 15

EFFECT OF REFLECTIONS FROM FRONT SURFACE

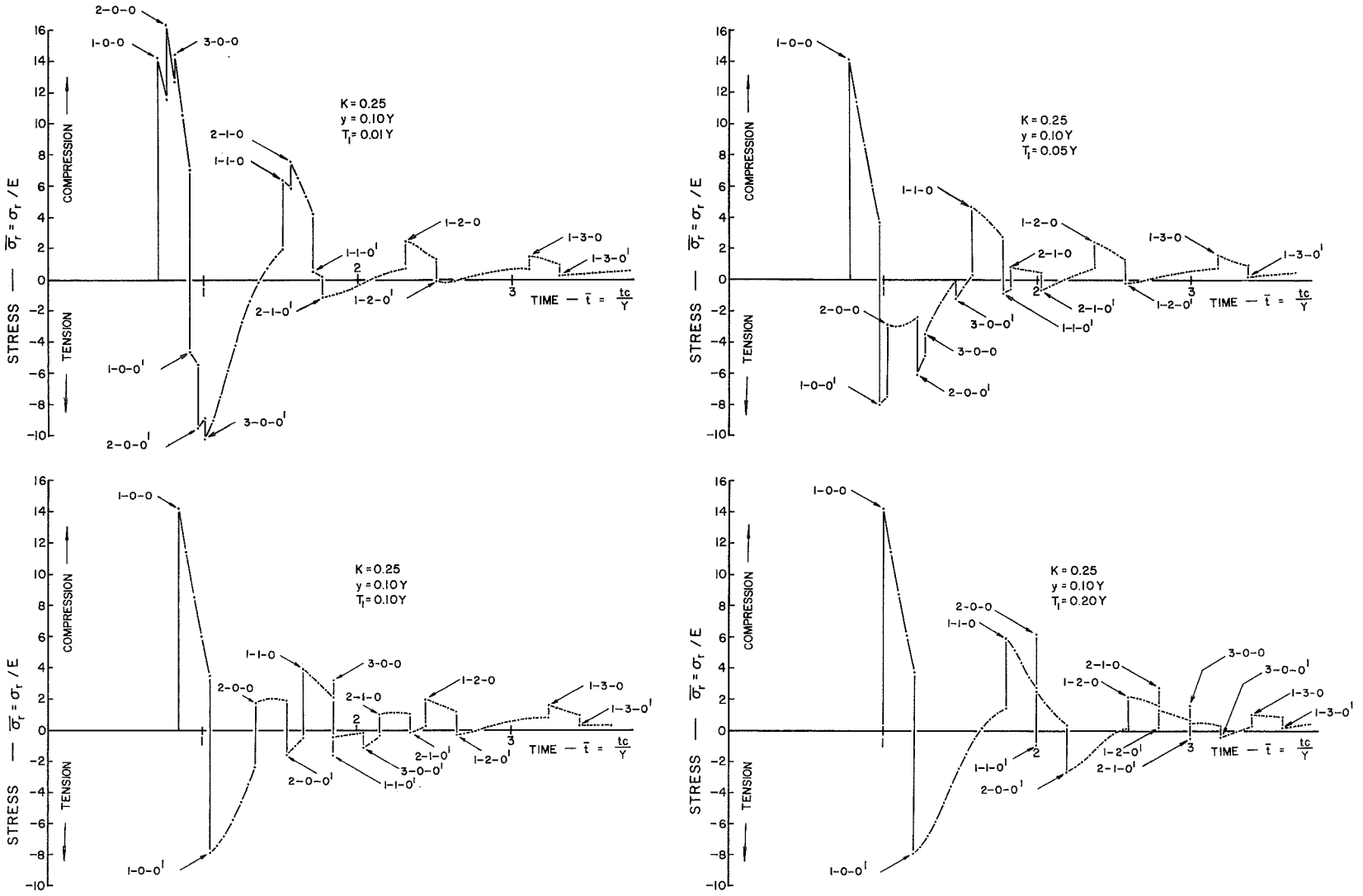

FIGURE 16

STRESS-TIME-LAMINATION THICKNESS RELATIONS ($\bar{p}_o$ = CONSTANT, K=0.25, y=0.10Y)

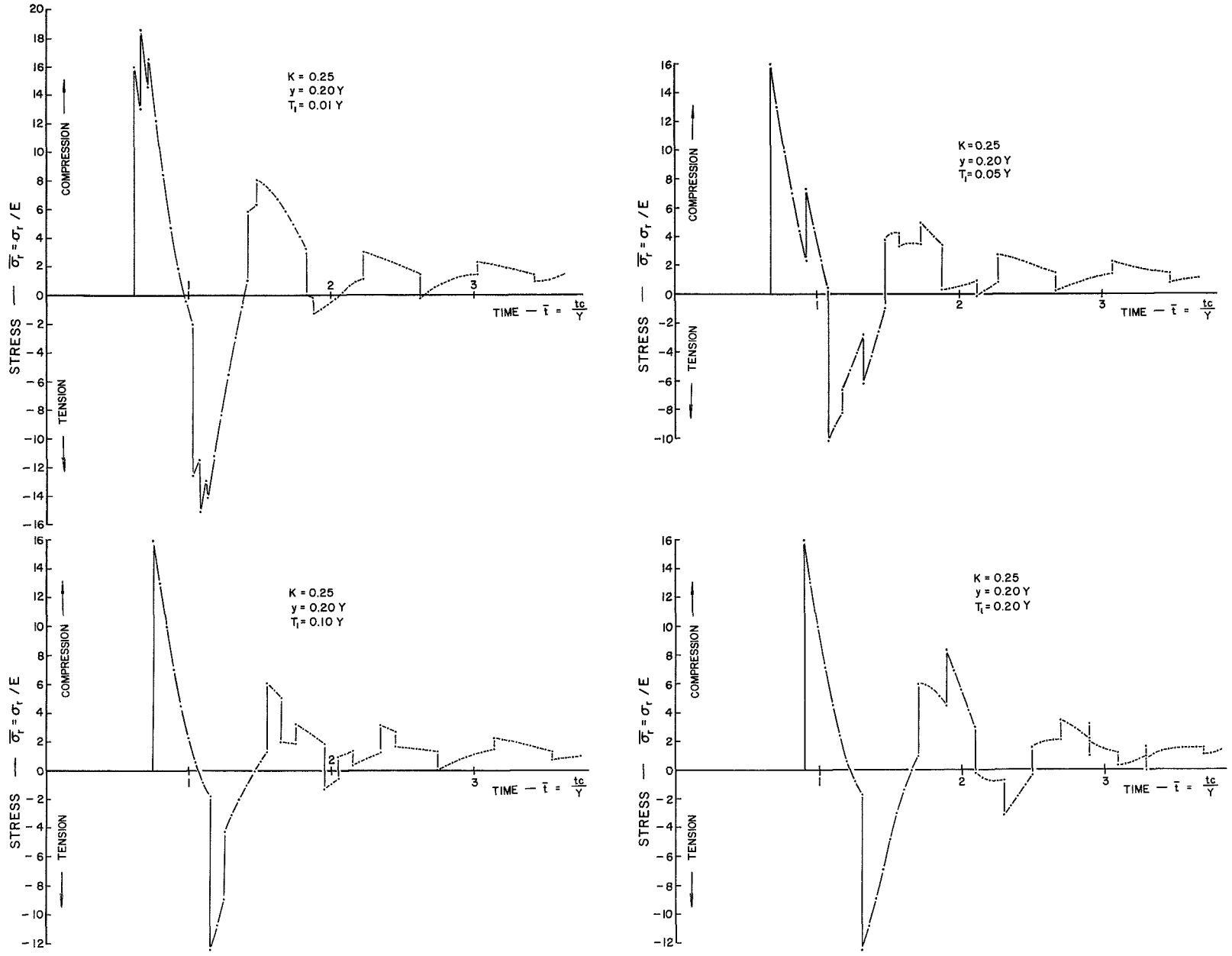

FIGURE 17

STRESS-TIME-LAMINATION THICKNESS RELATIONS ($\bar{p}_o$ = CONSTANT, K = 0.25, y = 0.20Y)

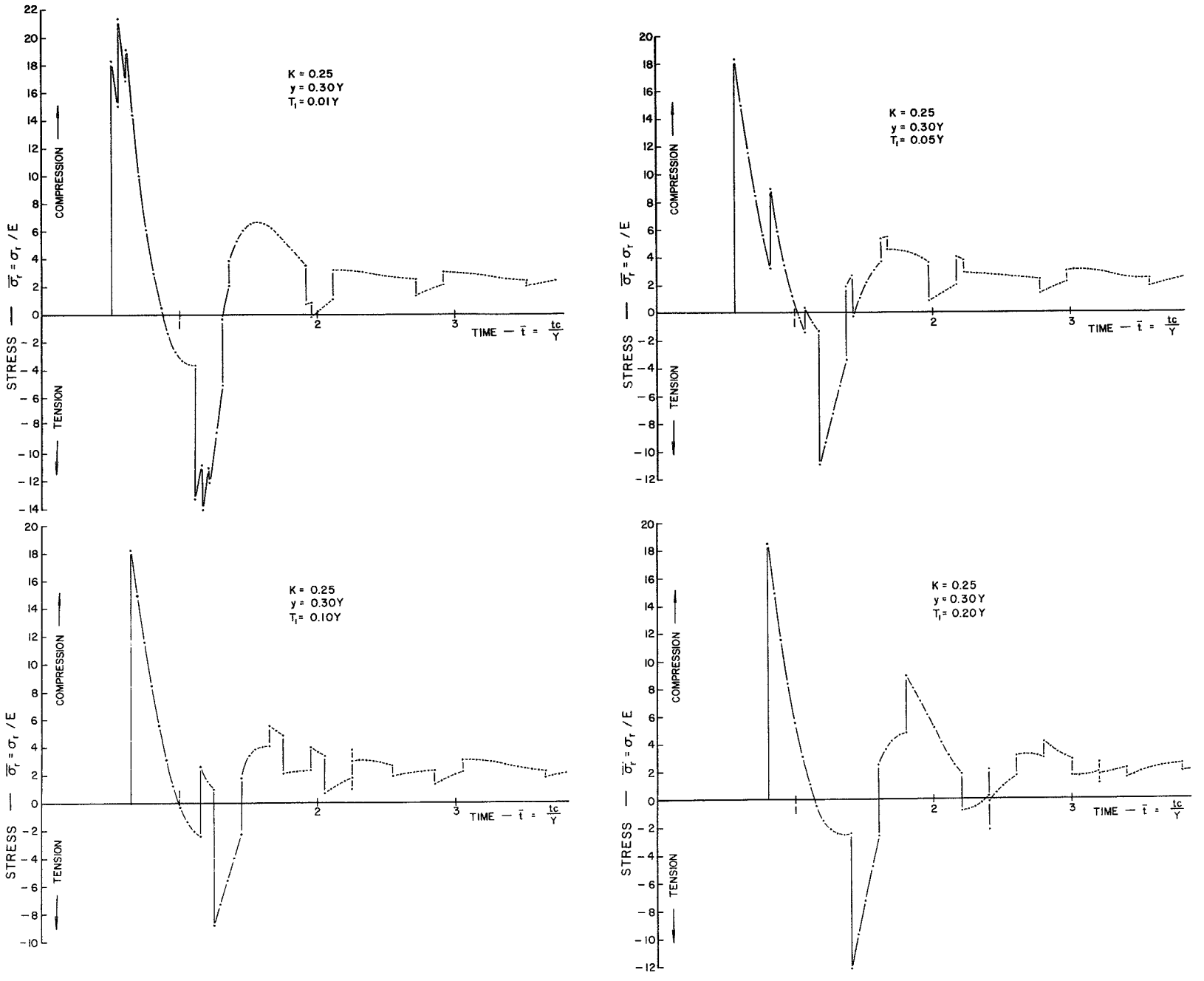

FIGURE 18

STRESS-TIME-LAMINATION THICKNESS RELATIONS ($\bar{p}_o$ = CONSTANT, K = 0.25, y = 0.30Y)

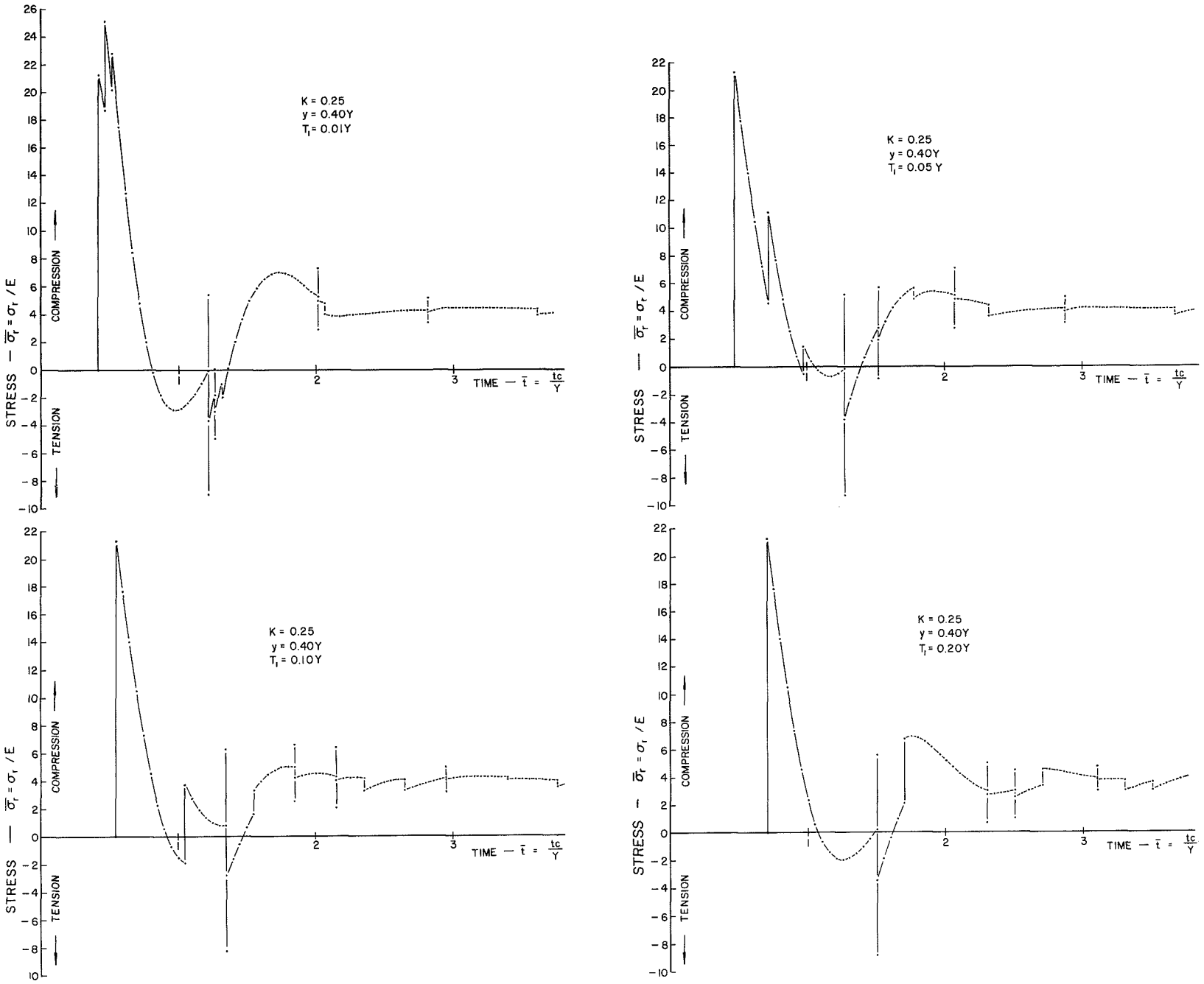

FIGURE 19

STRESS-TIME-LAMINATION THICKNESS RELATIONS ($\bar{p}_o$ = CONSTANT , K =0.25 , y =0.40Y)

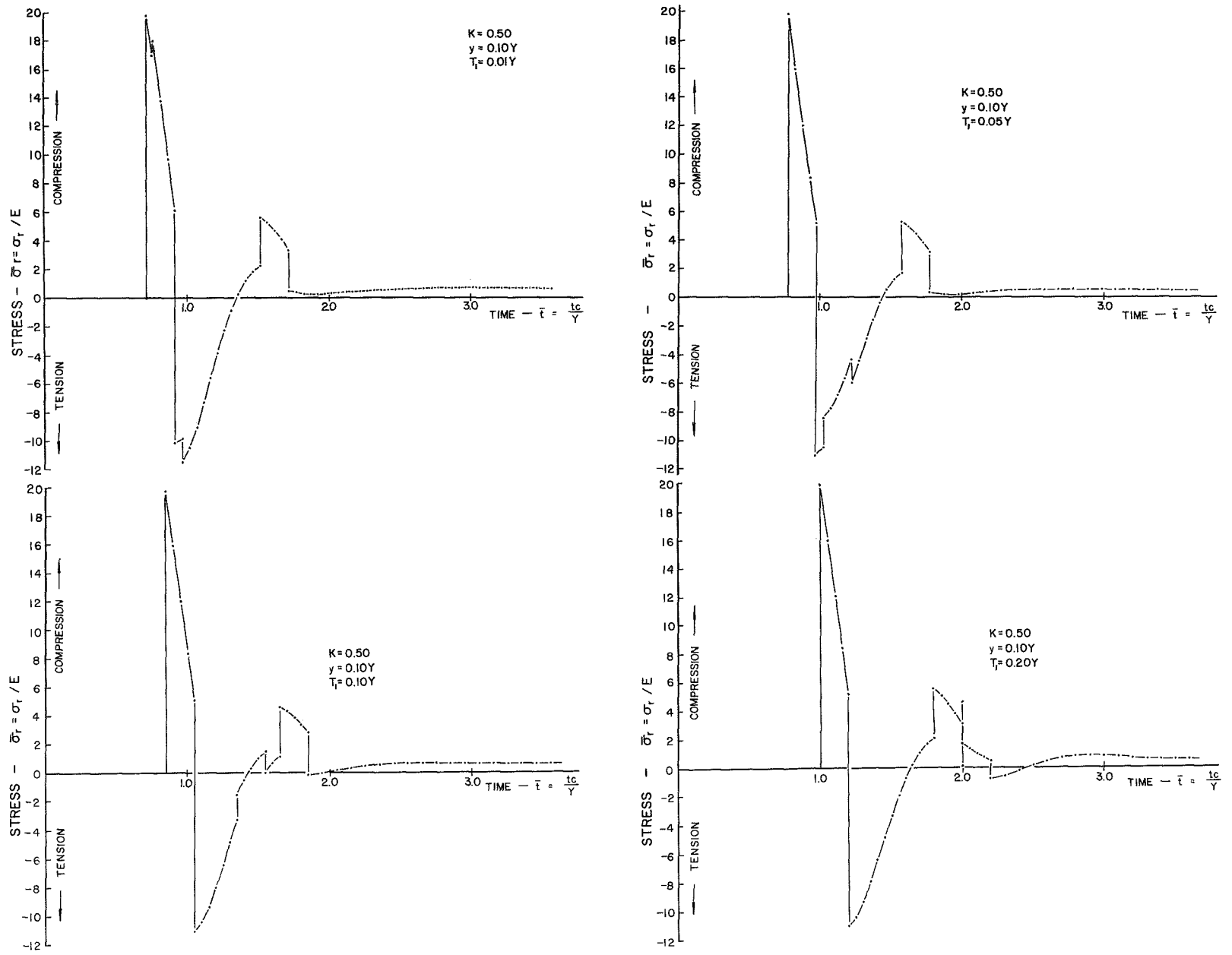

FIGURE 20

STRESS-TIME-LAMINATION THICKNESS RELATIONS ($\bar{p}_o$ = CONSTANT , K =0.50 , y =0.10Y)

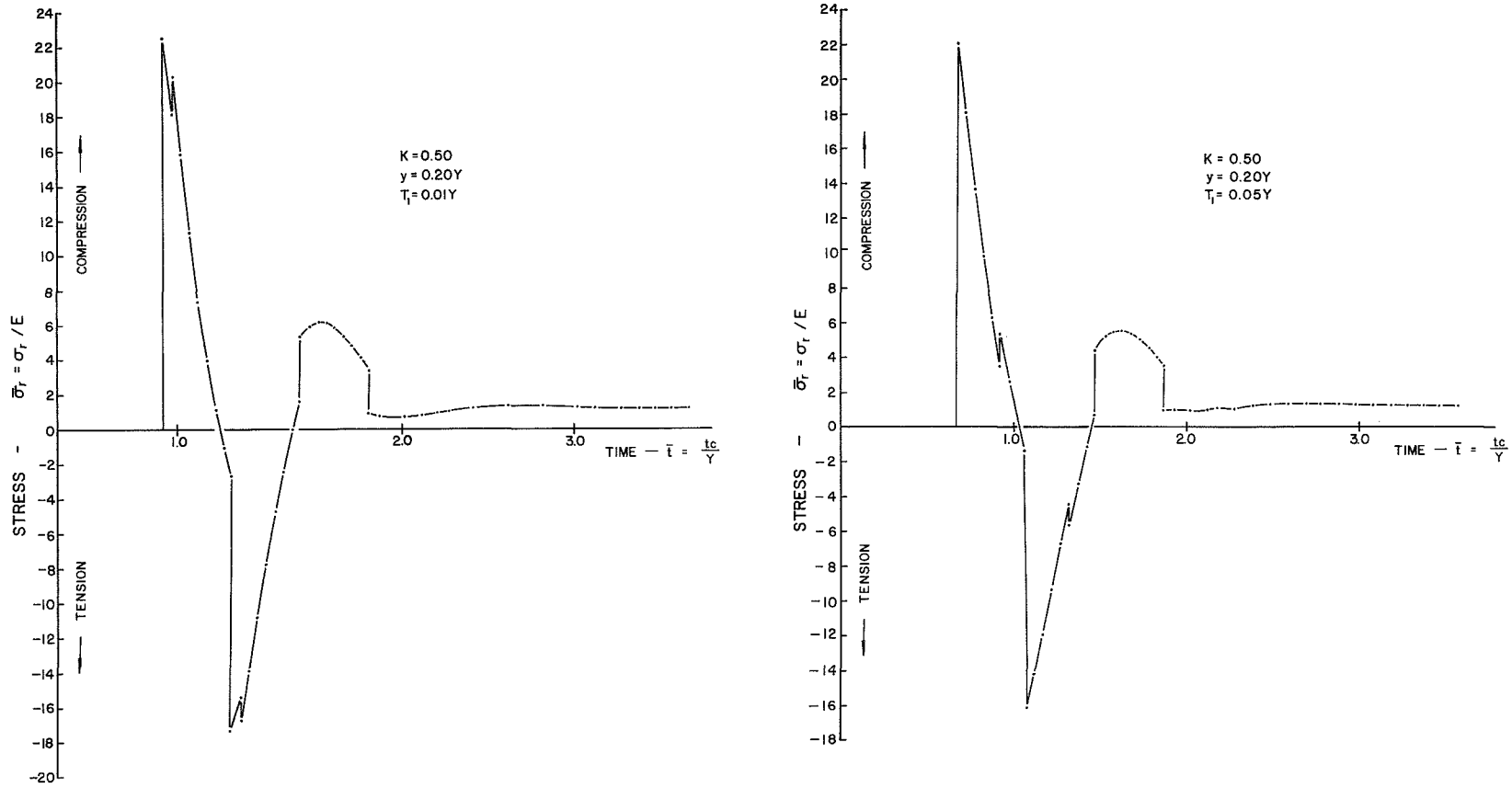

FIGURE 21

STRESS-TIME-LAMINATION THICKNESS RELATIONS

($\bar{p}_o$ = CONSTANT , K =0.50 , y =0.20Y)

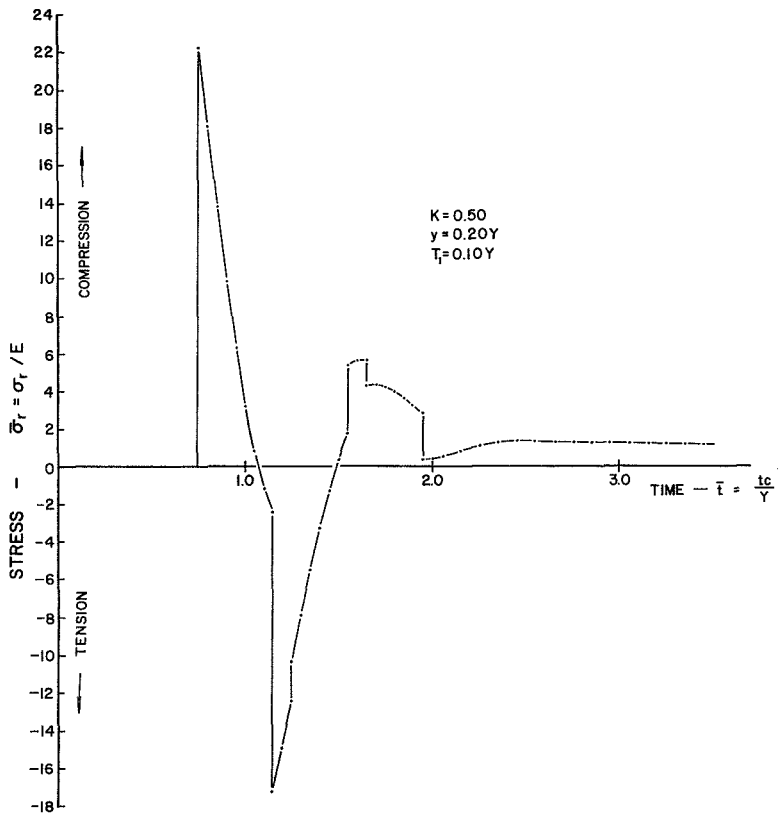

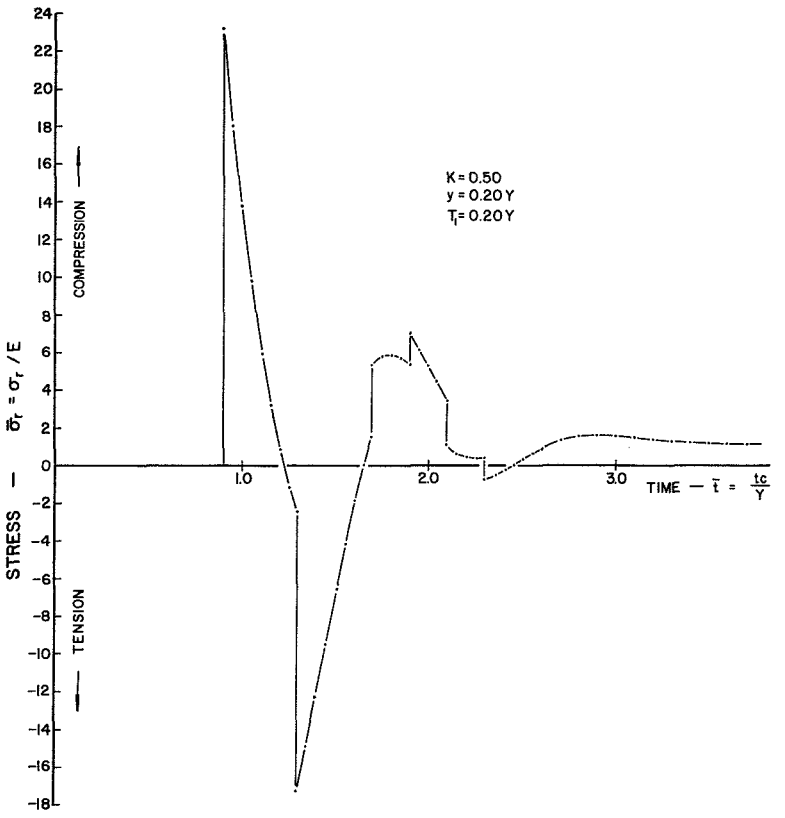

FIGURE 21 CONCLUDED

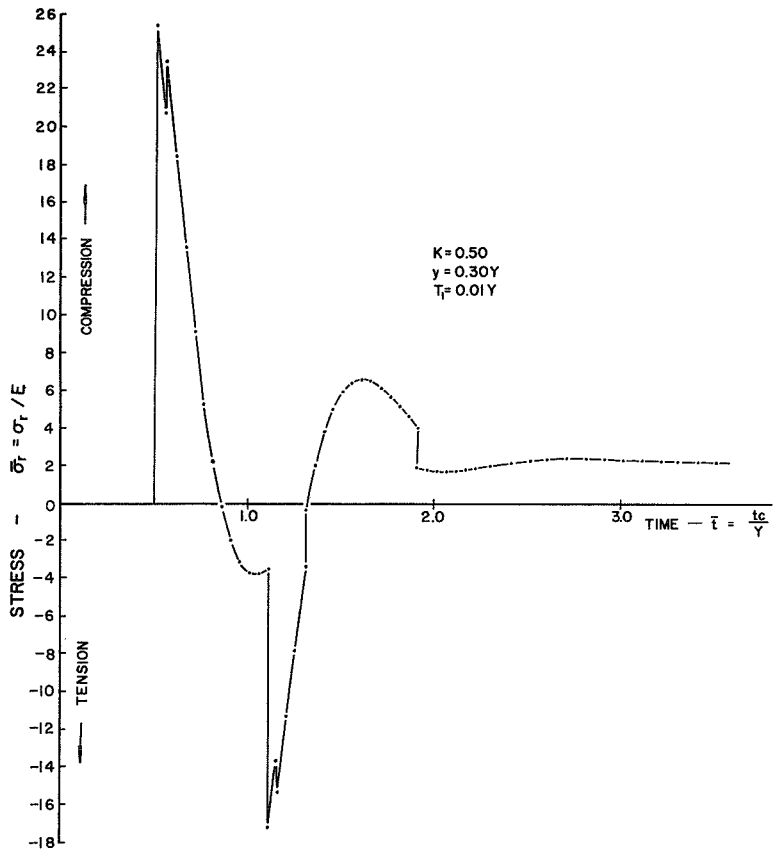

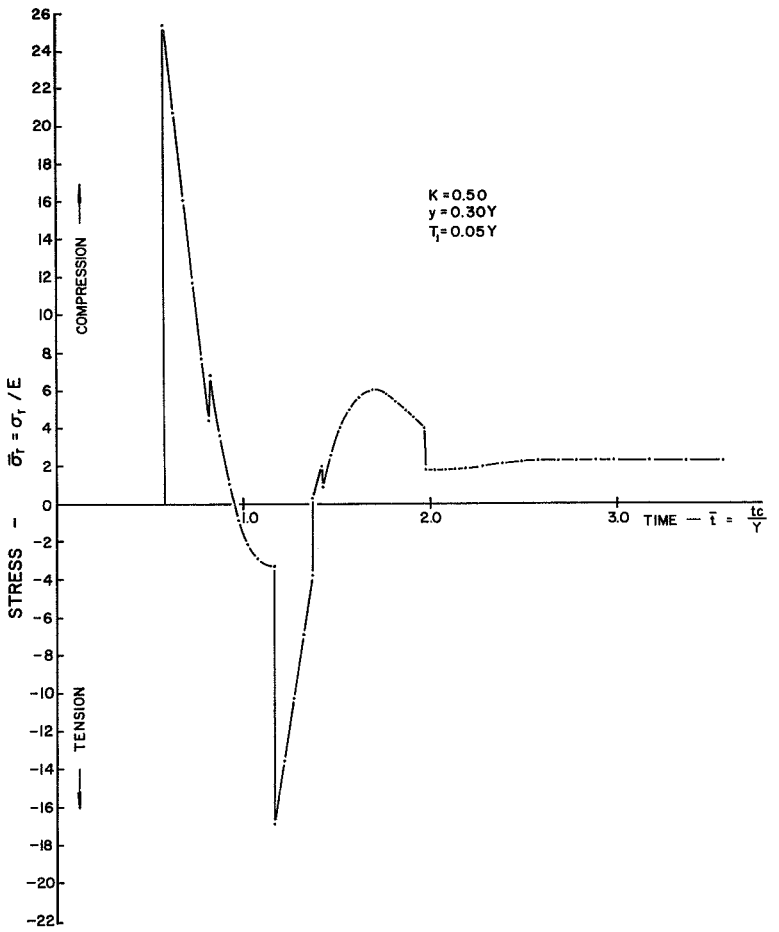

FIGURE 22

STRESS-TIME-LAMINATION THICKNESS RELATIONS

($\bar{p}_o$ = CONSTANT , K = 0.50 , y = 0.30Y)

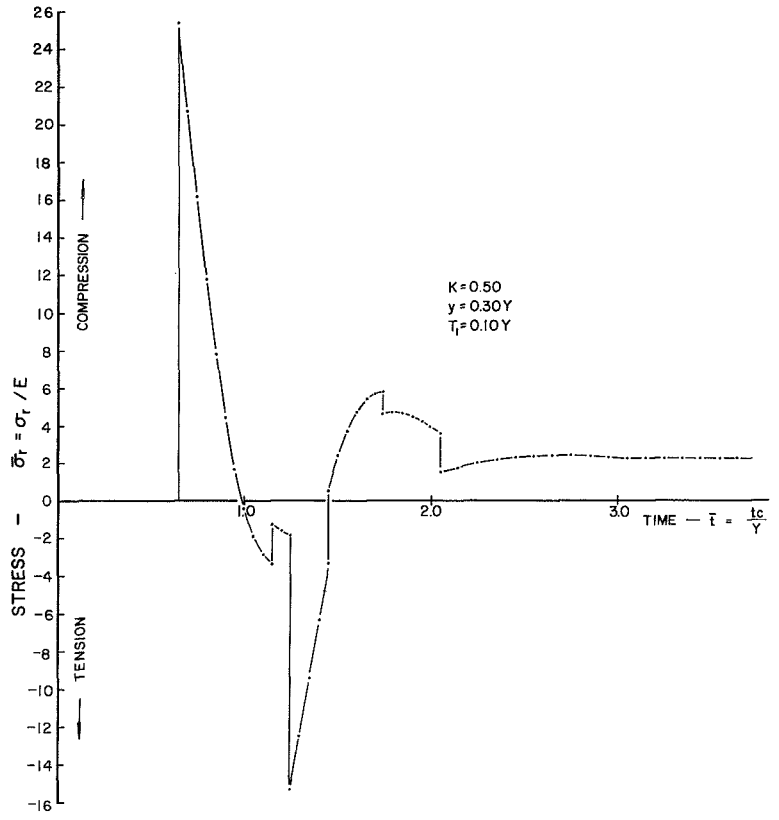

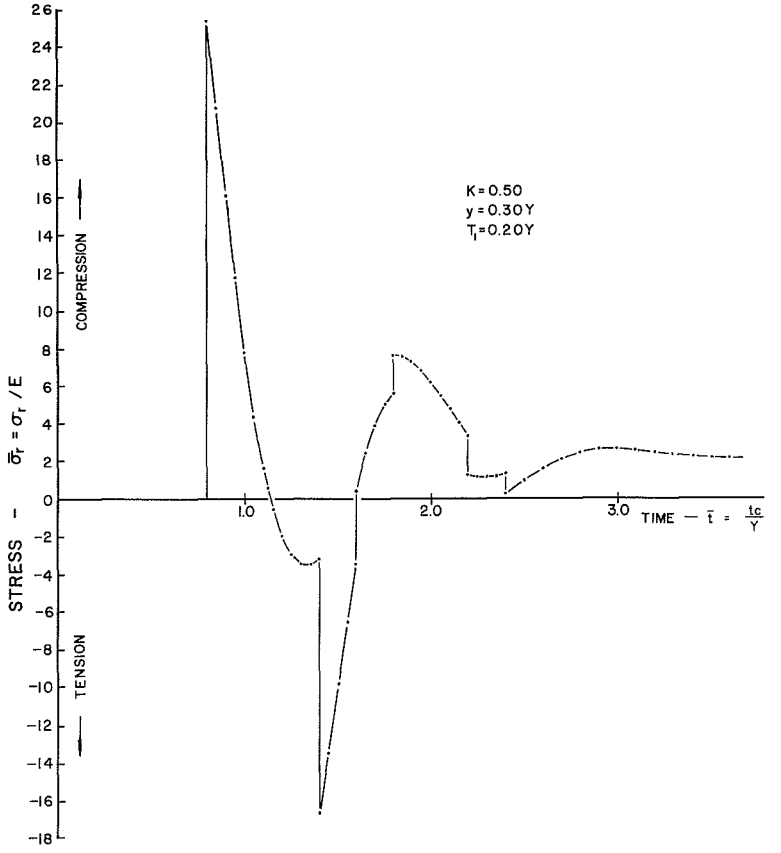

FIGURE 22 CONCLUDED

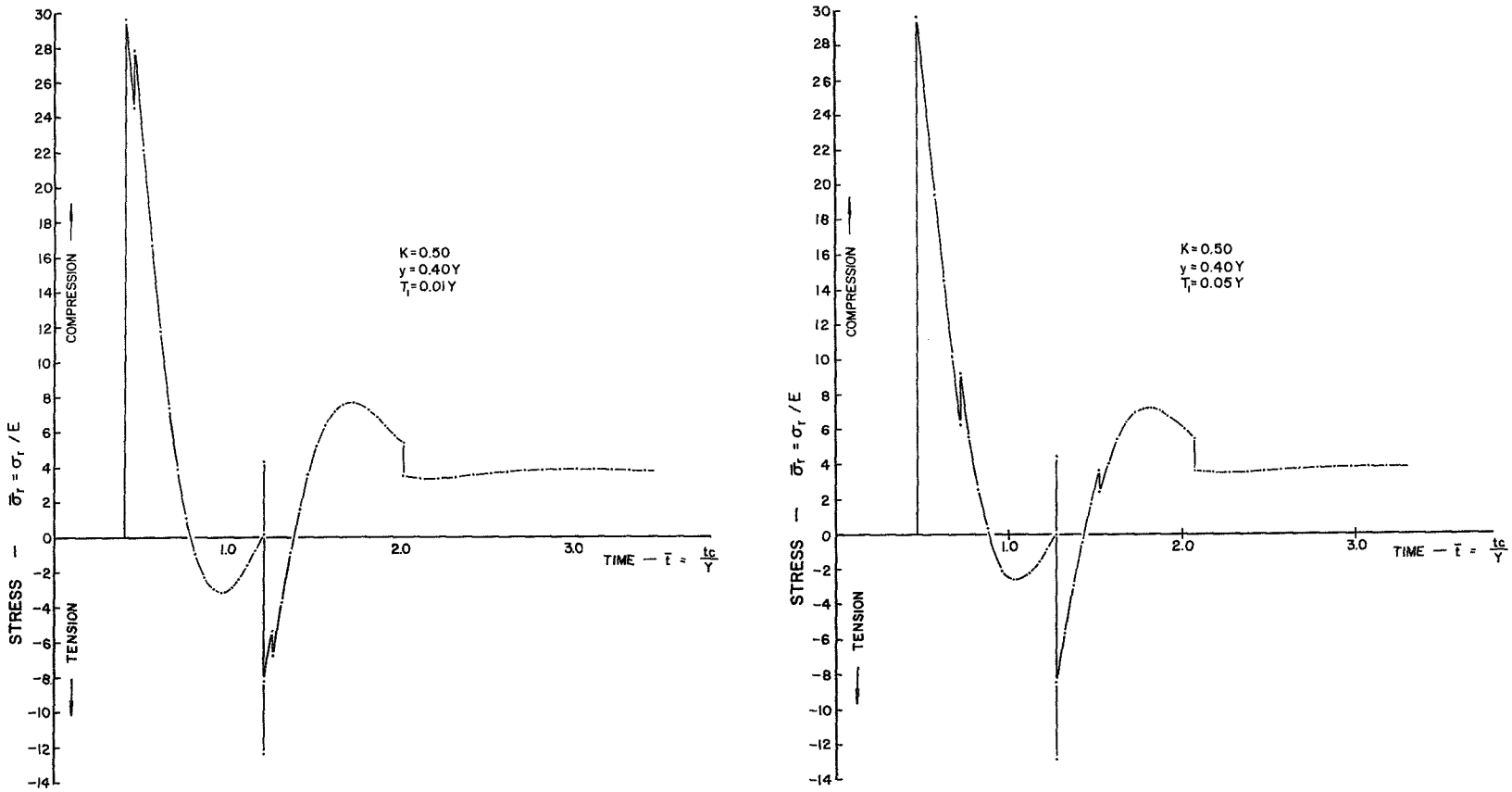

FIGURE 23

STRESS-TIME-LAMINATION THICKNESS RELATIONS

($\tilde{p}_o$ = CONSTANT , K =0.50 , y =0.40Y)

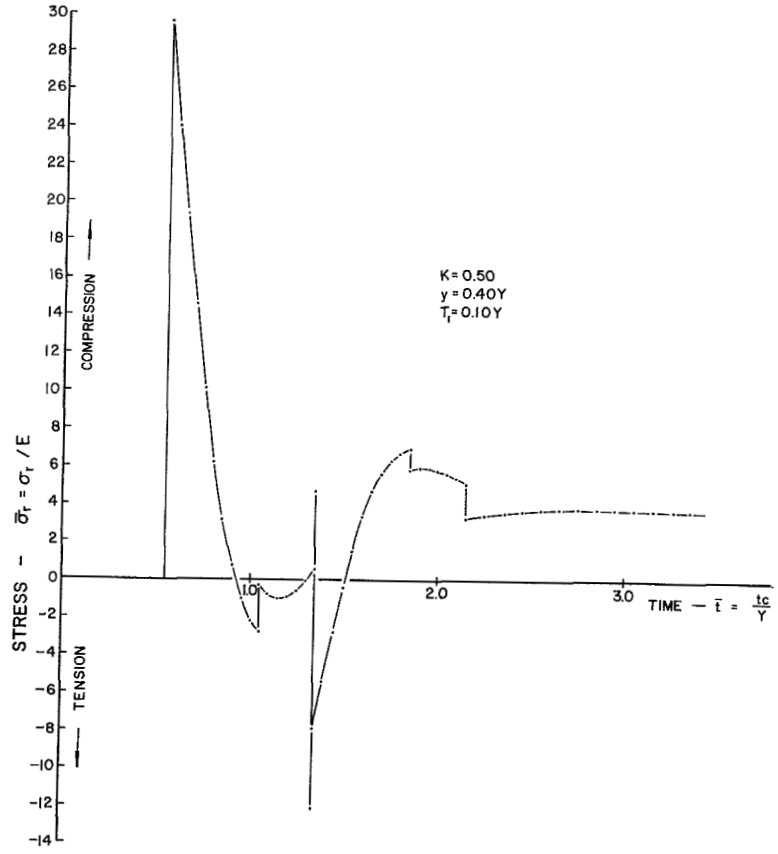

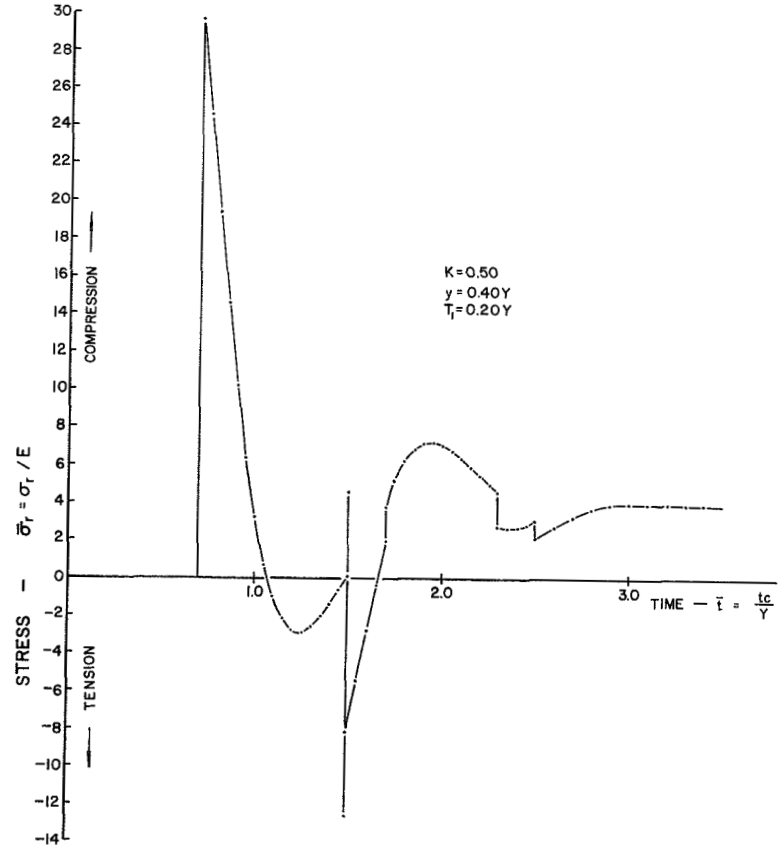

FIGURE 23 CONCLUDED

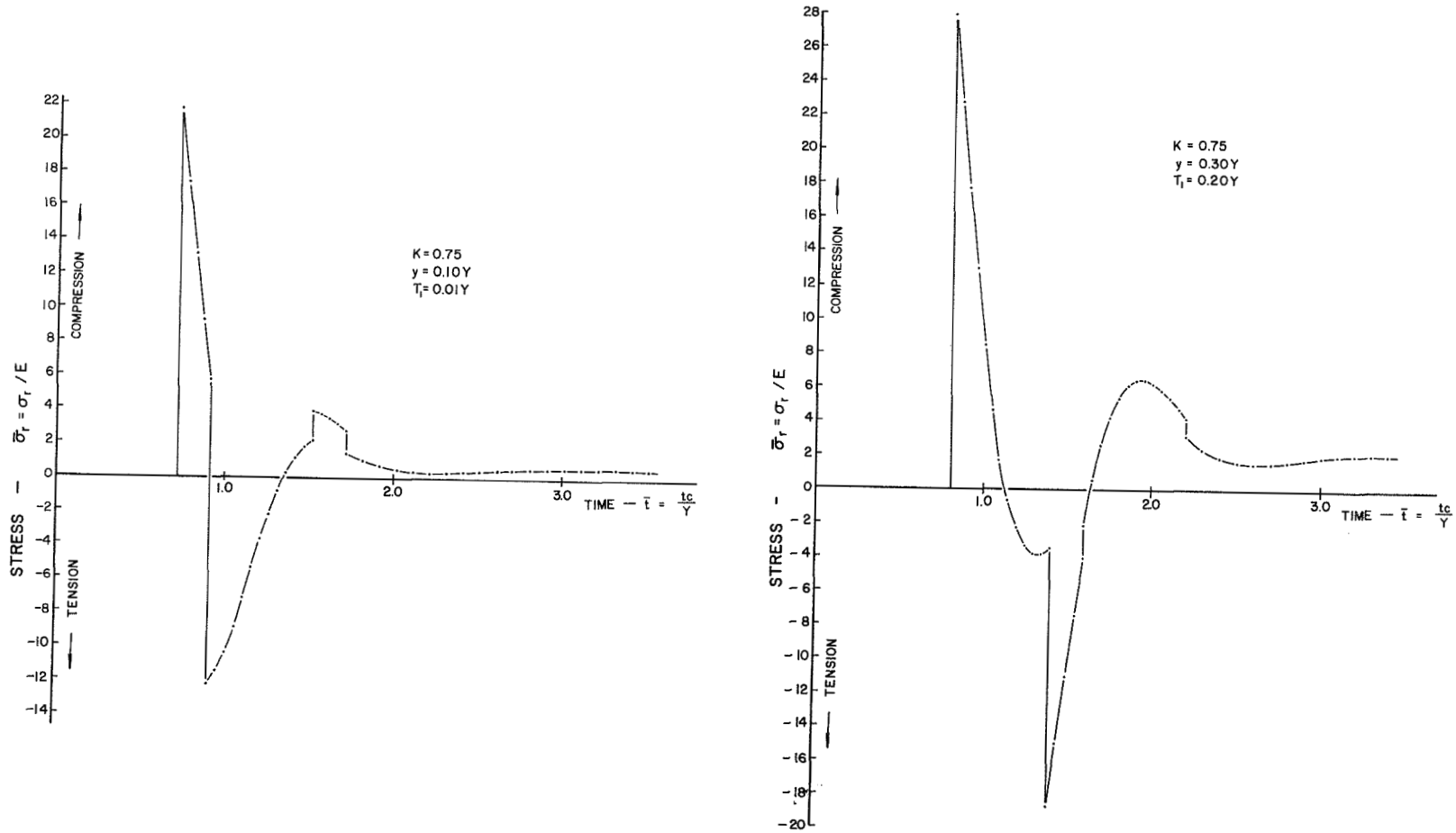

FIGURE 24

STRESS-TIME-LAMINATION THICKNESS RELATIONS

($\bar{p}_o$ = CONSTANT, K = 0.75)

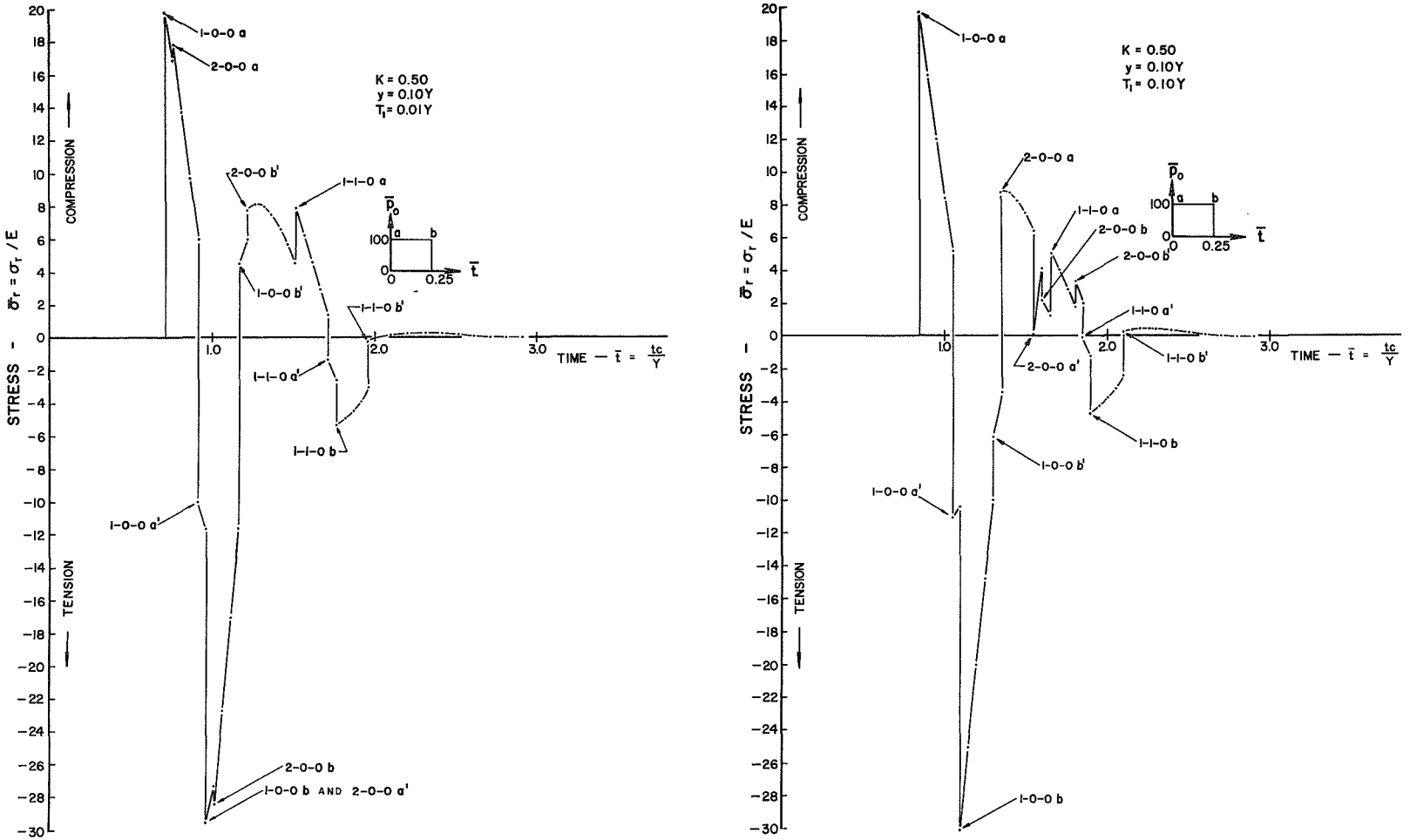

FIGURE 25

STRESS-TIME-LAMINATION THICKNESS RELATIONS

($\bar{p}_o$ = IMPULSE, L = 0.25)

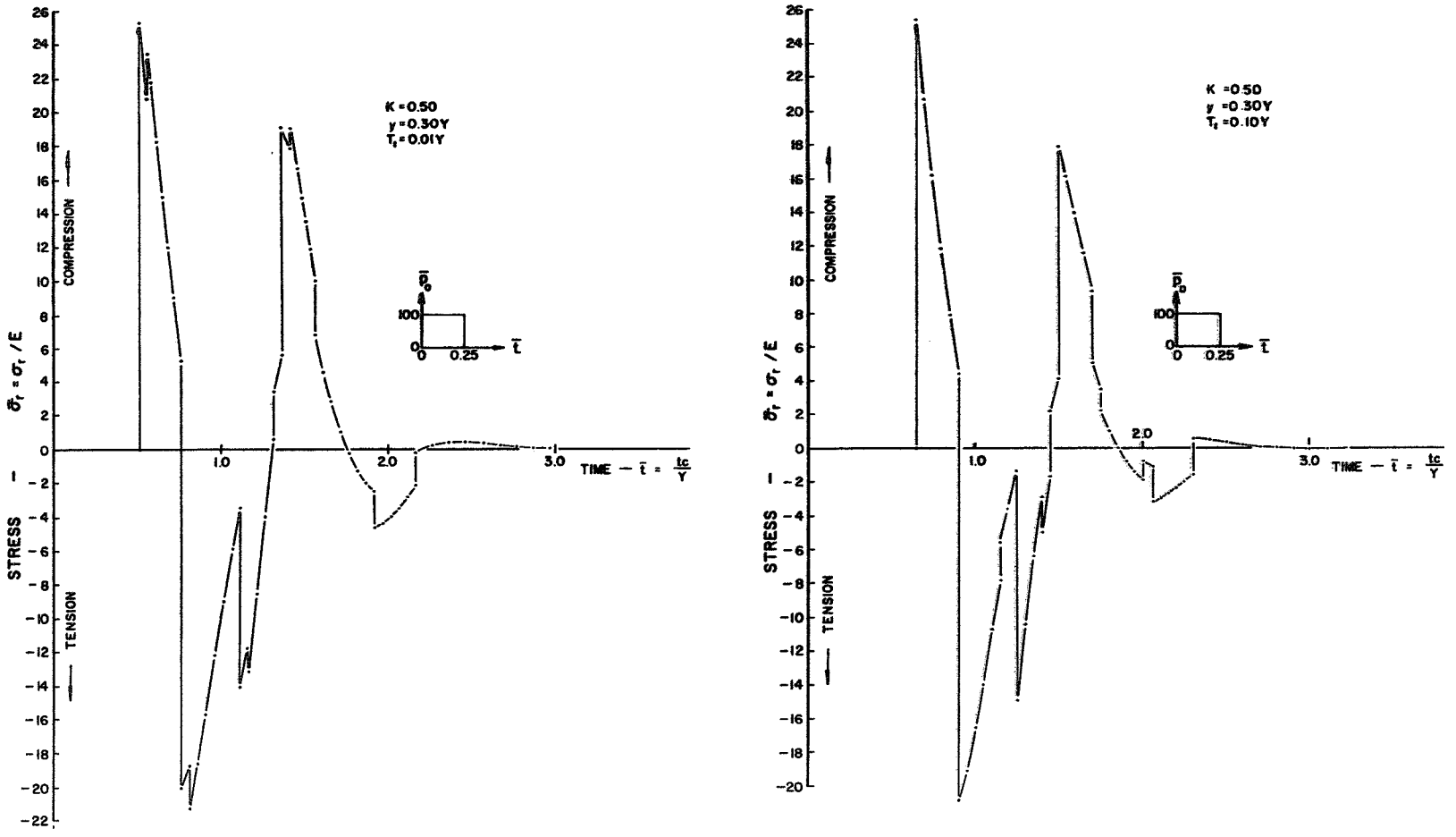

FIGURE 25 CONCLUDED

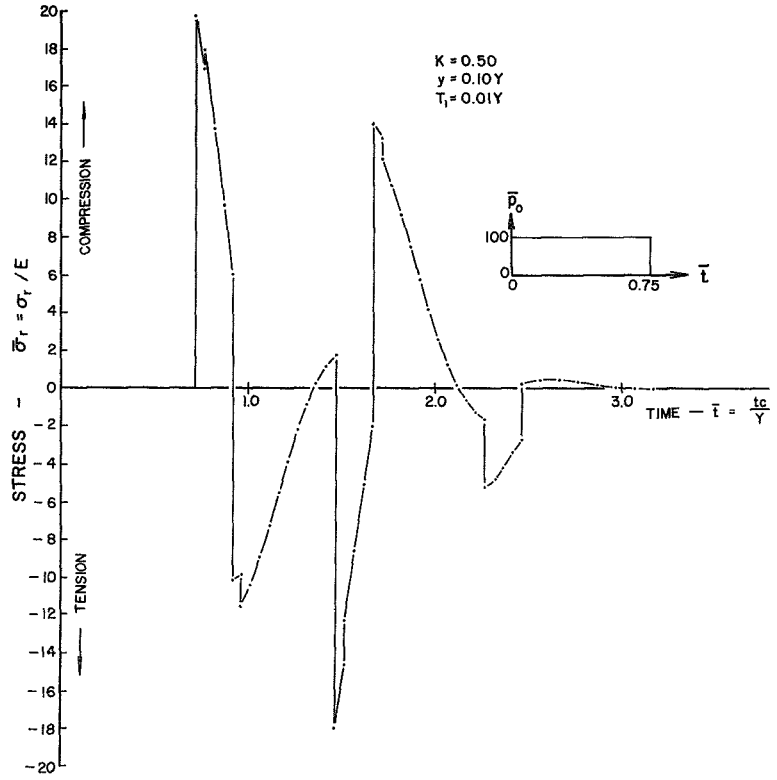

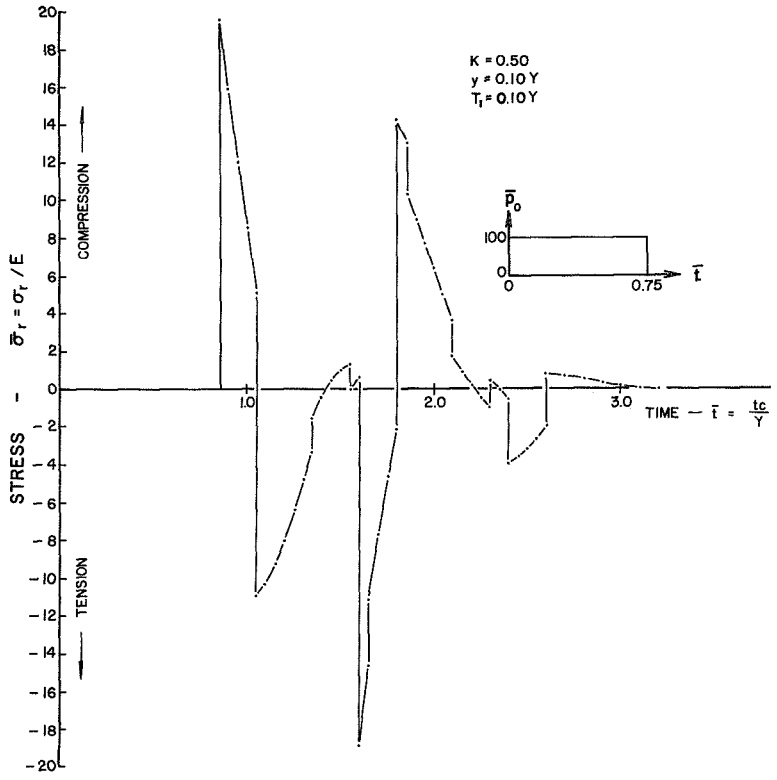

FIGURE 26

STRESS-TIME-LAMINATION THICKNESS RELATIONS

($\bar{p}_o$ = IMPULSE , L = 0.75)

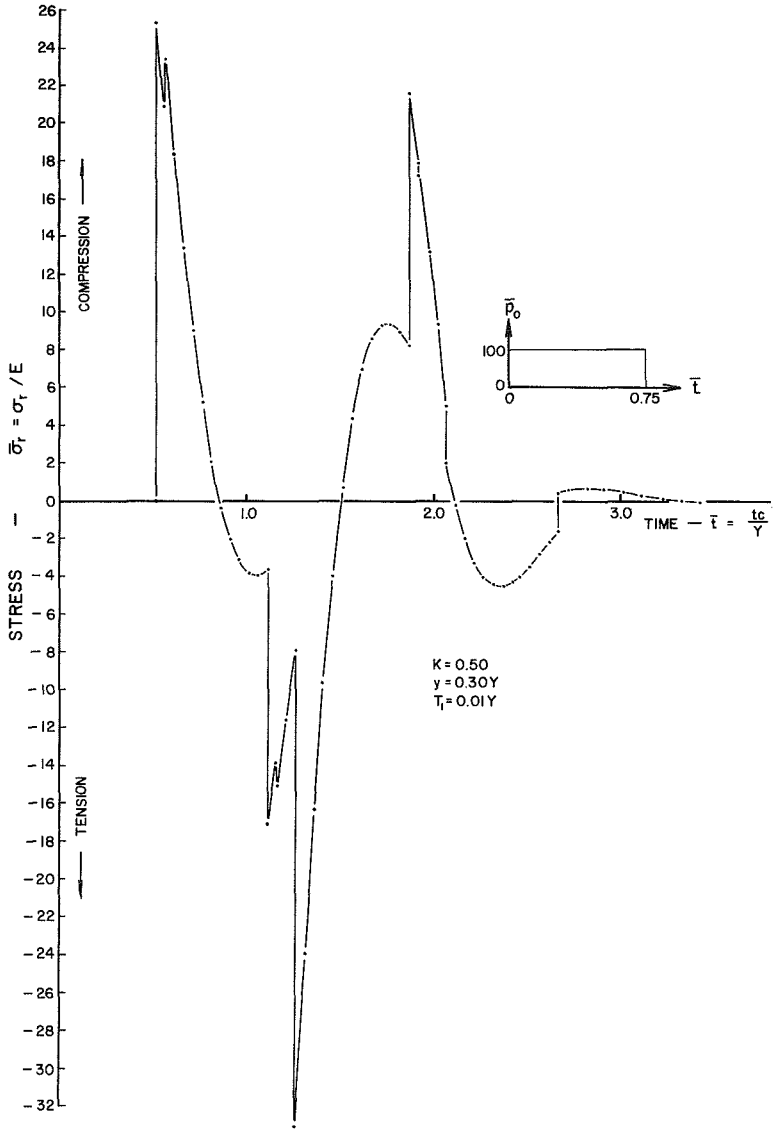

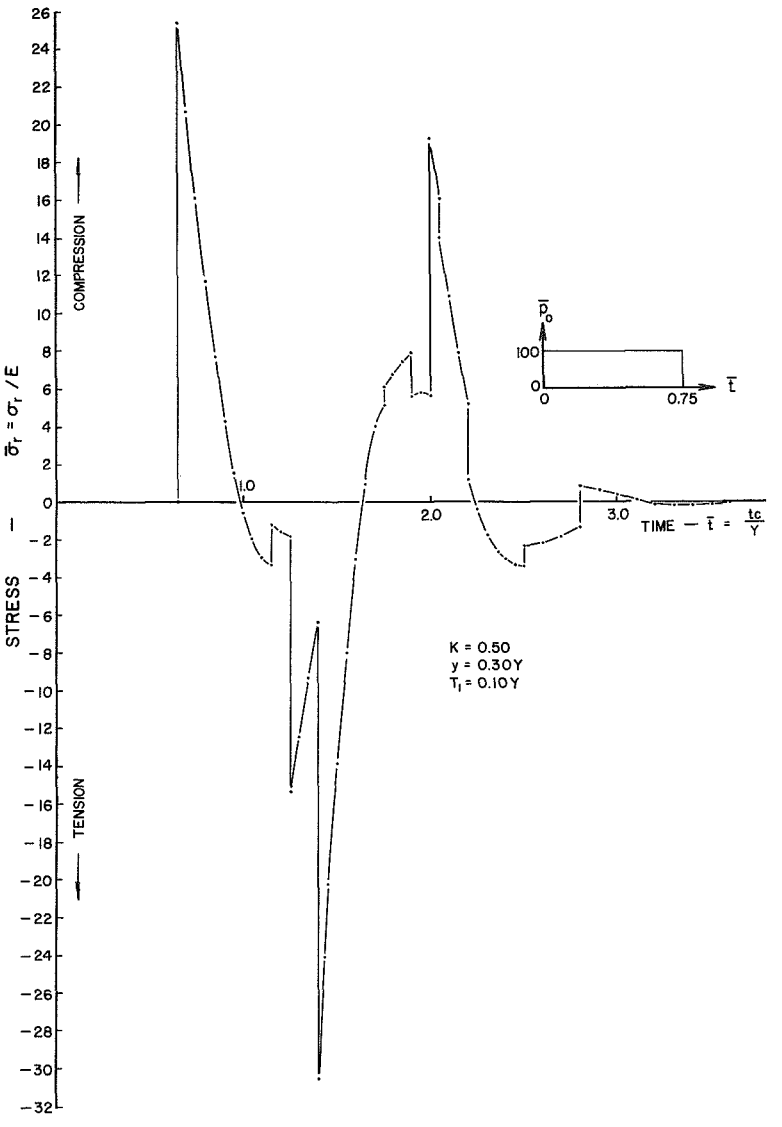

FIGURE 26 CONCLUDED

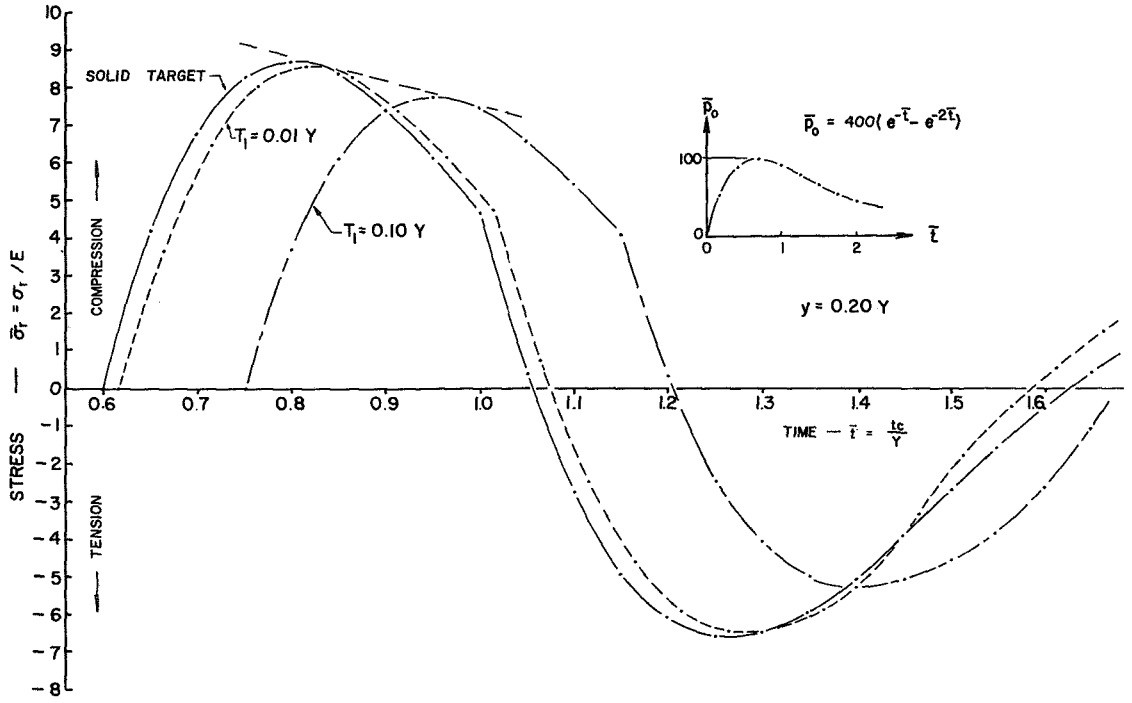

FIGURE 27

STRESS-TIME-LAMINATION THICKNESS RELATIONS

$[\bar{p}_o = 400(e^{-\bar{t}} - e^{-2\bar{t}})]$

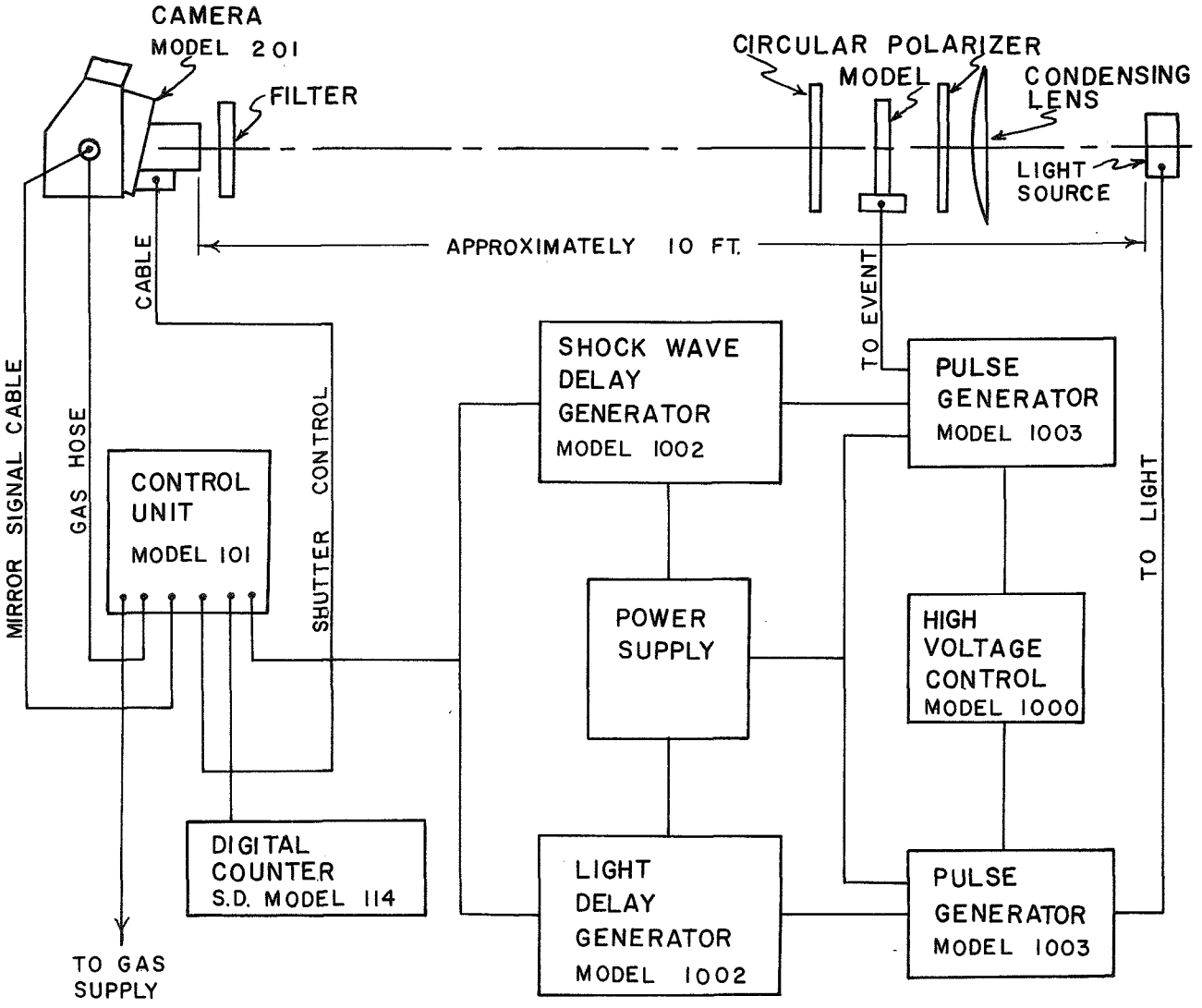

FIGURE 28

POLARISCOPE, CAMERA, AND CONTROLS

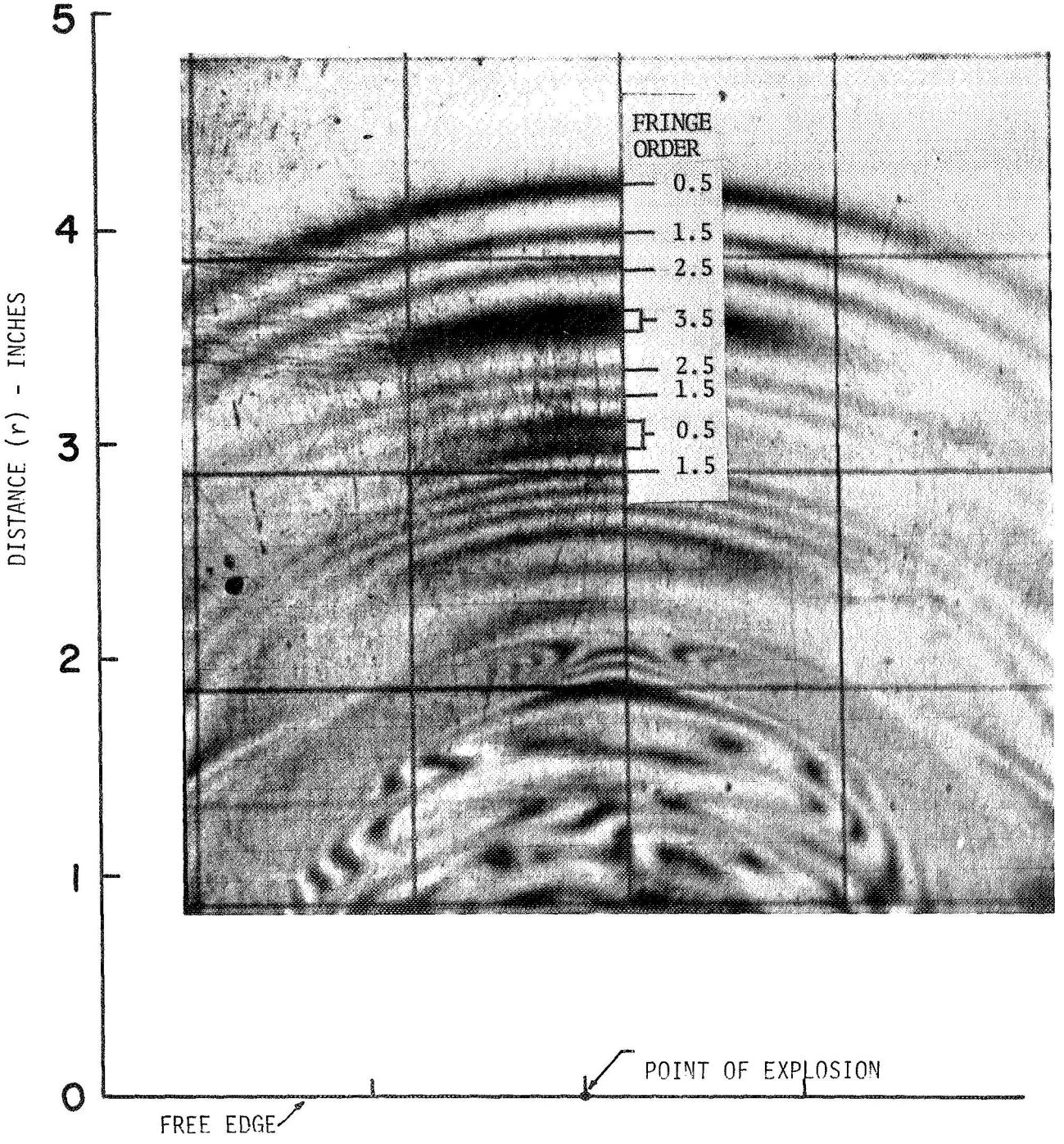

FIGURE 29

ILLUSTRATION OF FRINGE ORDER

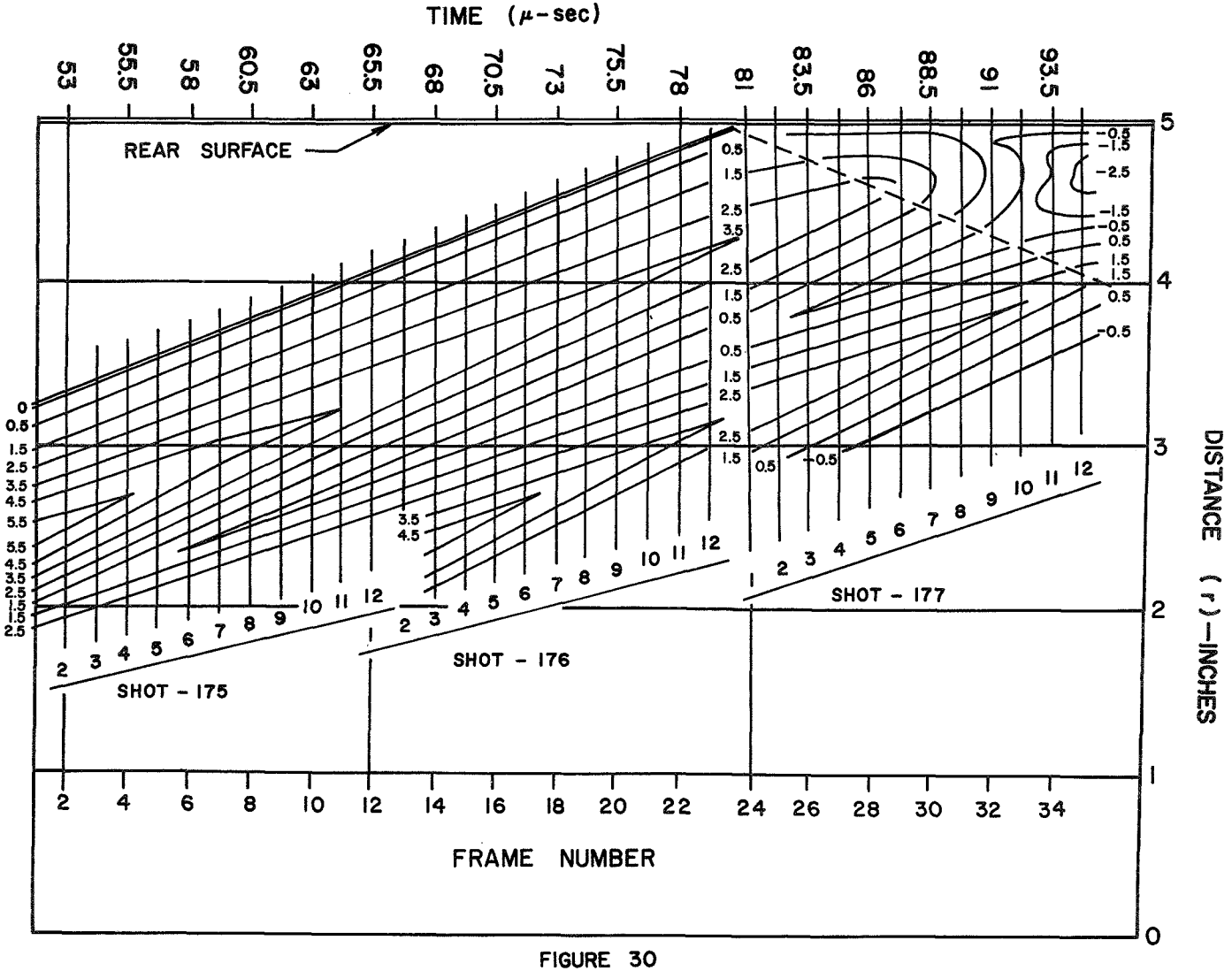

FIGURE 30

FRINGE LOCATIONS AT VARIOUS TIMES

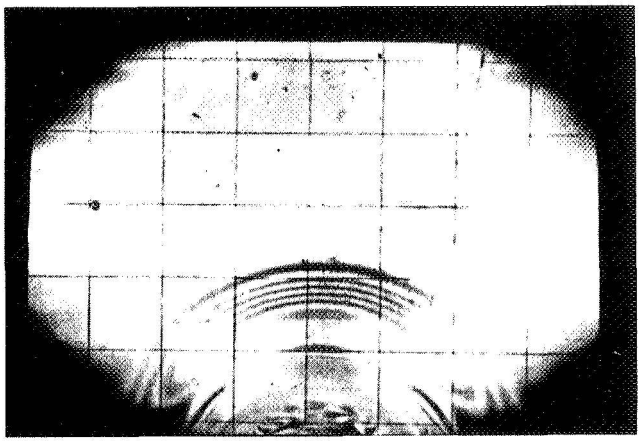

SHOT NUMBER 175, FRAME NUMBER 2

	N	R	UR	ET	ER	SIGMA R	SIGMA THETA
1	0.0	3.290	0.0	0.0	0.0	0.0	0.0
2	0.500	3.200	0.124	0.039	-2.721	-3.163	-1.163
3	1.500	3.050	0.937	0.307	-7.773	-9.182	-3.182
4	2.500	2.940	2.101	0.715	-13.085	-14.976	-4.976
5	3.500	2.830	3.815	1.348	-17.972	-20.406	-6.406
6	4.500	2.720	6.052	2.226	-22.614	-25.442	-7.442
7	5.500	2.580	9.518	3.689	-26.671	-29.534	-7.534
8	5.500	2.480	12.220	4.927	-25.433	-27.537	-5.537
9	4.500	2.380	14.426	6.061	-18.779	-19.256	-1.256
10	3.500	2.280	15.965	7.007	-12.313	-11.280	2.720
11	2.500	2.200	16.712	7.537	-6.203	-3.877	6.123
12	1.500	2.130	16.936	7.752	-0.328	3.149	9.149
13	1.200	2.070	16.931	8.169	1.541	5.427	10.227
14	1.500	2.020	16.861	8.347	0.067	3.786	9.786

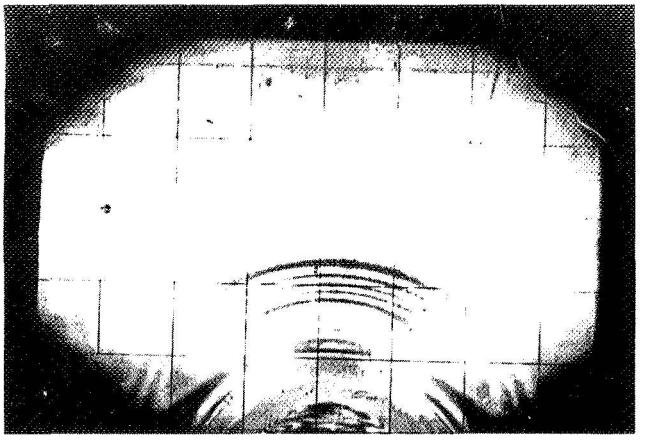

SHOT NUMBER 175, FRAME NUMBER 4

	N	R	UR	ET	ER	SIGMA R	SIGMA THETA
1	0.0	3.490	0.0	0.0	0.0	0.0	0.0
2	0.500	3.360	0.124	0.037	-2.723	-3.166	-1.166
3	1.500	3.210	0.937	0.292	-7.988	-9.206	-3.206
4	2.500	3.080	2.213	0.731	-13.049	-14.918	-4.918
5	3.500	2.950	4.330	1.408	-17.852	-20.213	-6.213
6	4.500	2.840	6.928	2.303	-22.531	-25.358	-7.358
7	5.500	2.700	10.015	3.708	-26.652	-29.532	-7.532
8	5.500	2.590	12.277	4.921	-20.039	-27.321	-7.321
9	4.500	2.580	12.826	4.971	-19.969	-21.016	-4.016
10	3.500	2.470	14.656	5.931	-13.389	-13.514	-1.986
11	2.500	2.390	15.473	6.445	-7.465	-5.686	4.314
12	1.500	2.300	15.863	6.647	-1.393	1.446	7.446
13	0.800	2.210	15.794	7.149	2.733	6.367	9.569
14	1.500	2.160	15.755	7.235	0.080	4.086	8.086

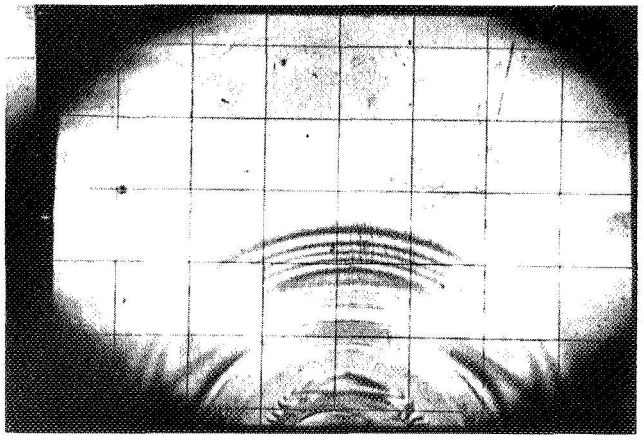

SHOT NUMBER 175, FRAME NUMBER 6

	N	R	UR	ET	ER	SIGMA R	SIGMA THETA
1	0.0	3.590	0.0	0.0	0.0	0.0	0.0
2	0.500	3.510	0.110	0.031	-2.729	-3.175	-1.175
3	1.500	3.360	0.925	0.275	-8.005	-9.233	-3.233
4	2.500	3.220	2.408	0.748	-13.052	-14.923	-4.923
5	3.500	3.090	4.427	1.433	-17.887	-20.270	-6.270
6	4.500	2.980	6.666	2.235	-22.605	-25.427	-7.427
7	4.500	2.790	11.133	3.490	-20.850	-22.596	-4.596
8	3.500	2.670	13.239	4.459	-14.361	-14.583	-0.583
9	2.500	2.570	14.365	5.589	-8.211	-7.115	2.885
10	1.500	2.470	14.882	6.025	-2.255	0.040	6.040
11	0.700	2.370	14.870	6.274	2.410	5.603	8.603
12	1.500	2.290	14.848	6.484	-1.796	0.780	6.780

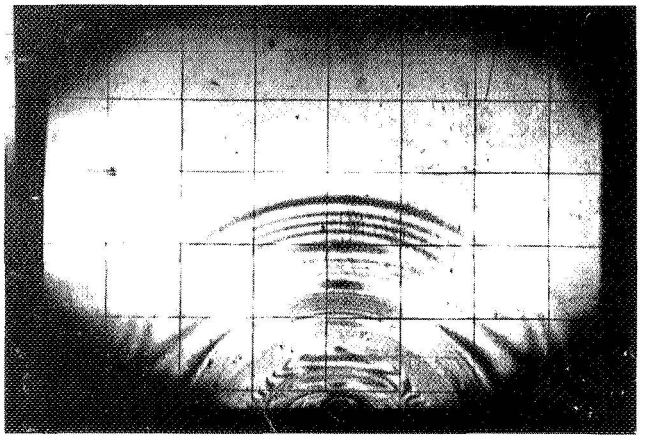

SHOT NUMBER 175, FRAME NUMBER 8

	N	R	UR	ET	ER	SIGMA R	SIGMA THETA
1	0.0	3.750	0.0	0.0	0.0	0.0	0.0
2	0.500	3.670	0.110	0.030	-2.730	-3.177	-1.177
3	1.500	3.510	0.979	0.277	-8.001	-9.227	-3.227
4	2.500	3.370	2.463	0.731	-13.069	-14.950	-4.950
5	3.500	3.230	4.639	1.436	-17.884	-20.264	-6.264
6	4.500	3.090	7.470	2.418	-22.422	-25.133	-7.133
7	4.500	2.880	9.992	3.353	-21.487	-23.624	-5.624
8	3.500	2.840	12.532	4.413	-14.907	-15.463	-1.463
9	2.500	2.750	13.596	4.945	-8.855	-8.154	1.846
10	1.500	2.640	14.236	5.393	-2.887	-0.979	5.021
11	0.500	2.550	14.237	5.583	2.823	5.779	7.779
12	0.500	2.510	14.123	5.627	2.867	5.849	7.849

FIGURE 31

STRESS WAVE PHOTOGRAPHS AND COMPUTED RESULTS

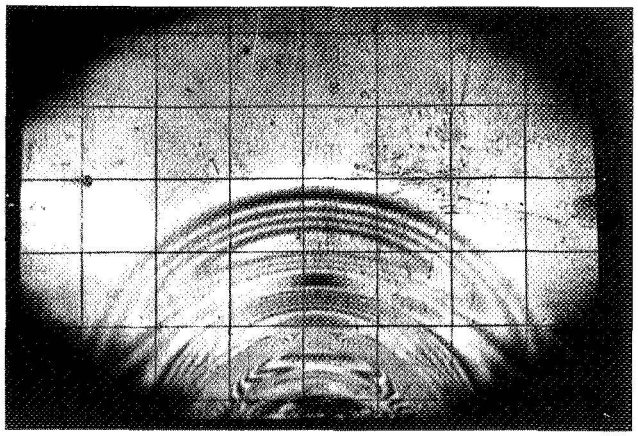

SHOT NUMBER 175, FRAME NUMBER 10

	N	R	DR	ET	ER	SIGMA R	SIGMA THETA
1	0.0	3.880	0.0	0.0	0.0	0.0	0.0
2	0.500	3.810	0.097	0.025	-2.735	-3.185	-1.185
3	1.500	3.660	0.913	0.249	-8.031	-9.275	-3.275
4	2.500	3.310	2.500	0.714	-13.086	-14.978	-4.978
5	3.500	3.360	4.838	1.440	-17.880	-20.258	-6.258
6	4.500	3.190	8.254	2.391	-22.249	-24.854	-6.854
7	4.500	3.150	9.164	2.909	-21.731	-24.340	-6.340
8	3.500	3.010	11.771	3.911	-15.409	-16.273	-2.273
9	2.500	2.920	12.883	4.412	-9.388	-9.013	0.987
10	1.500	2.810	13.594	4.834	-3.446	-1.880	4.120
11	0.500	2.700	13.642	5.052	2.292	4.923	6.923
12	0.350	2.670	13.560	5.079	3.147	5.933	7.333
13	0.500	2.650	13.500	5.066	2.336	4.994	6.994

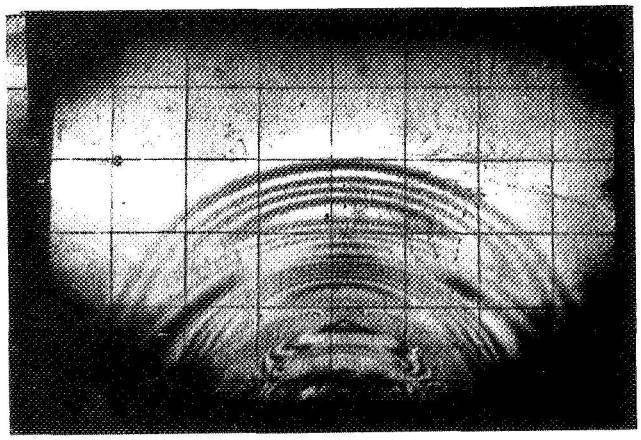

SHOT NUMBER 175, FRAME NUMBER 12

	N	R	DR	ET	ER	SIGMA R	SIGMA THETA
1	0.0	4.040	0.0	0.0	0.0	0.0	0.0
2	0.500	3.970	0.097	0.024	-2.736	-3.187	-1.187
3	1.500	3.810	0.967	0.254	-8.026	-9.268	-3.268
4	2.500	3.660	2.560	0.700	-13.100	-15.001	-5.001
5	3.500	3.500	5.050	1.443	-17.877	-20.253	-6.254
6	3.500	3.200	10.869	3.397	-15.923	-17.102	-3.102
7	2.500	3.090	12.280	3.974	-9.826	-9.719	0.281
8	1.500	2.980	13.036	4.373	-3.907	-2.625	3.375
9	0.500	2.870	13.140	4.578	1.818	4.159	6.159
10	0.200	2.830	13.033	4.605	3.501	6.138	6.938
11	0.500	2.780	12.899	4.640	1.880	4.258	6.258

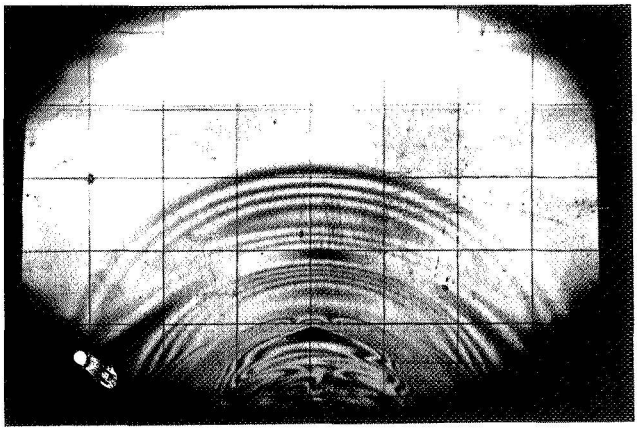

SHOT NUMBER 176, FRAME NUMBER 3

	N	R	DR	ET	ER	SIGMA R	SIGMA THETA
1	0.0	4.200	0.0	0.0	0.0	0.0	0.0
2	0.500	4.130	0.097	0.023	-2.737	-3.188	-1.188
3	1.500	3.970	0.966	0.244	-8.036	-9.284	-3.284
4	2.500	3.800	2.773	0.730	-13.070	-14.952	-4.952
5	3.500	3.640	5.259	1.445	-17.875	-20.250	-6.250
6	3.500	3.390	10.060	2.968	-16.352	-17.794	-3.794
7	2.500	3.280	11.521	3.513	-10.287	-10.464	-0.464
8	1.500	3.140	12.534	3.932	-4.288	-3.239	2.761
9	0.500	3.020	12.698	4.205	1.445	3.556	5.556
10	0.200	2.970	12.583	4.237	3.133	5.543	6.343
11	0.500	2.920	12.468	4.270	1.510	3.661	5.661

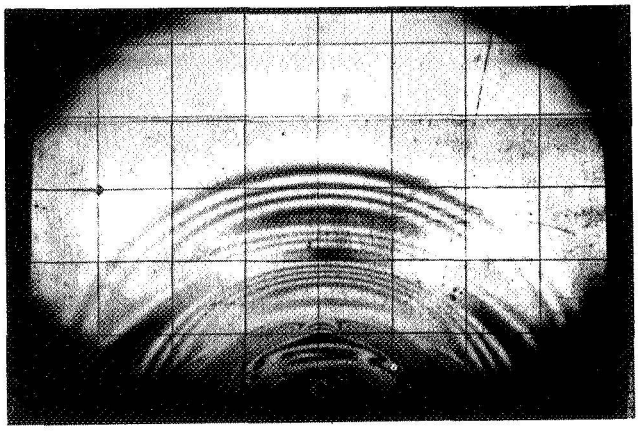

SHOT NUMBER 176, FRAME NUMBER 5

	N	R	DR	ET	ER	SIGMA R	SIGMA THETA
1	0.0	4.350	0.0	0.0	0.0	0.0	0.0
2	0.500	4.280	0.097	0.023	-2.737	-3.189	-1.189
3	1.500	4.120	0.966	0.235	-8.045	-9.298	-3.298
4	2.500	3.940	2.880	0.731	-13.069	-14.950	-4.950
5	3.500	3.770	5.521	1.464	-17.856	-20.219	-6.219
6	3.500	3.560	9.465	2.659	-16.661	-18.292	-4.292
7	2.500	3.420	11.356	3.321	-10.479	-10.773	-0.773
8	1.500	3.300	12.255	3.714	-4.566	-3.688	2.312
9	0.500	3.170	12.469	3.933	1.173	3.118	5.118
10	0.100	3.120	12.354	3.960	3.408	5.741	6.141
11	0.500	3.070	12.238	3.986	1.226	3.204	5.204

FIGURE 31 CONTINUED

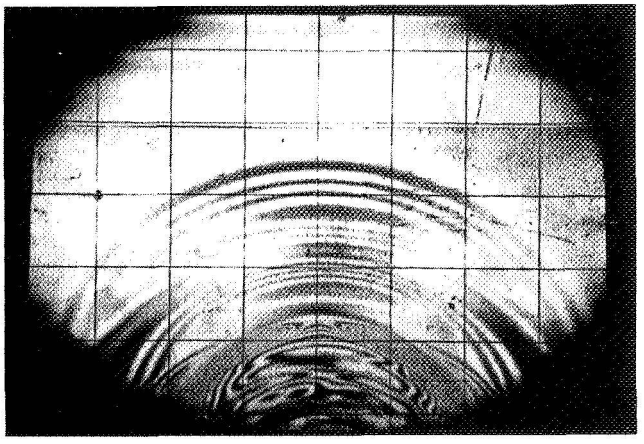

SHOT NUMBER 176, FRAME NUMBER 7

	N	R	UR	ET	ER	SIGMA R	SIGMA THETA
1	0.0	4.520	0.0	0.0	0.0	0.0	0.0
2	0.500	4.440	0.110	0.025	-2.735	-3.186	-1.186
3	1.500	4.260	1.089	0.256	-8.024	-9.265	-3.265
4	2.500	4.080	2.999	0.735	-13.065	-14.943	-4.943
5	3.500	3.910	5.640	1.443	-17.877	-20.254	-6.254
6	3.500	3.740	8.791	2.350	-16.970	-18.790	-4.790
7	2.500	3.610	10.594	2.935	-10.865	-11.396	-1.396
8	1.500	3.470	11.692	3.369	-4.911	-4.243	1.757
9	0.500	3.350	11.932	3.562	0.802	2.519	4.519
10	0.0	3.280	11.778	3.591	3.591	5.792	5.792
11	0.500	3.210	11.623	3.621	0.861	2.614	4.614

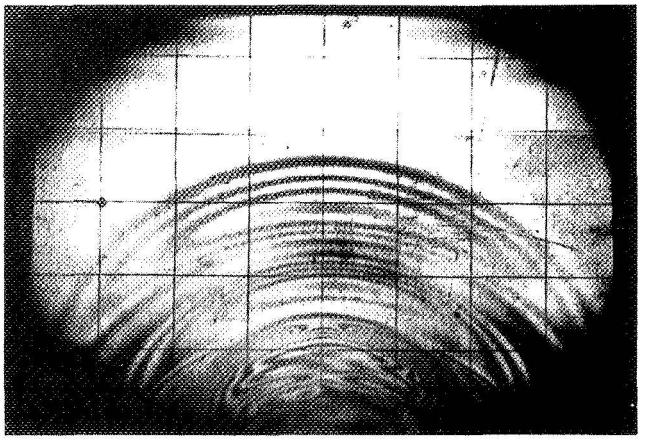

SHOT NUMBER 176, FRAME NUMBER 9

	N	R	UR	ET	ER	SIGMA R	SIGMA THETA
1	0.0	4.670	0.0	0.0	0.0	0.0	0.0
2	0.500	4.590	0.116	0.024	-2.736	-3.187	-1.187
3	1.500	4.420	1.036	0.234	-8.046	-9.299	-3.299
4	2.500	4.220	3.160	0.749	-13.051	-14.921	-4.921
5	3.500	4.050	5.800	1.432	-17.888	-20.271	-6.271
6	3.500	3.930	7.977	2.030	-17.290	-19.307	-5.307
7	2.500	3.770	10.239	2.716	-11.084	-11.748	-1.748
8	1.500	3.620	11.447	3.162	-5.118	-4.577	1.423
9	0.500	3.520	11.671	3.316	0.556	2.122	4.122
10	-0.050	3.430	11.481	3.347	3.623	5.721	5.521
11	0.500	3.350	11.313	3.377	0.617	2.221	4.221

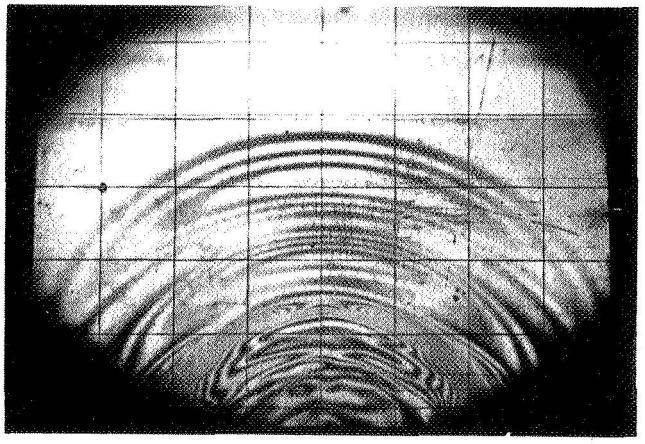

SHOT NUMBER 176, FRAME NUMBER 11

	N	R	UR	ET	ER	SIGMA R	SIGMA THETA
1	0.0	4.830	0.0	0.0	0.0	0.0	0.0
2	0.500	4.740	0.124	0.026	-2.734	-3.184	-1.184
3	1.500	4.560	1.104	0.242	-8.038	-9.287	-3.287
4	2.500	4.370	3.122	0.715	-13.085	-14.977	-4.977
5	3.500	4.190	5.924	1.414	-17.906	-20.300	-6.300
6	3.500	4.120	7.175	1.742	-17.578	-19.772	-5.772
7	2.500	3.950	9.627	2.437	-11.363	-12.198	-2.198
8	1.500	3.800	10.878	2.863	-5.417	-5.060	0.940
9	0.500	3.670	11.205	3.053	0.293	1.698	3.698
10	-0.100	3.570	11.006	3.083	3.635	5.618	5.218
11	0.500	3.470	10.809	3.115	0.355	1.798	3.798

FIGURE 31 CONCLUDED

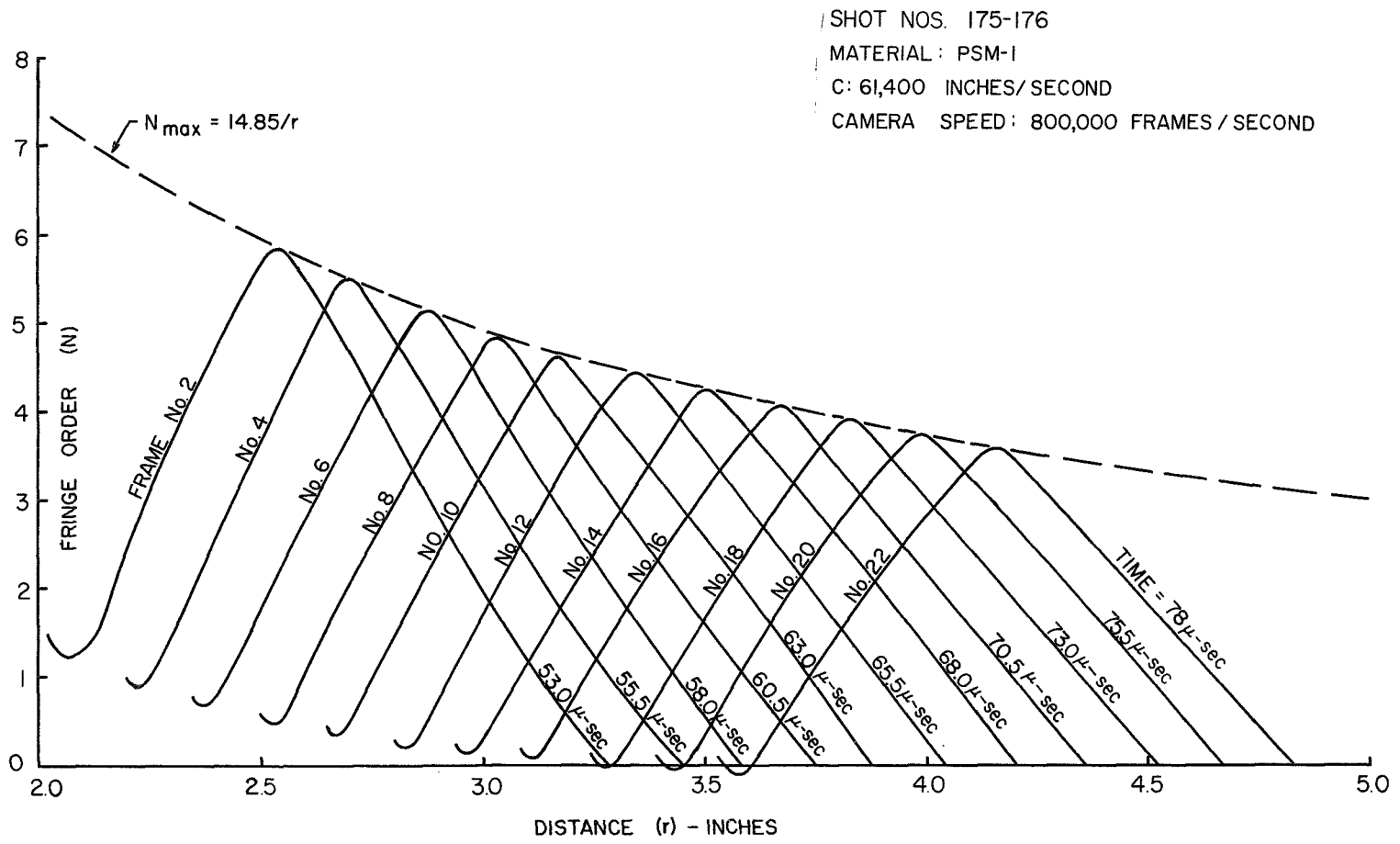

FIGURE 32

FRINGE NUMBER - DISTANCE - TIME RELATIONS

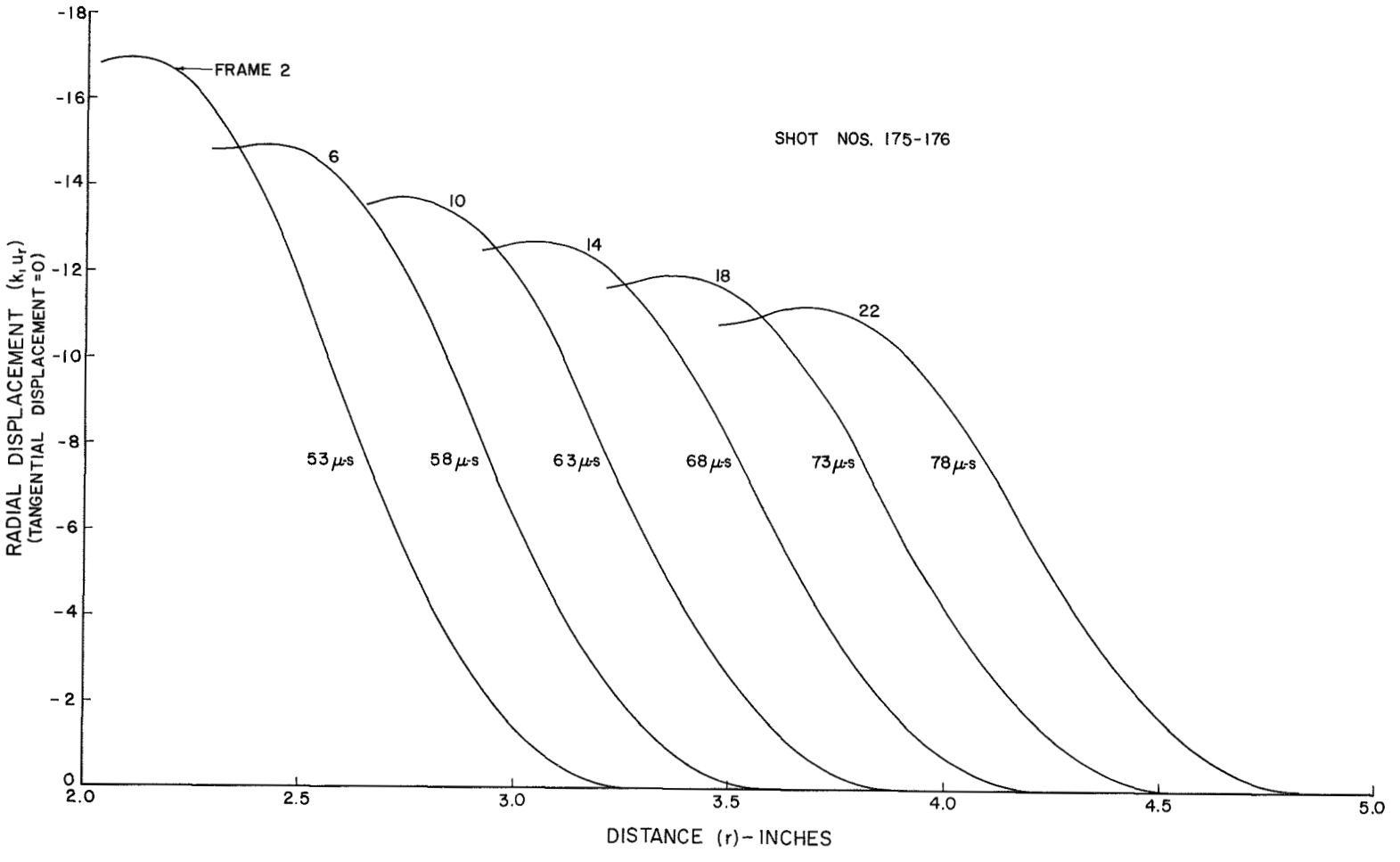

FIGURE 33

DISPLACEMENT - DISTANCE - TIME RELATIONS

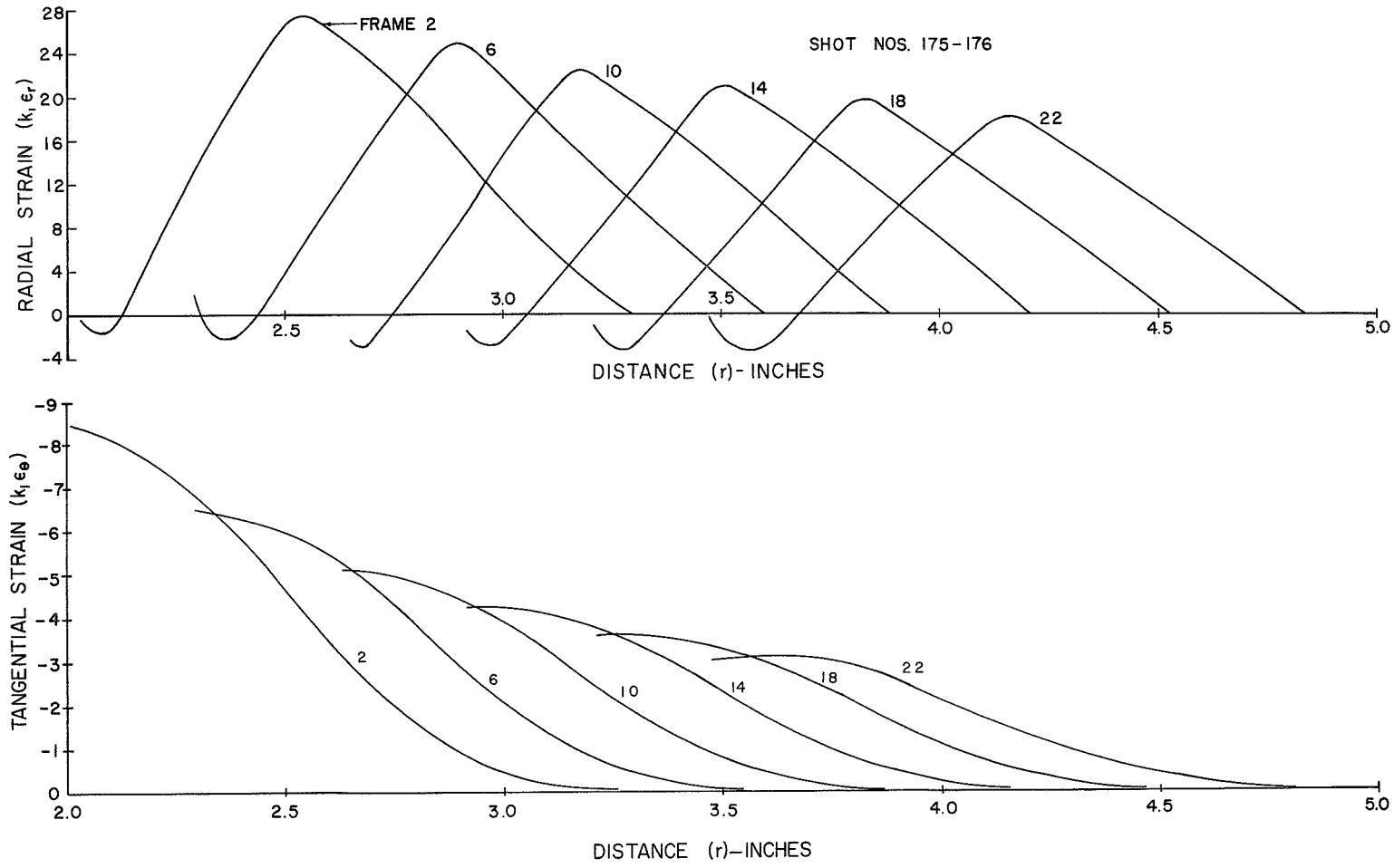

FIGURE 34

STRAIN-DISTANCE-TIME RELATIONS

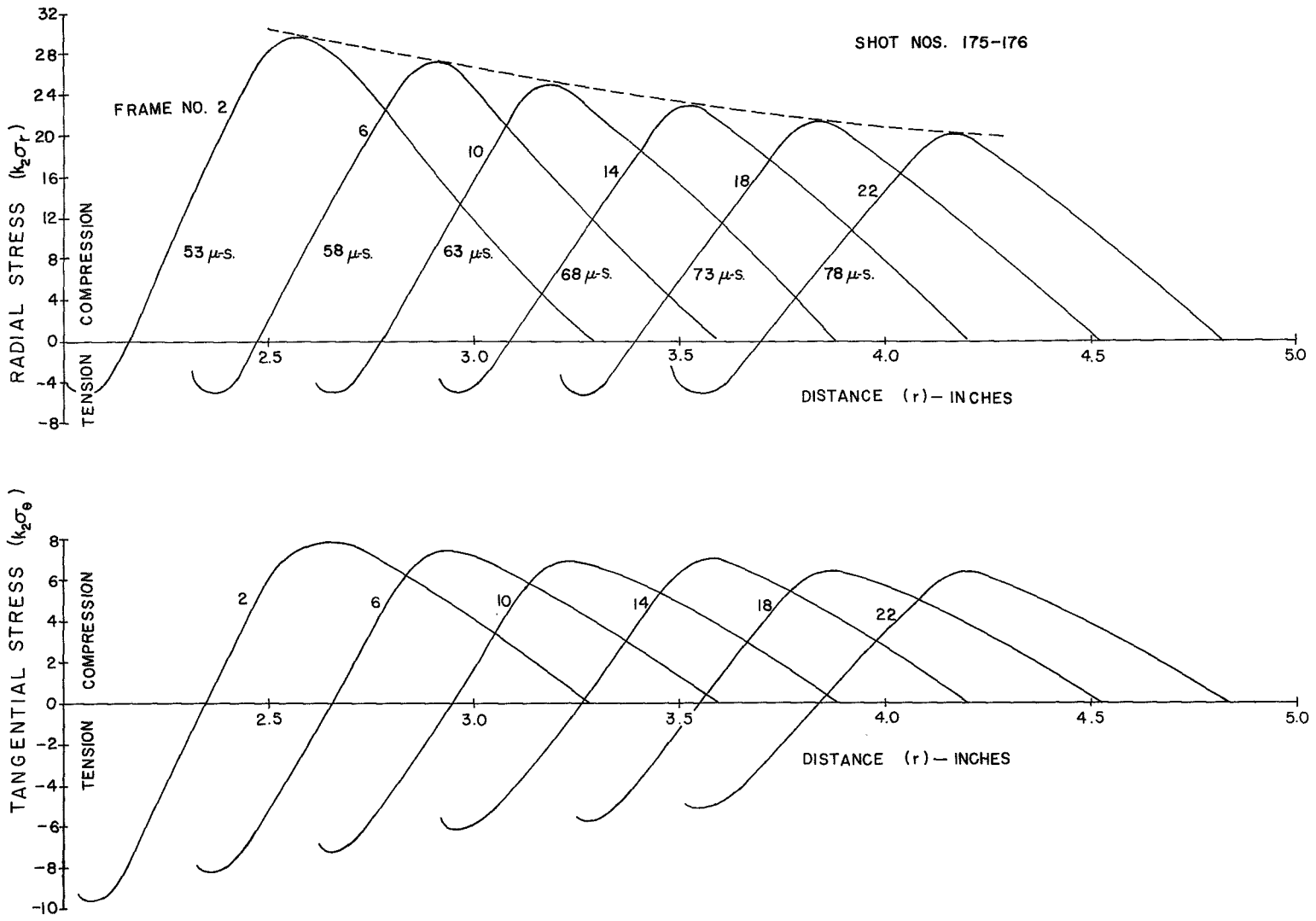

FIGURE 35

STRESS-DISTANCE-TIME RELATIONS

$\frac{1}{8}$" ALUMINUM LAMINATE (SHOT 240)

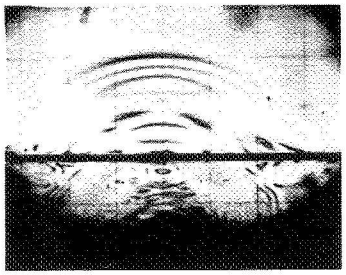

FRAME 1

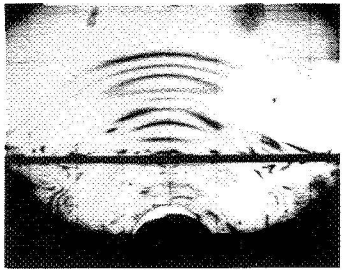

FRAME 2

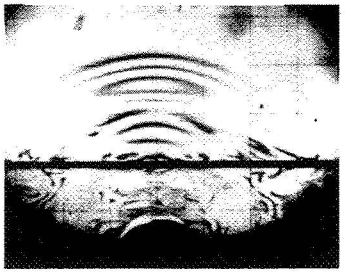

FRAME 3

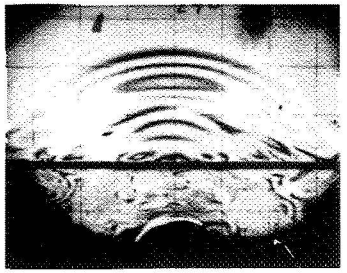

FRAME 4

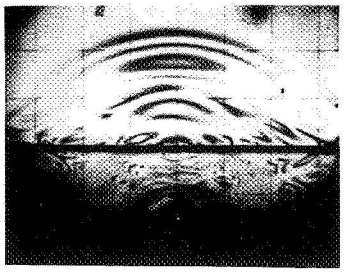

FRAME 5

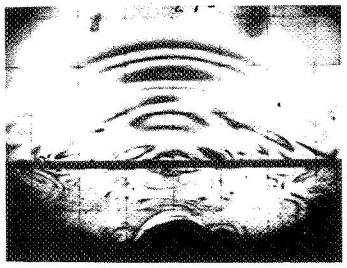

FRAME 6

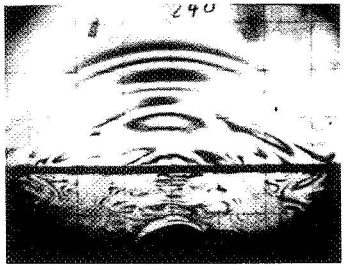

FRAME 7

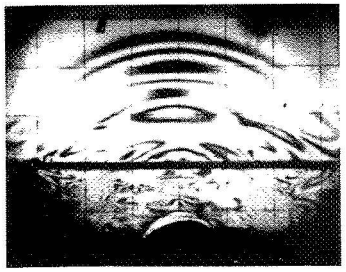

FRAME 8

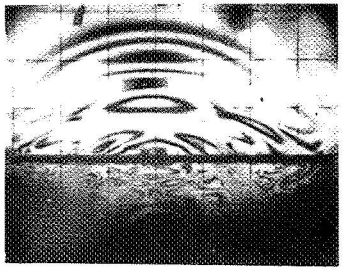

FRAME 9

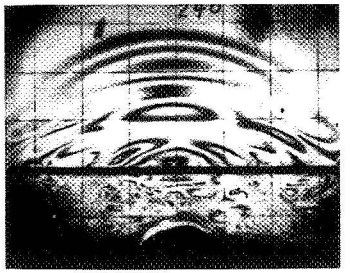

FRAME 10

FIGURE 36

STRESS WAVES THROUGH $\frac{1}{8}$ INCH ALUMINUM LAMINATE

1" ALUMINUM LAMINATE (SHOT 226)

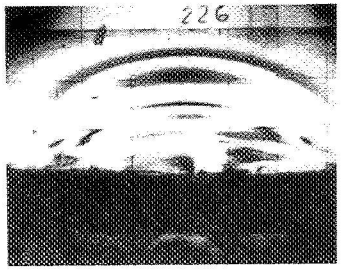

FRAME 1

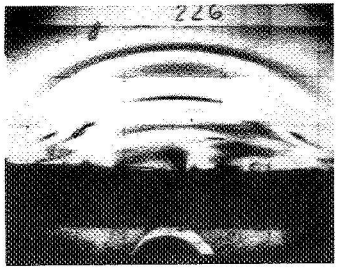

FRAME 2

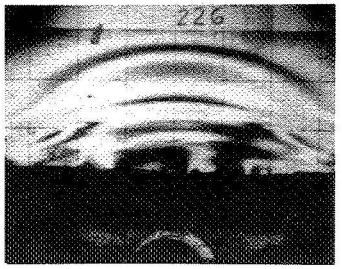

FRAME 3

FRAME 4

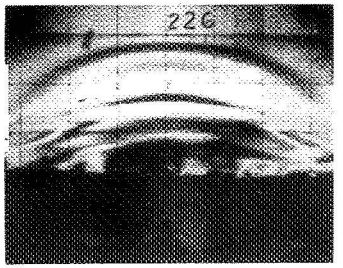

FRAME 5

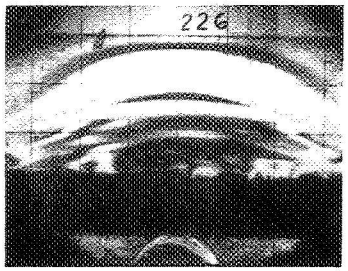

FRAME 6

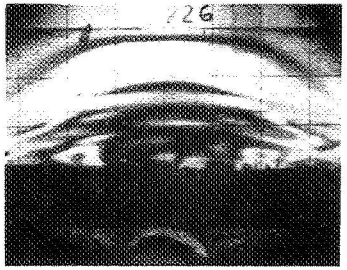

FRAME 7

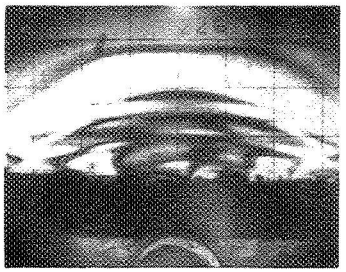

FRAME 8

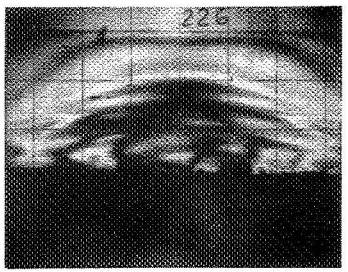

FRAME 9

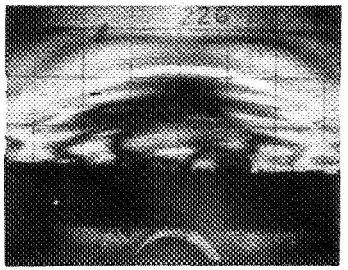

FRAME 10

FIGURE 37

STRESS WAVES THROUGH 1 INCH ALUMINUM LAMINATE

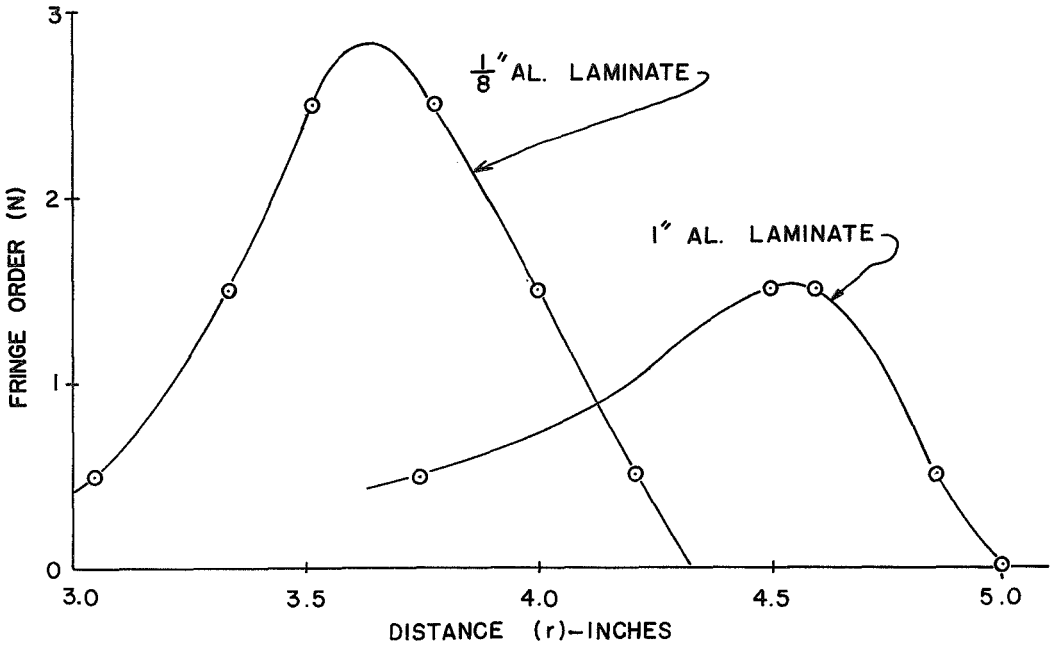

1/8 INCH LAMINATE							
	N	R	UR	ET	ER	SIGMA R	SIGMA THETA
1	C.C	4.330	0.0	0.C	0.C	C.C	0.0
2	C.5CC	4.210	0.166	0.039	-2.721	-3.162	-1.162
3	1.5CC	4.CCC	1.302	0.326	-7.954	-9.152	-3.152
4	2.5CC	3.78C	3.609	0.955	-12.845	-14.589	-4.589
5	2.85C	3.7CC	4.702	1.271	-14.461	-16.337	-4.937
6	2.85C	3.6CC	6.127	1.702	-14.C30	-15.642	-4.242
7	2.5CC	3.51C	7.285	2.076	-11.724	-12.781	-2.781
8	1.5CC	3.33C	8.835	2.653	-5.627	-5.398	C.602
9	1.CCC	3.22C	9.287	2.884	-2.636	-1.8CC	2.2CC
10	C.5CC	3.C5C	9.47C	3.107	C.347	1.785	3.785

1 INCH LAMINATE							
	N	R	UR	ET	ER	SIGMA R	SIGMA THETA
1	C.C	5.CCC	C.C	0.0	C.C	0.0	0.C
2	C.5CC	4.86C	0.193	0.040	-2.720	-3.162	-1.162
3	1.CCC	4.76C	0.6CC	0.126	-5.394	-6.24C	-2.248
4	1.5CC	4.6CC	1.669	0.363	-7.917	-9.092	-3.092
5	1.5CC	4.5CC	2.452	0.545	-7.735	-8.799	-2.799
6	1.2CC	4.3CC	3.797	0.883	-5.741	-6.318	-1.518
7	1.CCC	4.2CC	4.308	1.026	-4.494	-4.797	-0.797
8	C.7CC	4.CCC	5.015	1.254	-2.610	-2.494	C.3C6
9	C.5CC	3.75C	5.499	1.466	-1.294	-0.861	1.139

FIGURE 38

FRINGE ORDER AND COMPUTED RESULTS - ALUMINUM LAMINATES

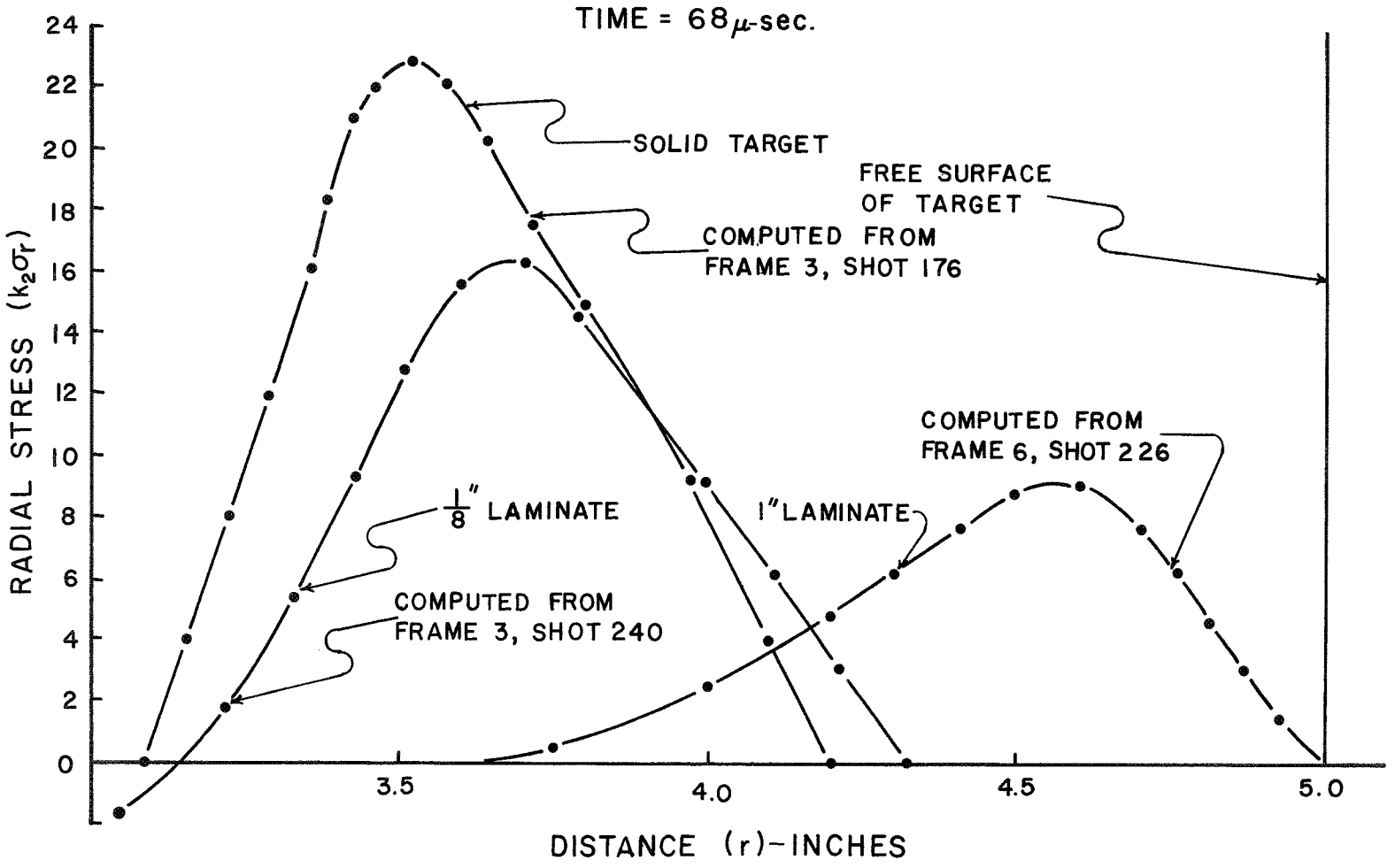

FIGURE 39

COMPARISON OF STRESSES IN HOMOGENEOUS AND LAMINATED TARGETS

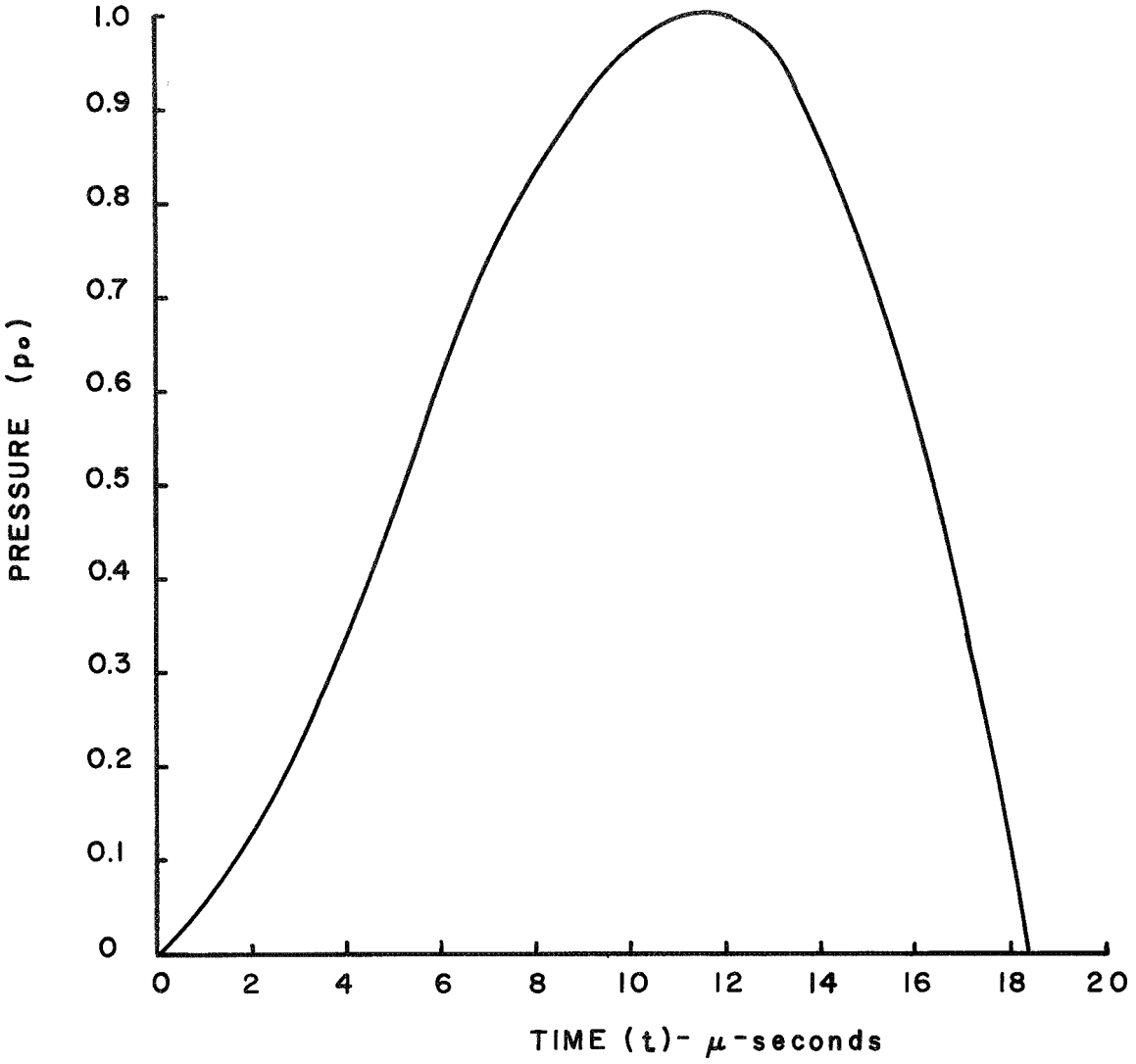

$$p_o = 9161\, e^{-0.01t} - 52194\, e^{-0.02t} + 116950\, e^{-0.03t} - 129079\, e^{-0.04t} + 70283\, e^{-0.05t} - 15121\, e^{-0.06t}$$

FIGURE 40

FORCING FUNCTION TO SIMULATE EXPERIMENTAL IMPULSE

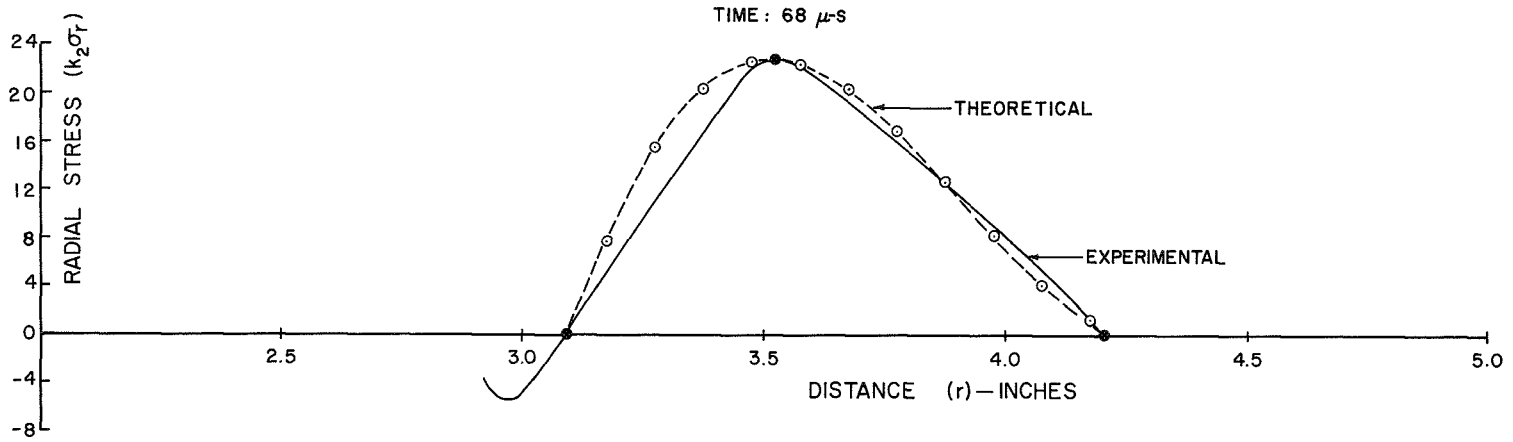

FIGURE 41

MATCHING THEORETICAL STRESS WAVE WITH EXPERIMENTAL STRESS WAVE

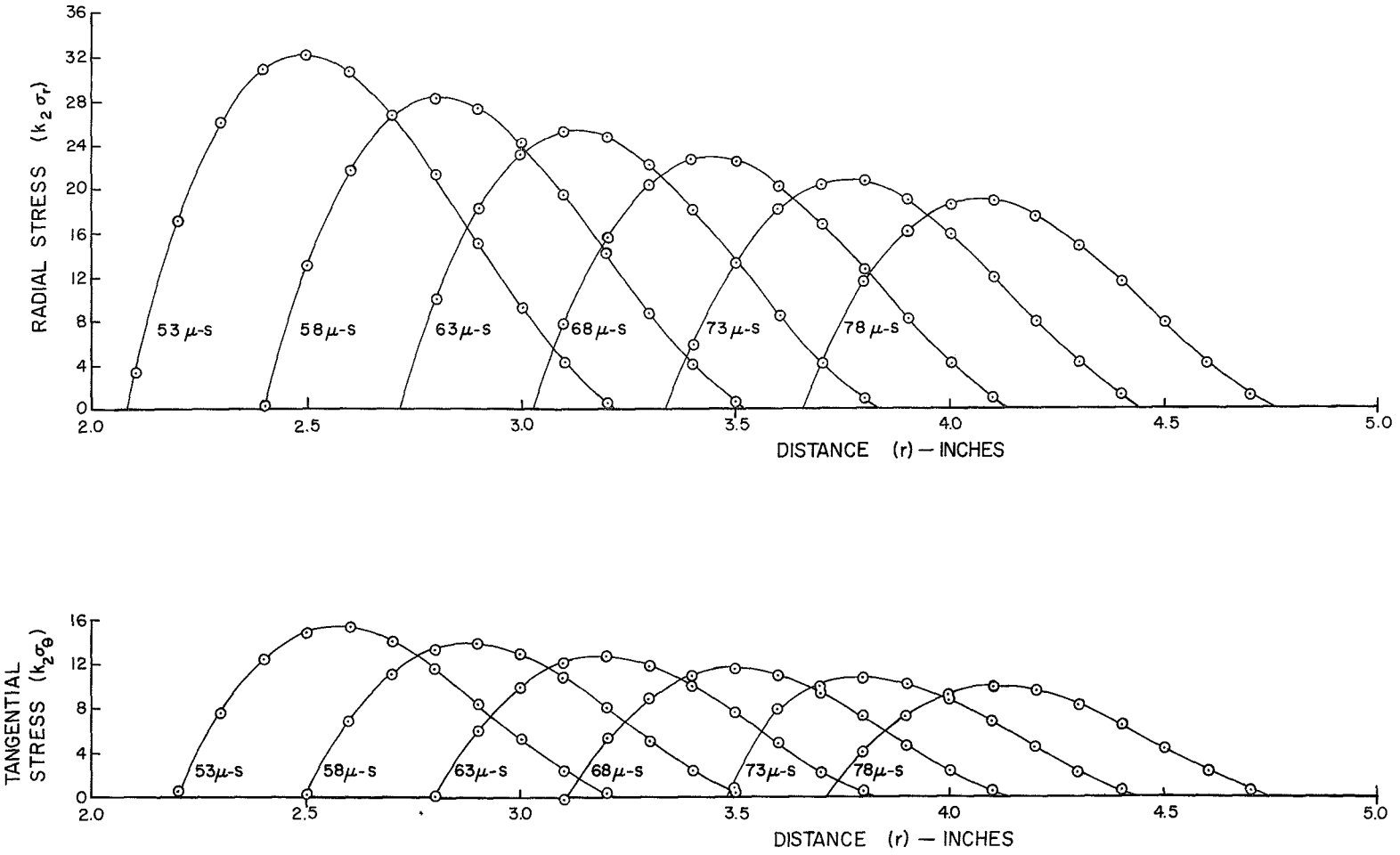

FIGURE 42

THEORETICAL STRESS-DISTANCE-TIME RELATIONS

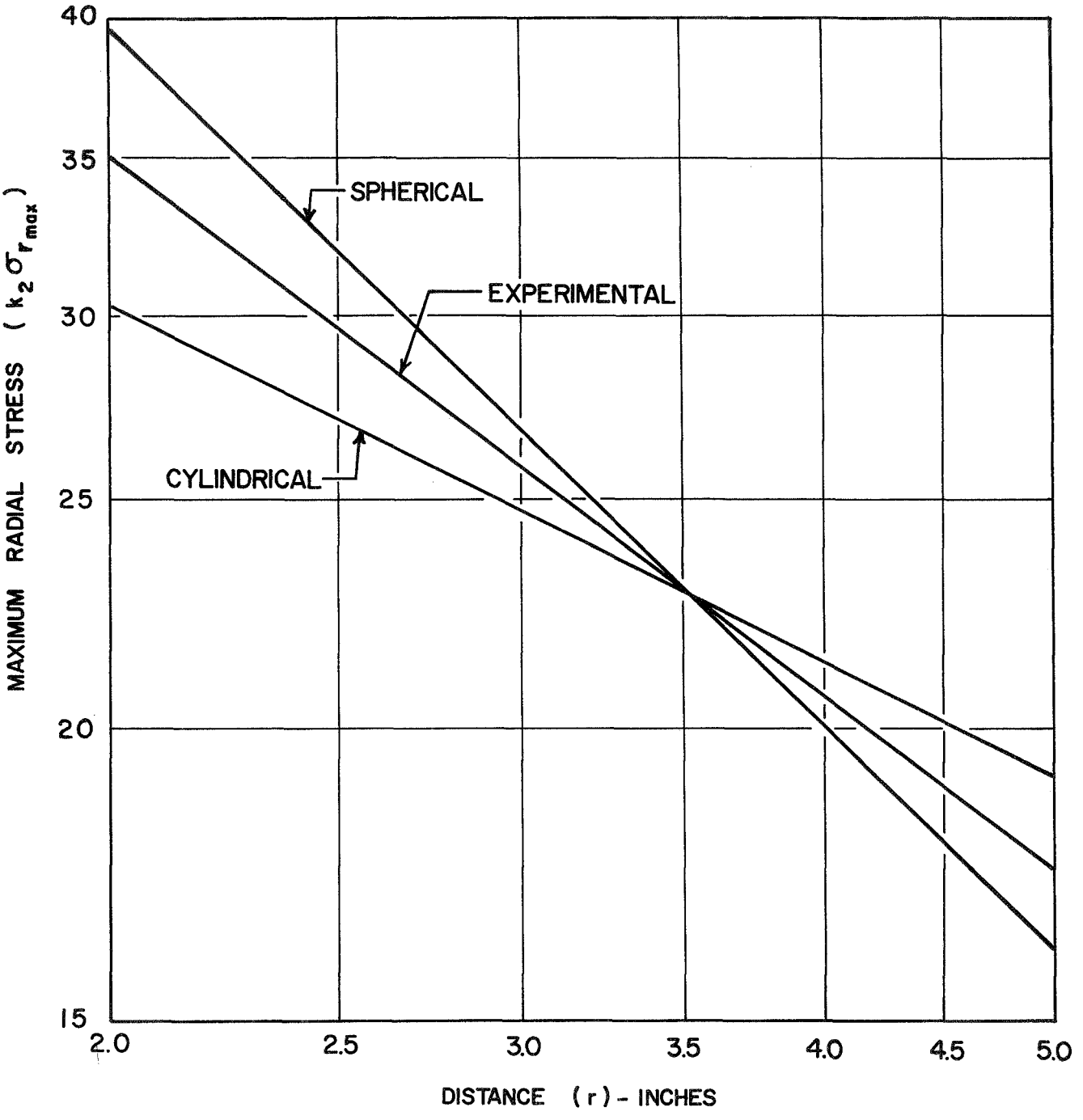

FIGURE 43

STRESS WAVE ATTENUATION

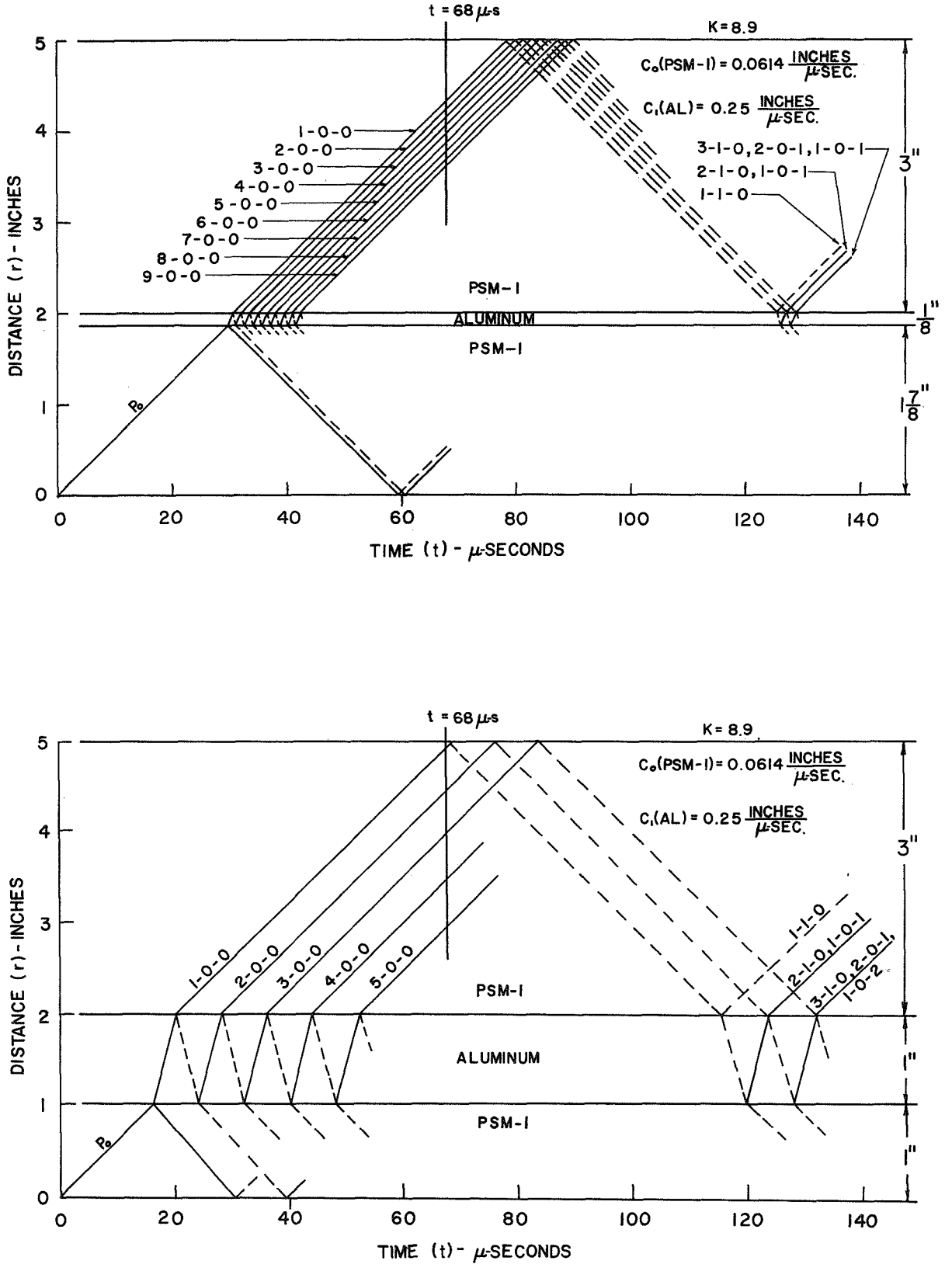

FIGURE 44

DISTANCE-TIME RELATION OF STRESS WAVES IN LAMINATED TARGETS

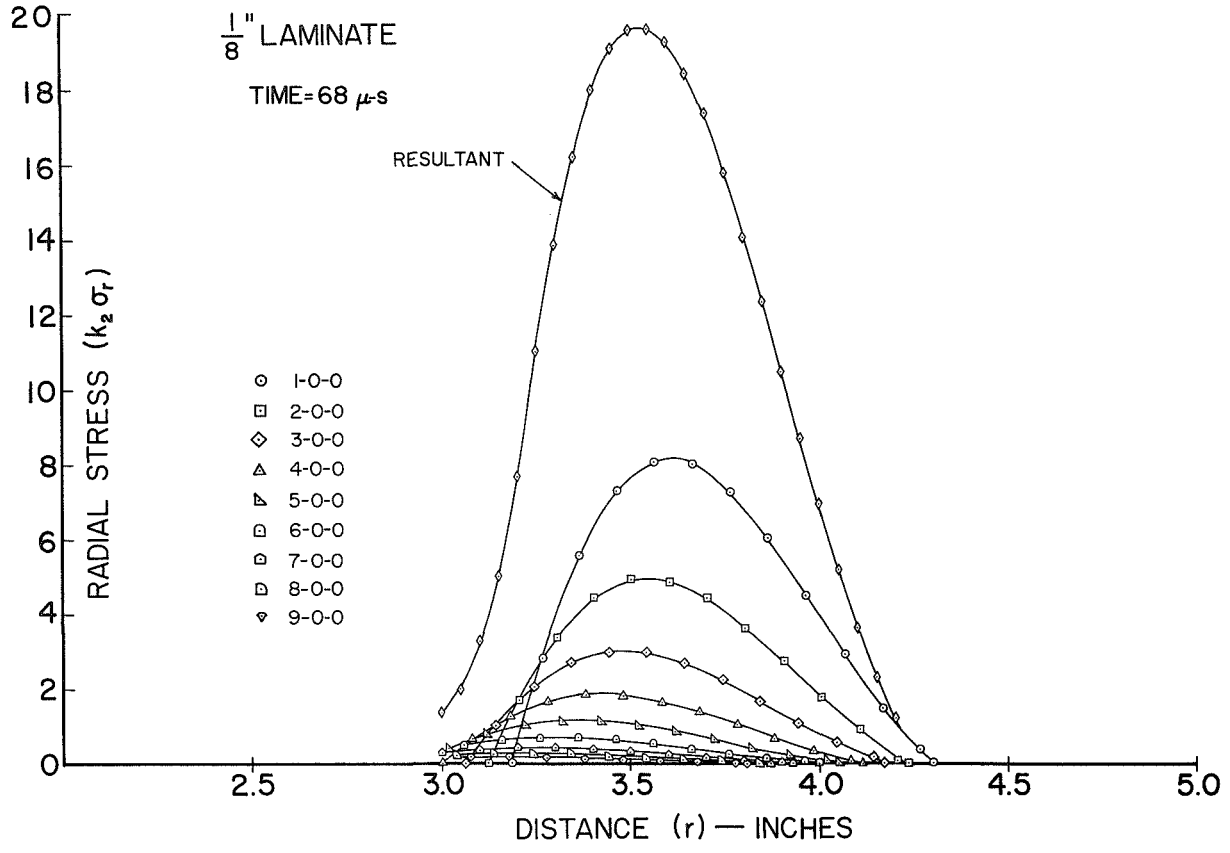

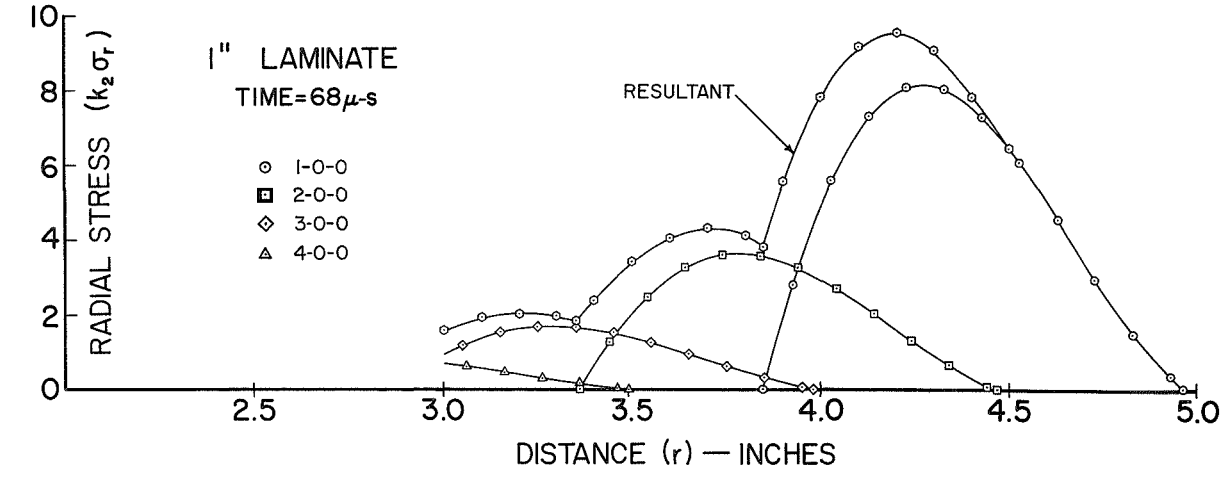

FIGURE 45

SUPERPOSITION OF TRANSMITTED STRESS WAVES IN LAMINATED TARGETS

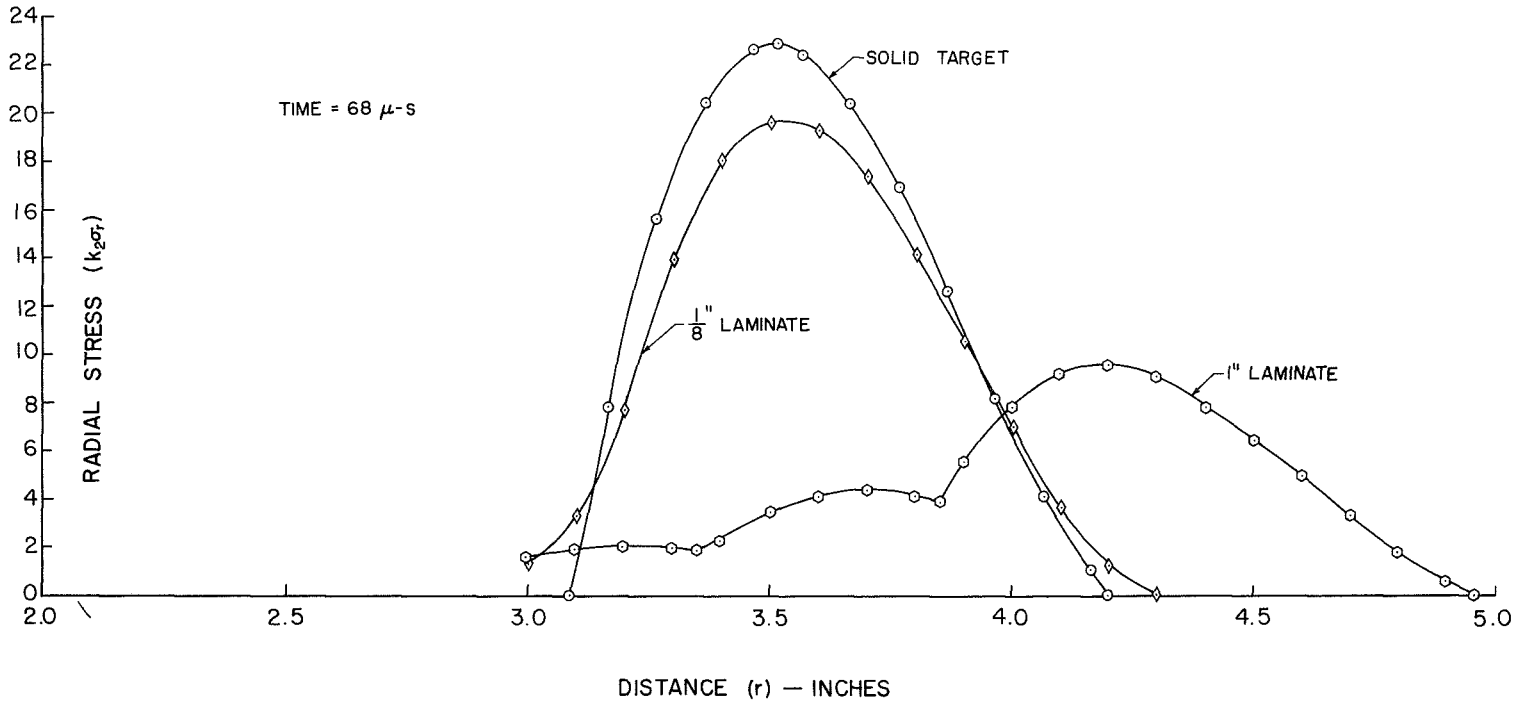

FIGURE 46

COMPARISON OF THEORETICAL STRESSES IN HOMOGENEOUS AND LAMINATED TARGETS

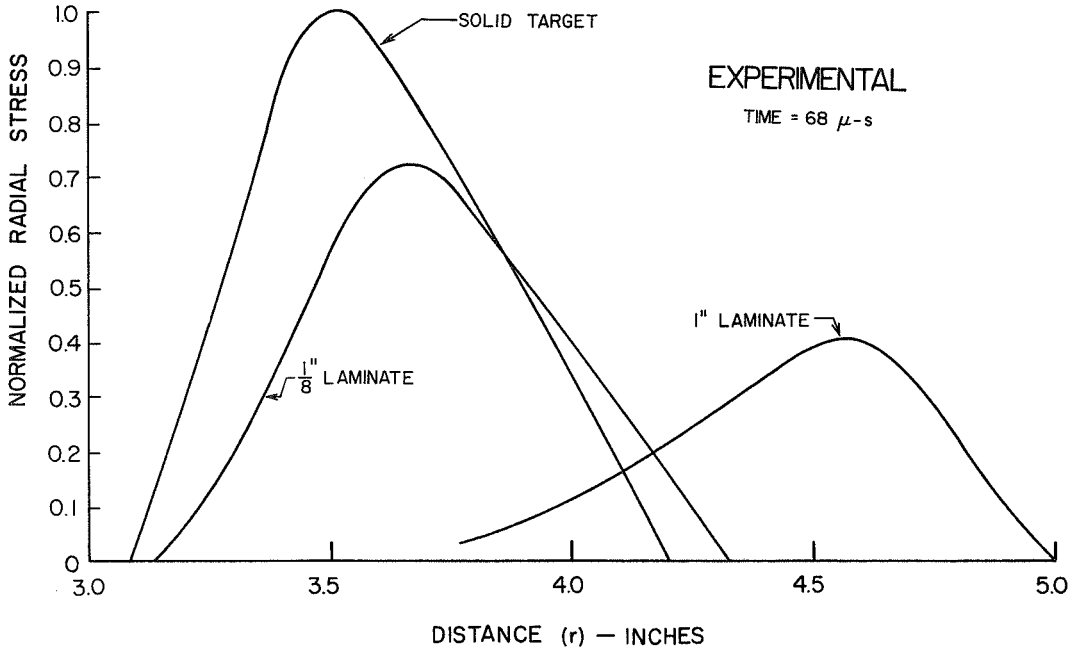

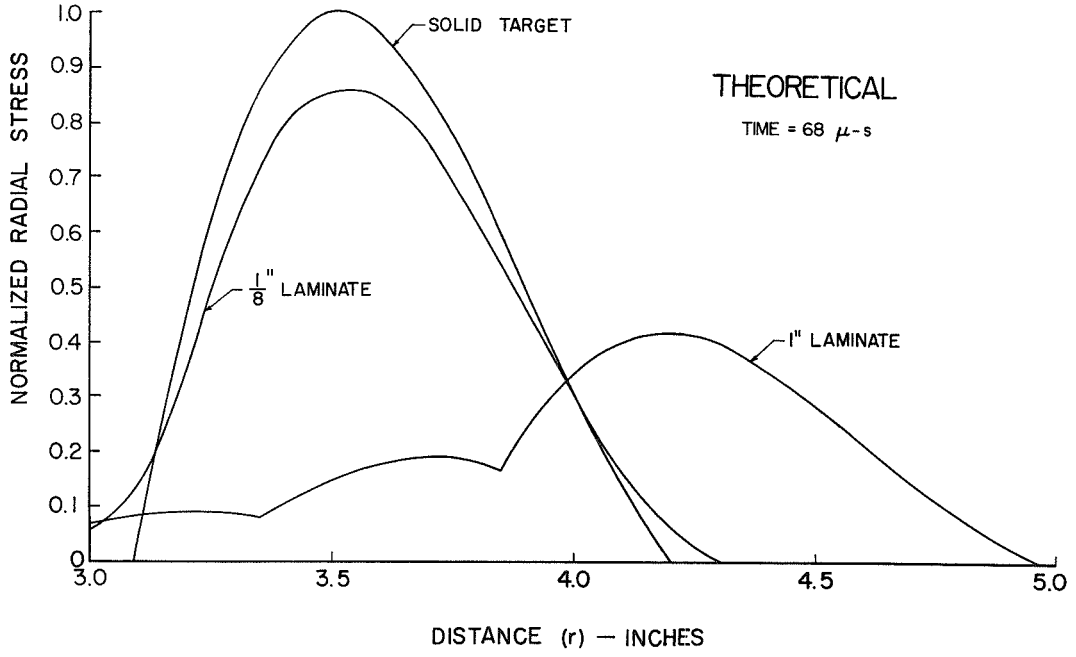

FIGURE 47

COMPARISON OF EXPERIMENTAL AND THEORETICAL RESULTS

TABLE I

MATERIAL PROPERTIES

	DENSITY (ρ) $LB \cdot SEC^2 \cdot FT^{-4}$	WAVE VELOCITY (c) $FT \cdot SEC^{-1}$	CHARACTERISTIC IMPEDANCE (ρc) $LB \cdot SEC \cdot FT^{-3}$
Steel	15.2	19,500	29.6×10^4
Silver	20.4	13,400	27.3×10^4
Copper	17.2	14,000	24.1×10^4
Lead	22.0	7,100	15.6×10^4
Mercury	26.3	4,500	11.8×10^4
Glass	5.0	22,300	11.15×10^4
Aluminum	5.22	20,900	10.9×10^4
Lucite	2.3	8,700	2.0×10^4
PSM-1	2.36	5,100	1.20×10^4
Water	1.94	5,200	1.01×10^4

1st \ 2nd	Steel	Silver	Copper	Lead	Mercury	Glass	Aluminum	Lucite	PSM-1	Water
Steel	-	0.92	0.81	0.53	0.40	0.38	0.37	0.068	0.041	0.034
Silver	1.08	-	0.88	0.57	0.43	0.41	0.40	0.073	0.044	0.037
Copper	1.23	1.13	-	0.65	0.49	0.46	0.45	0.083	0.050	0.042
Lead	1.90	1.75	1.54	-	0.76	0.71	0.70	0.128	0.077	0.065
Mercury	2.51	2.31	2.04	1.32	-	0.94	0.92	0.169	0.102	0.086
Glass	2.65	2.45	2.16	1.40	1.06	-	0.98	0.179	0.108	0.091
Aluminum	2.72	2.50	2.21	1.43	1.08	1.02	-	0.183	0.110	0.093
Lucite	14.80	13.65	12.00	7.80	5.90	5.57	5.45	-	0.600	0.510
PSM-1	24.67	22.75	20.08	13.00	9.83	9.29	9.08	1.67	-	0.842
Water	29.30	27.00	23.90	15.40	11.68	11.00	10.80	1.98	1.19	-

Impedance Mismatch, $K = \left[\frac{\rho_t c_t}{\rho_0 c_0}\right]$

TABLE II

IMPEDANCE MISMATCH FOR VARIOUS COMBINATIONS OF MATERIALS